
Electro-Acoustic Modulation of Surface Acoustic Waves on Thin-Film Lithium Niobate Substrate

*A senior design project submitted in partial fulfillment of the requirements for the degree
of Bachelor of Science*

at

Harvard University

Nicolas Weninger

S.B. Degree Candidate in Electrical Engineering

Faculty Advisor: Prof. Marko Lončar

Supervising Advisor: Dr. Linbo Shao

Harvard University School of Engineering and Applied Sciences

Cambridge, MA

March 2020

Abstract

Surface Acoustic Waves (SAWs) are an important physical phenomenon that could allow for universal coupling between solid state systems such as two-level quantum systems, and for applications in modern high-data rate signal processing. Their slow propagation speed, inability to disperse to vacuum and ability to be used on-chip with piezoelectric materials results in SAWs being an attractive alternative to photons and photon-coupling of such systems. Lithium Niobate (LN) is an appropriate material for this use. The high piezoelectric coupling coefficient, demonstrated non-linear effects, and well-established fabrication techniques make Lithium Niobate (LN) an ideal material for use with SAWs.

Current passive SAW devices still present challenges. It is currently not possible to couple and drive different isolated two-level quantum systems without active SAW modulation, and current passive SAW filters do not allow for as versatile signal processing as active SAW modulation would.

This project demonstrates active electro-acoustic modulation on an LN platform with a fabricated prototype device. More specifically, I design, simulate and fabricate structures on an LN substrate that demonstrate SAW amplitude modulation with a dynamic range of 4 dB, and 180° phase modulation, which can be controlled to give a frequency shift. I also design a benchtop control mechanism for the device.

A Note on COVID-19

Due to the emergency de-densifying measures Harvard University took on the advice of public health officials regarding the COVID-19 outbreak in the spring semester of 2020, I was unable to complete the build and validation of the final product. This report presents a detailed protocol of the validation steps that would have been undertaken, and documents the progress made on the project up until the emergency measures were taken.

This is a most unfortunate and unceremonious conclusion to the project; however, I am fully cognizant of the extraordinary challenge we face as a global community in fighting COVID-19, and find myself fortunate to live in a time where I am able to complete much of my education, including this thesis, remotely. I can only wish that the world emerges soon from these strange times, and once we do, I have no doubt that those who lived through them will not soon let them be forgotten.

Contents

| | |
|---|-----------|
| 1. Introduction and Motivation | 1 |
| 1.1 Surface Acoustic Waves and Existing Applications | 1 |
| 1.2 Lithium Niobate Substrate | 4 |
| 1.3 Active Modulation | 4 |
| 1.4 Problem Statement | 5 |
| 1.5 End User | 5 |
| 1.6 Project Goals | 7 |
| 2. Background Research | 8 |
| 2.1 The Inter-Digital Transducer on Lithium Niobate | 8 |
| 2.2 Acoustics and Quantum Systems | 10 |
| 2.3 Acoustics in Signal Processing | 12 |
| 2.4 Potential Modulation Mechanisms | 13 |
| 3. Design Approach, Goals and Technical Specifications | 14 |
| 3.1 Project Design Approach | 14 |
| 3.2 Design Goals and Constraints | 15 |
| 3.3 Unknown Aspects | 17 |
| 3.4 Technical Specifications and Justifications | 17 |
| 3.4.1 Overall System Specifications | 17 |
| 3.4.2 Phase Modulator Specifications | 20 |
| 3.4.3 Amplitude Modulator Specifications | 21 |
| 3.4.4 Control System Specifications | 22 |

| | |
|--|-----------|
| 3.5 Technical Specifications Summary | 23 |
| 4. Modelling..... | 24 |
| 4.1 Approach | 24 |
| 4.2 Model Setup | 25 |
| 4.2.1 Parameterisation | 25 |
| 4.2.2 Geometry | 26 |
| 4.2.3 Material | 27 |
| 4.2.4 Physics Models | 28 |
| 4.2.5 Common External Circuitry | 29 |
| 4.2.6 Model Mesh | 30 |
| 4.2.7 Model Output | 31 |
| 4.3 Identity Model Geometry and Results | 32 |
| 4.4 Gain Modulator Geometry and Results | 35 |
| 4.5 Phase Modulator Geometry and Results | 41 |
| 4.5.1 Surface Electrode Model Geometry and Results | 41 |
| 4.5.2 Naïve Model Geometry and Results | 43 |
| 5. Device Fabrication..... | 46 |
| 5.1 Mask Design | 46 |
| 5.2 Fabrication Protocol | 49 |
| 5.3 Fabrication Results | 51 |
| 6. System Design and Construction..... | 53 |
| 6.1 Printed Circuit Board | 53 |
| 6.1.1 Identity Circuit | 54 |
| 6.1.2 Gain Circuit | 54 |
| 6.1.3 Phase Circuit | 57 |
| 6.1.4 Additional Design Considerations | 58 |
| 6.1.5 Considerations for Future PCB Iterations | 59 |
| 6.2 Control System | 60 |
| 7. Design Evaluation and Testing | 62 |
| 7.1 Testing Methodology | 62 |

| | |
|--|-----------|
| 7.2 Identity Device Testing | 65 |
| 7.3 Gain Device Testing | 66 |
| 7.4 Phase Device Testing | 68 |
| 8. Conclusion | 70 |
| 8.1 Specification Evaluation | 71 |
| 8.2 Potential Future Work | 73 |
| Acknowledgements | 75 |
| References | 76 |
| | |
| A. Fabrication Mask Generation Code | 80 |
| B. PCB Schematic and Board Layout | 87 |
| C. PCB Bill of Materials | 89 |
| D. Project Budget | 90 |
| E. Supplemental ES100 Questions | 91 |

List of Figures

| | |
|---|----|
| Figure 1-1: Stakeholder Map – divided between academia and industry stakeholders. | 6 |
| Figure 2-1: Scanning electron microscope Image of an IDT. The image depicts a top-down view of an IDT, where the black lines are deposited metal ‘fingers’ on a substrate. Alternating fingers are electrically connected to the same terminal. [16]. | 9 |
| Figure 2-2: Cross-Section of two IDT finger-pairs. Dark shading indicates a ground connection, while light shading indicates an AC-signal connection. | 9 |
| Figure 2-3: Diagram of Tx/Rx IDT pair. The Tx IDT is connected to an AC source and the RX IDT is connected to an impedance matched load R. The red arrow indicates the direction of travel of the SAW [17]. | 10 |
| Figure 3-1: Abstracted Block Diagram of the project. The items indicated in red are within the scope of the project, and those in black are will be implemented with known methods. | 14 |
| Figure 3-2: System Model Diagram of the project, demonstrating in more detail the layout of individual components within the project. The items indicated in red are within the scope of the project, and those in black are will be implemented with known methods. | 15 |
| Figure 4-1: Geometry of LN substrate divided into 6 regions. The substrate is still one single piece. The white box is a placeholder for the SAW modulation structures discussed in later sections. | 28 |
| Figure 4-2: External circuitry for the Tx/Rx IDT pair with 50 Ω impedance matching. | 29 |
| Figure 4-3: Identity model with a 200 MHz SAW. The Tx IDT is on the left and the Rx IDT is on the right as marked, with 50 μm spacing in the middle. White lines indicate the divides between regions 1-6. (a) ‘Fine’ mesh setting, with bulk transmission of the SAW and unrealistic displacement of the base observed. (b) Custom triangular mesh setting, where the maximum allowed spacing is, $\lambda/4$. | 31 |

- Figure 4-4: Geometry of the identity model, depicted not to scale in order to better visualise the geometry. Boxes labelled "IDT" represent the geometric extent of the fingers for a given IDT. (a) Side cross-sectional view. λ is the SAW wavelength. (b) Top-down view showing additional circuitry.....33
- Figure 4-5: Identity model coarse frequency sweep results for $\lambda = 20\mu\text{m}$ geometry. The red dotted line indicates the specified lower bound for intrinsic attenuation.34
- Figure 4-6: Identity model frequency sweep results for both wavelength geometries, as indicated by the legend. The red dotted line indicates the specified lower bound for intrinsic attenuation. The $\lambda = 20\mu\text{m}$ data is lower resolution, as the peak can be identified from this data without the need for higher resolution studies. Further studies were only done on the new geometry.35
- Figure 4-7: Geometry of the gain modulation model, depicted not to scale in order to better visualise the geometry. Boxes labelled "IDT" represent the geometric extent of the fingers for a given IDT. λ is the SAW wavelength. (a) Side cross-sectional view. (b) Top-down view showing additional circuitry.....36
- Figure 4-8: Gain modulator coarse frequency sweep results for $\lambda = 20\mu\text{m}$ geometry, showing attenuation levels for 10, 20 and 30 IDT finger-pairs. The identity case is included as a comparison. The red dotted line indicates the specified lower bound for intrinsic attenuation.37
- Figure 4-9: Gain modulator resistance parameter sweep results for $\lambda = 20\mu\text{m}$ geometry, showing attenuation and phase shift for 10, 20 and 30 IDT finger-pairs.....38
- Figure 4-10: Gain model frequency sweep results for both wavelength geometries, as indicated by the legend.39
- Figure 4-11: Gain modulator resistance parameter sweep results for $\lambda = 20\mu\text{m}$ and for $\lambda = 19\mu\text{m}$ geometry, showing attenuation and phase shift for the 20 IDT finger-pair variant. The orange and blue arrows visually indicate the dynamic range.....40
- Figure 4-12: Surface electrode design of the SAW phase modulator. The positive and negative electrodes are connected to a DC power source. L represents the width dimension of the surface electrodes. λ is the SAW wavelength.....41
- Figure 4-13: Surface electrode design phase modulator amplitude and phase shift data. Two electrode widths are tested. Every 10th data point is plotted for clarity.....42

- Figure 4-14: Geometry of the naïve phase modulation model, depicted not to scale in order to better visualise the geometry. Boxes labelled "IDT" represent the geometric extent of the fingers for a given IDT. λ is the SAW wavelength. (a) Side cross-sectional view. (b) Top-down view showing additional circuitry..... 43
- Figure 4-15: Naïve design phase modulator amplitude and phase shift data. 10, 20, 30 and 40 finger-pairs on the phase modulation IDT is tested, as indicated in the legend. Every 3rd data point is plotted for clarity. 44
- Figure 5-1: Screenshot of the mask in KLayout. The distance between the blue markers is 2.5 mm. (a) Identity device. (b) Gain device with 20 finger-pairs. (c) Gain device with 10 finger-pairs. (d) Gain device with 30 finger-pairs. (e) Phase device with 40 finger-pairs. 48
- Figure 5-2: (a) SAW device fabrication: bilayer lift-off technique with photolithography and metal deposition of aluminium [27]. Red is the photoresist, the black in the exposure step is the mask, and the black in subsequent steps is the deposited metal. The bottom row are scanning electron microscope image of IDT fingers after (a) development, (b) metallisation, and (c) lift-off [42]. 49
- Figure 5-3: Select images from the fabrication process. (a) Sample cleaning to remove residue from dicing. (b) Photoresist spin-coating. (c) Samples after EE-3 metal deposition. (d) Two of four samples after lift-off and clean. 51
- Figure 5-4: Optical images of fabricated devices. (a) Zoomed in photo of an IDT showing the individual fingers. (b) Identity device. (c) Phase device (with 20 fabricated finger-pairs). (d)-(f) Gain devices (with 5, 10, and 20 fabricated finger-pairs). 52
- Figure 6-1: Identity circuit. (a) Schematic with SMA connectors and wire-bond pads. (b) Corresponding PCB layout..... 54
- Figure 6-2: Gain control circuit. (a) AD5174 digital rheostat schematic. (b) SPI digital interface schematic. (c) corresponding PCB layout, which also show the headers for the manual rheostat (labelled GAIN1). 56
- Figure 6-3: (a) Gain circuit Tx/Rx IDT interface schematic with 2x1 0.1" header connected to gain modulation IDT. (b) Corresponding PCB layout, showing the SMA connectors X1, X3 and the manual rheostat header GAIN1..... 57
- Figure 6-4: Phase circuit. (a) Schematic with additional SMA connector for the phase modulator, (b) corresponding PCB layout..... 58
- Figure 6-5: Dual-supply power bus connector with decoupling capacitors. 59

| | |
|--|----|
| Figure 6-6: A drawing indicating the SPI connections to an Arduino UNO. The protoboard depicted is the size of the PCB. Black: ground. Blue: SYNC1/2. Red: SCLK. Yellow: DIN. The graphic is made using Fritzing. | 61 |
| Figure 7-1: A VNA makes measurements with respect to a reference signal. The measurements are presented to the user on a display or logged on a computer for further analysis..... | 65 |
| Figure B-1: Full schematic of the PCB as ordered. | 87 |
| Figure B-2: Screenshot of the PCB layout as ordered, without ground plane infill..... | 88 |

List of Tables

| | |
|---|----|
| Table 3-1: Design Goals and Constraints | 15 |
| Table 3-2: Summary of Project Specifications. The numbers on the left match the last two digits of the heading of the specification..... | 23 |
| Table 7-1: Summary of tests to be conducted. The test description and parameters are also given. | 64 |
| Table 8-1: Summary of the project specifications. Green means that they have been met. Yellow means that they were unable to be tested..... | 71 |
| Table C-1: PCB Bill of Materials and total quantities ordered for the project. | 89 |
| Table D-1: Total project budget..... | 90 |
| Table E-1: Supplemental ES100 Budget Questions | 91 |
| Table E-2: Supplemental ES100 Questions on Harvard CNS Usage..... | 91 |

Chapter 1

Introduction and Motivation

With the leaps and bounds being made in modern communication and computation technologies, the world has found itself at a challenging junction. Whereas previously we were able to rely on the seemingly limitless promise of Moore's Law to guarantee advances in computational power and complexity, we now face the looming threat of the end of these days, given by the fundamental limits of physics that prohibit further miniaturisation of existing silicon-based computing architectures [1].

Given the relentlessly increasing demand for better and faster computing for ever more intricate and ground-breaking tasks, there is a clear and immediate need for a new processing paradigm that is able to transcend the architectural and physical boundaries once set by the universal computing platform of silicon. Surface acoustic waves (SAWs) are one among many phenomena being proposed, as their usefulness in their current applications lend credibility to the idea that they could be used in advanced signal processing or quantum computing applications. By leveraging the unique properties that SAW devices have to offer, more efficient coupling between qubits and higher performance signal processing can be achieved.

This thesis explores one piece of the larger puzzle of how surface acoustic waves could become a powerful platform on which to base future computation and communication platforms.

1.1 Surface Acoustic Waves and Existing Applications

An acoustic wave is a type of energy propagation through a medium through compression and expansion of the structure of the medium itself. It is most often

characterised as a longitudinal wave. Some examples of acoustic waves are audible sound from a speaker, earthquakes, and ultrasound used for medical imaging.

The study of SAWs developed out of the use of bulk acoustic wave propagation for convenient electronic applications, like filters and crystal oscillators. SAW propagation in crystalline solids exhibits properties that have been exploited for a number of electronic devices to date. Because of their unique properties, devices like acoustic delay lines and crystal oscillators with high Q-factors were developed, and have found use cases in a variety of applications, such as medical devices and digital watches [2].

The unique properties that characterise SAWs are with reference to other wave phenomena that are used in similar applications, like photons. These properties make SAWs more attractive than photon-based systems in current electronics and in potential future applications [3]. SAWs have a propagation speed five orders of magnitude less than that of photons and very low attenuation for frequencies well into the megahertz and gigahertz regimes, when propagating through crystalline solids [4]. SAWs are mechanical waves and thus cannot propagate through vacuum, making them not subject to scattering or radiation losses into vacuum as with photons, meaning that they are able to better avoid unwanted energy loss during transit. Further, their longer wavelength compared to photons means that fabricating nanostructures for SAWs on-chip is easier than fabricating equivalent structures for photons with current silicon fabrication techniques, as the required structures for SAWs are larger, thus mitigating fabrication issues. The combination of these properties means that SAWs present a promising alternative to photon-based systems, which are harder to control and scale due to the above.

A further useful property of SAWs is that the energy concentration is near the surface of the solid, rather than spread throughout the volume of the media [4]. This subsequently means that the wave can be more easily tapped or modified while it is propagating, opening the door to a host of passive signal processing applications, such as oscillators, bandpass filters, pulse compression filters and PSK filters.

The push for smaller devices has already resulted in the use of SAWs in the signal processing domain [5], which was spurred by the invention of the Interdigital Transducer (IDT), which provides an effective method of transduction of electrical to SAW signals [6]. An IDT consists of interlocking metal finger-like structures deposited on top of a piezoelectric substrate. A varying electric potential is applied between these fingers, so as to induce a mechanical stress in the substrate via the piezoelectric effect, thus causing SAWs to be generated. Section 2.1 goes into further detail on IDTs.

IDTs paved the way for many of the above applications to be realised, as the inherent benefits of SAWs could be exploited.

In recent years with the rise of solid-state quantum computers – and associated quantum information theory – SAWs have found other use cases, aside from classical signal processing. SAWs can be coupled with electromagnetic fields via the piezoelectric effect, giving rise to other applications like faster communications processing, modulating light via the acousto-optic effect [7], and driving solid-state electron spins in certain materials [8]. The strong electromechanical coupling, high resonant frequency and near-surface confinement of SAWs provide the potential for higher Q-factors, as required for applications in quantum and high-fidelity classical signal processing [9].

In the above cases, modulation of the SAWs is done in a passive manner. The physical structures – for example, etched grooves or deposited metal – on the surface of the substrate through which a SAW travels will define the transfer function of the SAW signal, much like how the transfer function of an electric signal is defined by the components (and thus, the impedance) of the circuit through which it travels. Because the structures are built into the substrate of the device, the SAW transfer function cannot be changed.

A concrete example of a passive use case is SAW filters in mobile phone radios. Such radios require many different filters for each RF frequency in which they operate. In the frequency range up to 1 GHz – which include some ‘4G’ bands – SAW filters are almost exclusively employed, with increasing prevalence in higher frequency ranges [10]. SAW filters for cellular phones are fabricated in increasing volumes today, given the worldwide growth of mobile phone adoption, and competing filter technologies have not yet proven to be more space efficient or higher performing than SAW filters [10].

A device capable of changing this inherent transfer function such that the properties of the SAW signal can be changed in a non-predetermined manner would open the door to many new signal processing and quantum computing applications. Given the benefits of using SAWs in these domains, so-called active modulation could allow for better signal processing abilities in the same physical area as in current SAW filters, potentially allowing for higher bandwidth and bitrate communication protocols. In their quantum information application, an active modulation device could be used to not only transfer state or maintain coherence between qubits, but also to drive state and connect different types of quantum system together to fully leverage the benefits of each. In short, an active modulation SAW device puts us one step closer to realising commercial quantum computing.

1.2 Lithium Niobate Substrate

Converting between optical or electrical signals and SAWs is needed in order to make use of the benefits that SAW devices have to offer. This conversion is done using different on-chip nanostructures, all of which employ the piezoelectric effect [11] – the ability of a material to generate an electric charge in response to applied mechanical stress, and vice-versa. This subsequently necessitates the need for a material that is piezoelectric. The material that is widely used to demonstrate this piezoelectric coupling capacity and exhibits a high piezoelectric coupling coefficient is Lithium Niobate (LN). LN possesses additional properties that make it ideal for this application: at room temperature, the acoustic propagation loss due to electrical conductivity is significantly lower than for other piezoelectric materials (about half with respect to quartz) [12], [13]. LN can also have smaller device footprints due to faster SAW propagation speed, better signal dispersion performance, and is compatible with proven silicon fabrication techniques [14].

1.3 Active Modulation

In order for SAWs to be fully realised as a universal interface for coupling solid-state quantum systems or in advanced signal processing applications, there must be a way to modulate SAWs on-chip – shifting their frequencies to match the transition of interest, and modulating their amplitude. If we want to use SAWs to control things, or to manipulate information carried by them, we need a way to control them.

If this were achieved, one would not only be able to couple quantum systems like qubits together, but also change and drive the state of individual or multiple qubits using SAWs. Additionally in signal processing applications, by being able to modulate the information carrier, it is possible to conduct frequency filtering and signal differentiation with parameters that are user controlled, rather than statically determined by the geometry of the device. This allows for further miniaturisation of existing devices, and opens the door to higher information density signal modulation techniques.

Passive signal processing techniques have been demonstrated for SAWs, optical modulation of SAWs is possible [8], and active optical modulation techniques exist for photon coupling techniques. However, no technique currently exists for electrically controlled active modulation of SAWs – a necessary component to realise the full potential of on-chip SAWs in novel systems.

1.4 Problem Statement

The full potential of SAWs as a universal interface paradigm for solid-state systems and a versatile classical signal processor have yet to be realised, both in the lab and ultimately in consumer devices. This is because the frequency, phase and amplitude of SAWs cannot be yet actively modulated using electric signals on-chip during transit, with other optical methods using photon coupling being too challenging to control and scale.

1.5 End User

The client for this project is the Laboratory for Nanoscale Optics at the Harvard University John A. Paulson School of Engineering and Applied Sciences. The principal investigator and faculty head of the lab is Professor Marko Lončar. It is intended to be used within their larger research portfolio on SAWs to demonstrate coupling between different solid-state systems.

The potential target end users for an electro-acoustic SAW modulator are many, given the widespread current uses of SAWs in electronic consumer devices (e.g. as filters in mobile phone modems), and the potential future users of quantum information, communication and computation systems. Additional target end-users include:

- Quantum computing and communication engineers, who could use SAWs to create scalable networks of solid-state qubits
- Mobile telephone modem manufacturers, who would use SAW modulation to more compactly and efficiently demodulate and modulate signals on future network standards (5G and beyond).
- Research groups focusing on signal processing and other uses for SAWs. This is likely the most relevant group, seeing as the prototype device is highly unlikely to be ready for mass consumer manufacture by the conclusion of the project.

This device could have a measurable impact on the work of not only the Laboratory for Nanoscale Optics, but the wider research community, as it would enable a new suite of applications for an already well-characterised physical phenomenon. It may also open the door to new quantum computing architecture research that take advantage of the properties of different types of solid-state qubits. The consumer applications of SAW devices would be expanded to include next-generation wireless technologies beyond 5G.

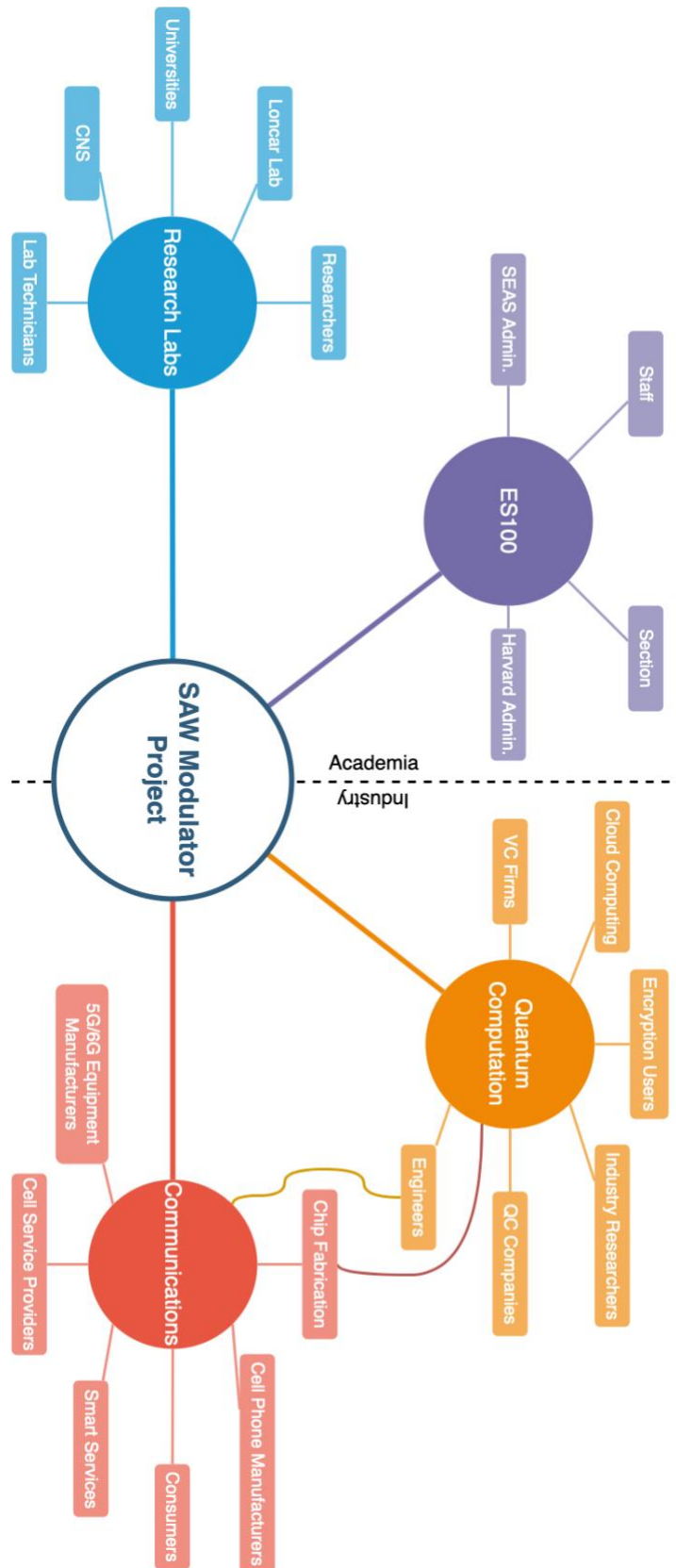


Figure 1-1: Stakeholder Map – divided between academia and industry stakeholders.

1.6 Project Goals

This project will demonstrate an active electro-acoustic modulation of SAWs on an LN substrate. This means that the degree of frequency and amplitude modulation of the SAW can be controlled electrically via fabricated structures on the LN substrate and an off-chip control system. The frequency will be indirectly modulated by taking advantage of phase and amplitude modulation effects.

While it is academically interesting to simply demonstrate that this phenomenon is possible, this modulator is ultimately intended for use in a larger system to support a research effort, and ultimately make its way into commercial use. Thus, the ultimate aim is to create a modulator that can be useful within a system in such a way as to be interesting to commercial applications. This is further outlined in the specifications in Chapter 3.

This project will design, prototype and validate an LN device capable of achieving the above goals. A benchtop control system for the device is also necessary for its intended application, the design for which will form an additional component of the deliverable.

Chapter 2

Background Research

A significant amount of literature exists for the application of SAWs in consumer electronics and to couple between solid-state quantum systems. However, as electro-acoustic modulation has been characterised as a need only fairly recently with increased interest in quantum computing and modern communication protocols in the past decade, little to no literature exists yet on the subject. This section will expand upon existing applications of SAWs and provide contextual information that is key to understanding the mechanisms by which SAWs operate.

2.1 The Inter-Digital Transducer on Lithium Niobate

To better understand the nature of SAW generation and propagation on piezoelectric substrates, it is useful to look at the Inter-Digital Transducer (IDT). Indeed the invention of the IDT proved pivotal in the development of acoustic systems, as it allowed the transduction of electric signals to SAWs in an efficient and easily characterizable manner [6]. Further developments in the field showed that this IDT structure on an LN substrate produces significantly higher SAW surface energy confinement and exhibits superior energy transmission characteristics from the electrical signal to the SAW than other piezoelectric substrates [12], meaning that the SAWs generated and received by LN IDTs are less attenuated than for other substrates.

An IDT is a metal structure that is deposited on the surface of the substrate, as shown in Figure 2-1. The metal is often gold or aluminium. Gold is chosen for its good electrical conductivity, which makes SAW transduction less prone to resistive losses.

However, the difference in conductivity between gold and aluminium is small ($\Delta\rho = 3.8 \times 10^{-9} \Omega m$). Gold is challenging to work with during fabrication while in contrast, aluminium is chosen for its comparatively easy fabrication [15]. Further, due to the higher density of gold than aluminium, gold attenuates the SAWs more due to mechanical losses. Accordingly, aluminium finds more applications in SAW-enabled devices, despite gold's good conductive properties.

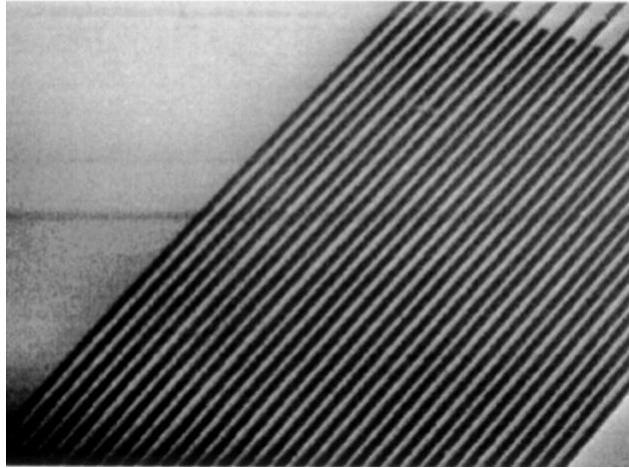


Figure 2-1: Scanning electron microscope Image of an IDT. The image depicts a top-down view of an IDT, where the black lines are deposited metal 'fingers' on a substrate. Alternating fingers are electrically connected to the same terminal. [16].

The IDT consists of interlocking structures – often called fingers. By virtue of how an IDT generates SAWs, the spacing of these fingers is dictated by the desired centre wavelength of the SAW that is being generated. A pair of fingers is spaced one wavelength apart, with quarter wavelength spacing between the fingers. The fingers are a quarter wavelength in width, as shown in Figure 2-2 [14].

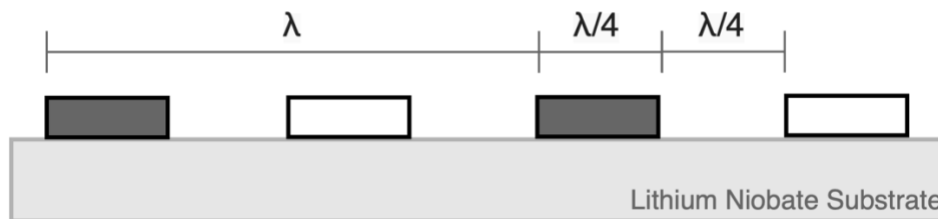


Figure 2-2: Cross-Section of two IDT finger-pairs. Dark shading indicates a ground connection, while light shading indicates an AC-signal connection.

In SAW generation, every other IDT finger is connected to the AC signal terminals, while the others are connected to ground. Due to the potential difference between fingers, a mechanical stress is generated in the piezoelectric LN substrate,

thereby producing the SAW. In SAW reception, the mechanical stress in the LN due to the SAW produces an electric potential. Being an electrical conductor, the receiving IDT has a current induced in it due to this potential, which in turn is manifested as the outgoing signal. When combined, the transmission (Tx) and reception (Rx) IDTs can be used on the same substrate to create a SAW device, as depicted in Figure 2-3.

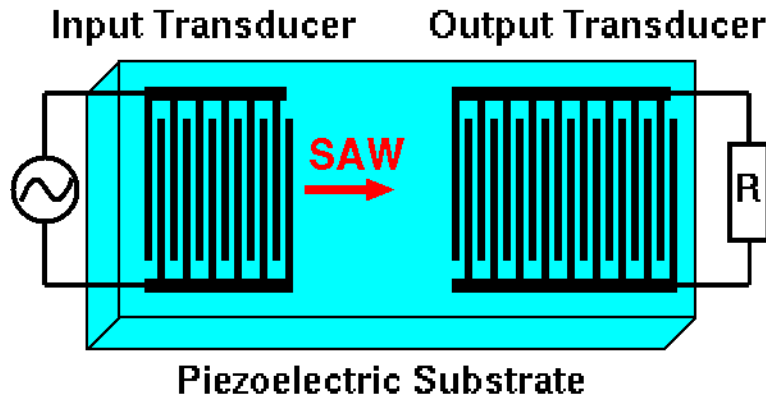


Figure 2-3: Diagram of Tx/Rx IDT pair. The Tx IDT is connected to an AC source and the RX IDT is connected to an impedance matched load R. The red arrow indicates the direction of travel of the SAW [17].

2.2 Acoustics and Quantum Systems

Several teams have shown the potential of acoustic coupling with different types of two-level quantum systems, which can be used for quantum information applications. This coupling means that the quantum state of qubits can be driven by acoustic waves, often represented in their quantised form, phonons.

A team demonstrated that SAWs could be used to drive the state of a two-level Nitrogen vacancy centre in Diamond – a potential candidate for qubit platforms [8]. Further, they have also demonstrated that it is possible to couple SAWs with electron spin states without decay of the spin coherence of the system [18]. These results establish the possibility for further development spin-based quantum diamond nitrogen vacancy centre acoustics, bridging the gap between quantum state control and SAWs, and demonstrating a potential application for this project.

Another cross-disciplinary team investigated the effect of atomic spin-strain coupling via the piezoelectric effect using SAWs of point defects in silicon carbide [19]. While silicon carbide systems were optically controllable, the team demonstrates that full quantum state control can also be achieved through spin-strain coupling via SAWs. In order to achieve this controllability, the SAW must be able to induce

different strains in the system, requiring different wave properties. Thus, if this qubit architecture were to be used in a system, there may be a need for active SAW modulation.

Further research has demonstrated that SAWs are even able to interact with superconducting qubits to carry quantum information [20], [21]. This is an exciting result, as superconducting qubits are currently implemented in existing quantum computing architectures, such as on IBM Q's commercially accessible quantum computers [22], and so superconducting qubits may require minimal additional basic research to significantly decrease their quantum decoherence rates, as the energy of a SAW will dissipate less easily as compared to photons. This result thus potentially indicates a way to mitigate the quantum error correction issues using SAWs, and further underlines the myriad of different potential applications of SAWs in the quantum information domain. It also suggests further potential applications for SAW active modulation, such as error correction between qubits, achieved by driving the state of the errored qubit to nominal.

While it may be important that SAWs are able to control individual qubits, SAWs must be able to scale control over a larger architecture in order for SAWs to be useful in eventual multi-qubit quantum computing platforms. Indeed, the ability to use SAWs to scale phonon networks between multiple qubits while maintaining coherence over sufficient periods of time has been demonstrated, providing a basis upon which to build quantum computation or communication platforms. It has been demonstrated that the previously mentioned diamond nitrogen vacancy qubit architecture can indeed be scaled to many qubits using SAWs, overcoming the challenges faced in scaling phonic networks [23]. This coupling could be further extended to 2D networks, and this architecture design is generalisable to other material systems than diamond [24]. Another group, in collaboration with Harvard University, have also demonstrated scalable quantum communication protocols within chip-scale qubit networks using propagating phonon wave packets, or SAWs [25]. These results indicate that SAWs are a viable method for large architecture quantum applications, and that the benefits of active modulation can also be realised at scale.

Traditionally, coupling between qubits was achieved through optical means, such as with lasers or on-chip photonics. However, given the above, SAWs provide a more efficient, less noisy and easier way to achieve this goal, which can be easily scaled over on-chip distances, unlike photonic systems. Given this, SAWs provide a universal interface for coupling solid-state quantum systems, and the ability to actively modulate them during transit on-chip opens the door to new quantum

computing paradigms and to potentially mitigating the issues faced by current quantum computing architectures, such as challenges with error correction and maintaining coherence.

Lastly, aside from using SAWs to control qubits, SAWs themselves have been demonstrated be able to take a fully controllable quantum superposition state, opening the door to macroscopic mechanical qubits that do not require esoteric materials or superconducting temperatures [26]. The ability to change the characteristics of these superposition states would mean that quantum computation could be performed directly using active modulation of the SAW.

2.3 Acoustics in Signal Processing

Aside from research applications in the field of quantum computing, SAWs on piezoelectric substrates have been in consumer electronics since the early days of handheld mobile phones [27], in the form of passive signal processing units [5]. Delay lines, frequency fitters, dispersive delay lines, and oscillators are all possible to implement with a SAW device. For example, a simple delay line would consist of an Tx/Rx IDT pair spaced an appropriate distance apart, as the SAW propagation speed is significantly slower than that of an electric signal. Oscillators can be achieved by designing two wavelength-appropriate Bragg reflators that are etched between the Tx/Rx IDT pair.

A key example of the use of SAW devices in consumer electronics is their ubiquity in mobile and cordless phones. The IEEE notes that “SAW filters have become the key components in mobile communication and multimedia applications” due to their versatility – by being able to integrate more than one filter function into one package – and superior impedance performance [27]. Reduced costs are also realised by eliminating many discrete components and reducing printed circuit board (PCB) size [27].

With increasingly crowded longer frequency spectrum space due to the high demand for mobile cellular services, ever faster communication standards have been moving to the unoccupied higher frequency spectrum [28]. This has put pressure on RF radio designers, as the higher frequencies that need to be processed in the small form factor of a mobile phone necessitate increasingly complex architectures, or sacrificing signal quality. Research has demonstrated that SAWs on an LN substrate meet the required performance standards for the LN architecture to be seriously considered for the front-end filtering requirements for 5G applications and beyond

[28]. Active modulation of SAWs would allow further minimisation the number of filters required and allow for higher performance of individual filters, which is increasingly important as the consumer pressure for smaller form factors increases.

2.4 Potential Modulation Mechanisms

In researching some ways in which to modulate a travelling SAW, one needs to first consider which properties of a wave one should modulate. The three parameters that characterise a wave are its frequency, amplitude and phase. If one achieves adequate modulation of two of the above, the third becomes indirectly modulatable – perhaps with some additional filtering of sidebands required [29].

Recent literature and unpublished literature from the Lončar group at Harvard University suggest a method by which amplitude could be modulated. To demonstrate narrow-band amplitude modulation, a third IDT is placed between the Tx/Rx IDT pair, to which an external resistance circuit using a basic op-amp layout is connected [30]. This resistance could be positive or negative, corresponding to attenuation and amplification respectively. The resonant nature of the third IDT, arising from its geometry only allows a certain frequency range around the centre frequency and harmonics thereof to be amplified. A cascade of such devices could be potentially used to amplitude modulate a discretised range of frequencies. However, should a SAW encounter an IDT not geometrically optimised for its wavelength or harmonics thereof, the SAW would be attenuated.

Modulating phase is somewhat easier than modulating frequency, as to do the latter, one would need to change the speed at which the wave propagates through the LN substrate (given by *wave propagation speed = frequency x wavelength*) before and at the point of reception by the IDT. Modulating just phase is conceptually simpler, as I would need to change the speed of propagation between transmission and reception. I propose two designs for this in section 4.5.

Chapter 3

Design Approach, Goals and Technical Specifications

3.1 Project Design Approach

The project design approach can be summarised in the system diagrams shown in Figures Figure 3-1 and Figure 3-2.

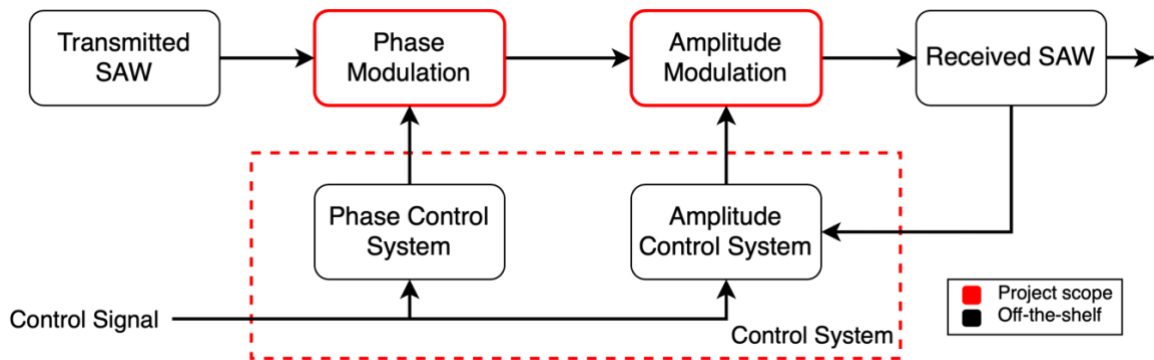


Figure 3-1: Abstracted Block Diagram of the project. The items indicated in red are within the scope of the project, and those in black are will be implemented with known methods.

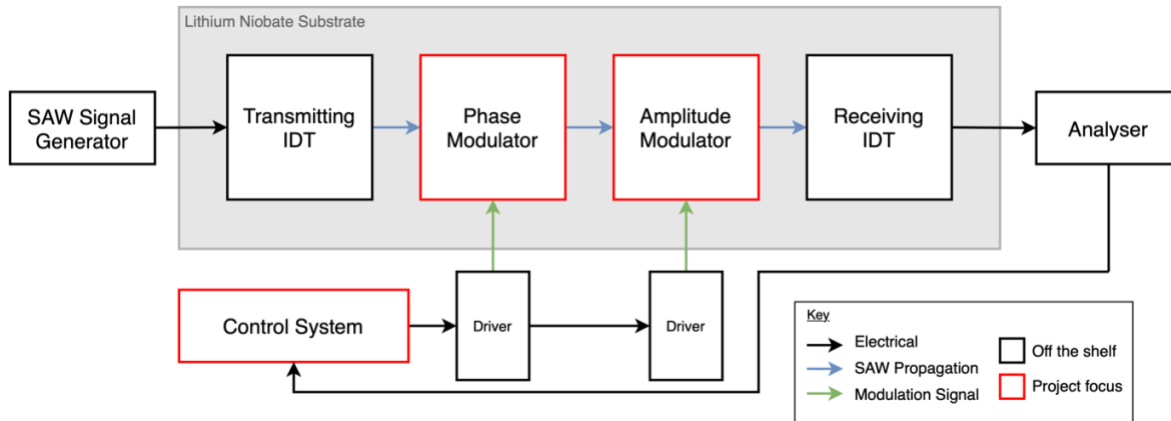


Figure 3-2: System Model Diagram of the project, demonstrating in more detail the layout of individual components within the project. The items indicated in red are within the scope of the project, and those in black are will be implemented with known methods.

The project focuses on the amplitude and phase modulation of a SAW. It uses off-the-shelf components and designs to complete the tasks that are necessary for the realisation of the product but are already well-characterised. This includes the SAW signal generator, which will be a bench-top signal generator for testing purposes, the Tx/Rx IDT pair, where the geometry is understood, and the driving mechanism, which will be off-the-shelf wherever possible. The SAW transmission performance of the final product will be analysed with a Vector Network Analyser (VNA).

Although the above diagrams portray a clear delineation of the project scope, certain aspects of other subsystems were ultimately included within the project scope. The number of fingers on the Tx/Rx IDT pair played a role in determining the characteristics of SAW propagation (Section 0), and the exact implementation of the driver circuitry required some design work (Chapter 6).

3.2 Design Goals and Constraints

Table 3-1: Design Goals and Constraints

| Constraint | Reasoning |
|--|---|
| Show in simulation the possibility of electro-acoustic SAW amplitude modulation. | The crux of this project depends on the ability to modulate SAWs. One degree of freedom of a wave is its amplitude. In order to design a device for fabrication, it needs to be verified that it will function as expected. This will also allow for characterisation the amplitude response of the device in simulation in order to see how accurate the |

| | |
|---|--|
| | fabrication process was, or whether there were any errors in the fabrication process. |
| Show in simulation the possibility of electro-acoustic SAW phase modulation. | Another degree of freedom of a wave is its phase. Previous research suggests that active phase modulation, combined with active frequency modulation and the appropriate filtering of sidebands will allow for frequency modulation while maintaining phase coherence [16]. This is also analytically the case [29]. |
| The design of the device must be able to be fabricated at Harvard CNS. | The ultimate intent of the project is to be able to fabricate a device. Thus, it is vital that the device be designed in such a way that it can be fabricated with the equipment available at Harvard CNS. Failure to do so will not result in a particularly useful final design. |
| Fabrication of the device is an additional desired outcome. | As above, demonstrating that the device can be fabricated is important to the success of the project, as it is intended for use within the lab's other research projects. |
| Physical device must be able to modulate phase and amplitude. | The fabricated device will be tested against these specifications and should meet all of them, if it is to be useful to the research agenda of the Lončar Lab. Additionally, this would also provide indication of whether this device could be modified to be useful to industry. |
| Device design must be usable within a lab space, not requiring unreasonable additional equipment. | As the device will be initially used in a lab environment, it is imperative that it can be usefully functional without the need for additional expensive or esoteric equipment that is not readily available – for example, not requiring an overly specialised power supply or computer interfaces. |
| The device must be designed and fabricated for a Lithium Niobate substrate. | The Lončar Lab has a very focused research agenda with regards to LN. As such, a given constraint by the Lab is that the SAW modulator be designed on an LN substrate. Additional benefits of this are the ability to tap into the existing expertise of the advisor and the Lab with regards to design and fabrication of LN devices. |
| The fabricated device will be mounted onto a printed circuit board (PCB). | The fabricated device will need to be handled by researchers on a bench and need a way to interface with external devices, such as signal generators and analysers. Connecting these external devices directly to the |

| | |
|--|---|
| | microscopic LN device is challenging. Therefore, mounting it on a PCB that interfaces the LN device with external devices is necessary. |
|--|---|

3.3 Unknown Aspects

This project is attempting to build an entirely new device for which no previous examples exist. Indeed, it is unknown to what extent modulation can be achieved and what properties active SAW modulation exhibits. Due to these uncertainties, it is challenging to concretely define the potential properties of the device, and so it is hard to estimate an efficiency, bandwidth, noise floor, or whether it maintains phase coherence. We will only be able to state minimum requirements that the device must meet to be useful and design to meet these requirements.

3.4 Technical Specifications and Justifications

3.4.1 Overall System Specifications

3.4.1.1 Physical Dimensions of Lithium Niobate Device

Quantitative Description

The physical size of all the features on the LN substrate, including the Interdigital Transducers (IDT) to generate and detect the SAWs must not exceed 1 mm x 1 mm or be smaller than 10 μ m x 10 μ m.

Justification

The nanofabricated LN portion of the device is the centrepiece of the project. If it is too small, the equipment the Lončar lab uses to interface with their nanofabricated devices will not be able to interface with the device as the physical connections will be too large for the LN device [31]. Conversely, if it is too large, the device will not be useful in compact signal processing applications. These values were obtained from my advisors as of yet unpublished paper, documenting his previous work [30]. In it, they demonstrate a SAW device where the IDT to generate the SAWs is approximately

200 μm^2 . At least two IDTs are needed to generate and detect the SAW. The amplitude and phase modulators will be the approximate dimension of the IDT for a given bandwidth by convention. Adding in extra buffer space for fabrication ease, it is reasonable to approximate the overall dimensions to be no smaller than $5 \times 200 \mu\text{m} = 1 \text{ mm}$.

Measurement

The CNS HAR-021 Optical Microscope with a CCD Camera will be used to observe and measure the size of the LN nanostructures. This instrument is appropriate as it is non-destructive to the sample and requires no special preparation. HAR-021 also has a 100x magnification lens, meaning that my sample is within the resolution scale of the instrument [32].

3.4.1.2 Physical Dimensions of Overall Device with Associated Connections (PCB)

Quantitative Description

The dimensions of the final product – including the PCB onto which the LN device is mounted – must not exceed 15 cm x 15 cm.

Justification

If the final PCB is too large, it becomes cumbersome to use on a lab benchtop and more expensive to manufacture. The Lab's previous PCBs onto which they have mounted SAW devices have had dimensions less than 15 cm x 15 cm [33]. This is therefore a reasonable upper bound, as the number of connections to external equipment is unlikely to be larger than the number of connections on comparable designs. In the case of my advisor's most recent publication, the number was seven [33].

Measurement

The PCB will be designed Altium or Eagle to design the PCB, which has a dimensioning tool integrated that we will use. This will be verified with callipers once the PCB is assembled.

3.4.1.3 Manufacturability of Device

Quantitative Description

The device must be able to be fabricated with the equipment available at Harvard CNS. Thus, the design of the modulator cannot have features that are less than 1 μm .

Justification

The device will be fabricated using a photolithography process, amongst other processes if required, such as ion beam etching. However, the photolithography process is the limiting factor in terms of resolution, given the equipment available at CNS. The CNS OL-10 (MLA150 Maskless Aligner) will be used, due to its high feature resolution and the lab's familiarity with the machine. The manufacturer has specified that OL-10 has a recommended maximum feature resolution of 1 μm [31], factoring in a margin for error.

Measurement

As above, CNS HAR-021 Optical Microscope with a CCD Camera will be used to observe and measure the size of the LN nanostructures. This instrument is appropriate as it is non-destructive to the sample and requires no special preparation [32]. Further, I will digitally design the device as to not have features less than 1 μm .

3.4.1.4 Insertion Loss Through Device

Quantitative Description

The fabricated LN device must have an intrinsic insertion loss with no amplitude modulation no greater than -20 dB.

Justification

Insertion loss is an important value for the overall system, as it indicates to what extent the losses are intrinsic and which are intentional with the modulator. 20 dB loss is a reasonable number, given that existing passive SAW filters see insertion losses of ~ 10 dB [34]. Given that my device will likely have more stages than a passive SAW filter, 20 dB loss is a reasonable upper bound without adversely impacting function.

Measurement

The output signal relative to the input signal at the SAW generation and detection IDTs respectively will be measured with a spectrum analyser. This test will be conducted with no amplitude modulation to measure the intrinsic losses.

3.4.1.5 Noise Factor

Quantitative Description

The noise factor of the device – from SAW generation to SAW reception – must not exceed 20 dB.

Justification

The noise factor is a useful number in determining how much additional noise is added by the system relative to the noise on the existing signal. Existing SAW passive filters used in radiofrequency applications have a noise factor of ~ 18 dB [35]. Thus, 20 dB noise factor is reasonable, as this will ensure that the device remains useful in application. Higher values may still make the device useful, but this is a safe educated approximation.

Measurement

The output signal relative to the input signal at the SAW generation and detection IDTs respectively will be measured with a spectrum analyser. With this, the input signal SNR and output signal SNR can be obtained, thus giving the noise factor.

3.4.2 Phase Modulator Specifications

3.4.2.1 Phase Modulation

Quantitative Description

The phase modulation must be able to shift the frequency of a SAW centred at 200 MHz by 10 MHz (200 ± 10 MHz).

Justification

The use of a phase modulator allows us to shift the frequency of the incoming SAW on chip. Previous work done in the lab chose a centre frequency for their SAWs of 200 MHz [30]; however it is worth noting that with current passive devices this can be

changed arbitrarily by geometrically scaling the design – to allowable limits given fabrication limitations.

The bandwidth of ± 10 MHz is chosen as the maximum bandwidth of next-generation mobile phone frequency allocations in the United States is 20 MHz [36]. As this device is potentially intended for use in future signal processing applications, it is reasonable to look at current bandwidth allocations for the type of signal that the device may process in the future.

Measurement

A vector network analyser (VNA) will allow for coherent measurement of the output signal relative to the input signal. Using a VNA, the maximum frequency bandwidth for a given control signal can be obtained.

3.4.3 Amplitude Modulator Specifications

3.4.3.1 Dynamic Range

Quantitative Description

The dynamic range of the amplitude modulator is at least within the range of 0 dB to -10 dB from baseline.

Justification

In order for the device to be functional, we must be able to at will ‘turn off’ the signal at will. Previous work by the Lončar Lab has demonstrated 10 dB attenuation from the baseline value to be a useful value for their research purposes [30].

Additionally, while it is desirable to be able to amplify the signal to compensate for losses, this can also be done at the SAW generation stage and thus is not a vitally important metric to constrain the design against.

Measurement

A VNA will be used to measure the dynamic range of the output signal relative to the input signal for a given frequency. A comparison of the amplitudes of the input and output signal allows for attenuation to be calculated.

3.4.4 Control System Specifications

3.4.4.1 Benchtop Operation

Quantitative Description

The external units that connect to the modulator must have power supplied from a standard 120 V AC RMS at 60 Hz.

The external units must all interface with the control system hardware – likely a computer – with either USB or Ethernet.

Justification

This device is ultimately intended for use in a lab and in a benchtop environment. The Lončar Lab environment has standard US mains outlets available, making the operation of a system that uses these connections easier, as opposed to three-phase supply or some other esoteric power supply.

Additionally, requiring the use of USB or Ethernet interfacing improves reliability due to the standardisation of the protocols, makes interfacing the devices easier from a setup perspective, and allows almost every computer to interface with them.

Measurement

This is a simple binary measurement by observation. At the end of the project, we will ensure that this specification is met.

3.4.4.2 User Safety and Noise Reduction

Quantitative Description

Connections to and from the control system to the PCB are to be made with coaxial cable or some other kind of shielded connection.

Justification

Using standard and well-understood connections like coaxial connections will reduce operator error and the chance of a short circuit from occurring. An additional benefit is that the shielding will reduce radio-frequency interference (RFI) noise on the control signal lines, reducing the noise on the LN substrate structures.

Measurement

This is a simple binary measurement by observation. A multimeter will be used to ensure that the voltage of the shielding remains at 0 V.

3.5 Technical Specifications Summary

Table 3-2: Summary of Project Specifications. The numbers on the left match the last two digits of the heading of the specification.

| | Description | Specification | Sub-System |
|------|--|---|----------------------------------|
| 1.1 | Physical size of all the features on the LN substrate | Between 1 mm x 1 mm and 10 μm x 10 μm | Overall System Size |
| 1.2 | Max. final product dimensions | 15 cm x 15 cm | |
| 1.3 | Fabricated with the equipment available at Harvard CNS | No features less than 1 μm | Manufacturability and usefulness |
| 1.4 | Max. allowable intrinsic insertion loss with no amplitude modulation | -20 dB | |
| 1.5 | Max. allowable noise factor | 20 dB | |
| 2.1 | Frequency shift about centre frequency | (200 \pm 10) MHz | Phase Modulator |
| 3.1 | Dynamic range of the amplitude modulator | 0 dB to -10 dB | Amplitude Modulator |
| 4.1a | Power | 120 V AC RMS at 60 Hz | Control System |
| 4.1b | Computer interfaces | USB or Ethernet | |
| 4.2 | Connections to and from the control system to the PCB | Coaxial | |

Chapter 4

Modelling

In order to make most use of the materials and fabrication time available at Harvard CNS, designing the geometric structure of the devices without needing to manufacture them to test whether they work under the operating parameters is an important step. This also allows for more rapid design iterations as opposed to needing to manufacture a new device every time. Design and modelling of the proposed device is therefore required as part of this project.

4.1 Approach

When deciding on a modelling technique, three main considerations were factored:

- Could the modelling be conducted within a reasonable timeframe (1-2 weeks)?
- Would the Lončar lab and the advisor be able to provide valuable advice for the process and subsequently use the results generated in other projects?
- Does the chosen technique model the device in a manner that reflects physical reality?

Two general modelling methods were considered: analytical and numerical. Analytical modelling would provide a good theoretical and rigorous foundation for the project; however, given the complexity of the system being designed, as well as the required mathematical sophistication and academic training required, it was concluded that analytical analysis would take too long, and would ultimately not be particularly useful in the more complex cases as the dimensionality of the problem increased. Further, the Lončar lab also refrains from detailed analytical analysis for these same reasons.

Numerical modelling does not provide a deep theoretical understanding of the physics; however, this technique has proven useful to the Lončar lab in the past by producing useful results that reflect reality, even in the case of their more complex microfabricated devices. Learning a new software tool to model a comparatively simple case would not prove too arduous, and if the project was completed with the software tool that was used by the lab, the work produced would be immediately useful to the advisor and his colleagues. Further, as the model grows in complexity, numerical modelling can still provide useful results.

Based on the above considerations and given the software resources available at Harvard SEAS, it was decided that the finite element analysis software tool COMSOL Multiphysics would be used. COMSOL is also available on the Harvard FASRC Cannon Computing Cluster, which allows for faster computation time as compared to running the model on a single desktop computer, and also allows for remote model setup. The geometry of the device is also be constructed in COMSOL, as this allows for better iteration time, as opposed to needing to re-export a model from an additional CAD program. Finally, the data produced by the COMSOL SAW device models that the Lončar lab has used in the past have been verified by measurement of fabricated devices, which is a positive indication that this modelling technique would indeed reflect the physical reality of the device.

To better isolate the individual physical effects, the gain modulation and phase modulation designs are modelled separately. This allows for a better understanding of parameter sensitivity with respect to the SAW transmission characteristics, thus allowing for a more comprehensive understanding of the behaviour each modulation subsystem to be obtained before attempting to combine them into the final design.

4.2 Model Setup

4.2.1 Parameterisation

Before constructing the geometry, the model was parameterised. This means that all geometric dimensions of the model are defined by changeable parameters that are defined early in the model tree. Thus if a property of the model that would impact its dimensions were to be changed later – for example, the centre frequency of the SAW – only one number would need to be changed and the model geometry would automatically update to reflect the change. The following geometric parameters are user-defined, with the remaining geometry being calculated from them.

- Centre wavelength of SAW
- Number of IDT finger-pairs of the Tx/Rx pair
- Geometric parameters of modulation structures (e.g. number of IDT finger-pairs of other IDTs)
- Width, depth and height of LN substrate
- Distance between Tx/Rx IDTs and edge of the LN substrate
- Distance between Tx/Rx IDTs and modulation structures
- Height of IDT deposited material

Other non-geometric values are parameterised such that the model solver would be able to change them automatically in order to conduct analyses of SAW transmission characteristics.

- Signal characteristics of the test SAWs, generated from an AC source (peak-to-peak voltage and frequency)
- Gain modulation parameters (e.g. impedance between IDT terminals)
- Gain modulation parameters (e.g. DC voltage applied to deposited structures)

4.2.2 Geometry

In designing the geometry, the device was modelled in 2D space rather than 3D space, discarding the depth dimension, defined here as the axis along which the IDT fingers lie. This preserves the dimension along which the SAW propagates, and the dimension of the height of the device. This greatly simplifies the geometry design and construction. Additionally, a 3D model uses significantly more computational resources and does not greatly improve the model outcome. The Loncar lab has demonstrated that the 2D case provides accurate results [12]. Given the limited computing resources on hand, this simplification to 2D was an acceptable trade-off. However, it is still worth noting that despite this, the modelling physics still requires and uses a depth value in the physics engine, so it still must be defined, even if it is not immediately visible in the displayed geometry. A value of 1000 μm was chosen, as this value has worked well for previous devices fabricated by the lab due to the edge effects contributing less to the overall device characteristics [33], while still remaining within the project's specified upper feature dimension of 1mm.

Common across all models is the Tx/Rx IDT pair geometry, which is defined by the specified centre wavelength of the SAW – refer to Figure 2-2 for the precise geometry. From the project specifications, the centre frequency must be 200 MHz

(Section 3.4.2.1). Using the LN materials datasheet from the vendor Roditi, the SAW propagation speed on the LN with a 127° cut – the specified crystallographic orientation that the lab devices use – was 3980 m/s [37]. We can use the relation between frequency f , wavelength λ and speed v to calculate the desired wavelength:

$$\lambda = \frac{v}{f} \quad [1]$$

As will be discussed later, both $\lambda = 20\mu\text{m}$ and $\lambda = 19\mu\text{m}$ were modelled due to the SAW propagation speed in the datasheet being incorrect, with the actual value for the given material properties being closer to 3800 m/s by inspection. The LN substrate geometry is partly defined by the geometry of the metal structures (such as the IDTs) in the two surface dimensions, and by the LN vendor in the height dimension. The height of the LN substrate is 100 μm .

4.2.3 Material

There are two materials in this model – aluminium and Lithium Niobate. Both of these materials are available in the standard COMSOL material library.

In setting up the LN material properties, three properties of the material need to be changed from their default values to define the cut angle of the material: the elasticity matrix, coupling matrix and relative permittivity. All three need to be rotated from their default values to reflect the 127° Y-cut orientation of the LN crystallographic coordinate system. This specific orientation means that the SAW will propagate along the X-Axis of the crystal coordinate frame [37], which is set to be the x-axis of the model frame (left to right in the diagrams presented here). The transformations chapter of Newnham’s textbook elaborates on how this is achieved [38]. I confirmed the calculated values with my advisor’s model for another project.

Additionally, the substrate is created and divided into six separate regions, as illustrated in Figure 4-1. All regions except region 3 are defined as ‘perfectly matched’, meaning that the acoustic impedance of the region and at the region boundaries is set such that there will be minimal acoustic wave reflections at the region boundaries. Only region 3 is not defined as perfectly matched, as this is where the IDT’s and modulation structures will be deposited, where impedance factors could impact device performance. This practice of defining perfectly matched regions significantly reduces computational load and allows one to see the important effects rather than the higher order effects caused by small reflections. While information about the

higher-order wave propagation effects, such as wave reflection, is lost in this choice, it does not significantly impact model accuracy.

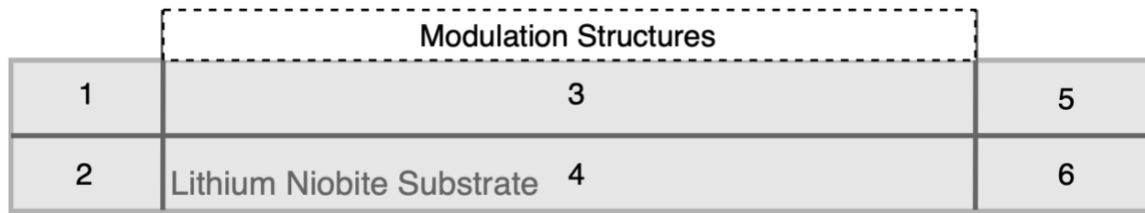


Figure 4-1: Geometry of LN substrate divided into 6 regions. The substrate is still one single piece. The white box is a placeholder for the SAW modulation structures discussed in later sections.

Aluminium was chosen as the material for the metal deposited structures, like the IDTs. Aluminium was chosen over copper or gold for several reasons. First, the Lončar lab has experience with fabrication of Aluminium IDTs. Secondly, aluminium has a much lower density than copper or gold while still being easy to fabricate with, and therefore will not attenuate a SAW as much as alternative material choices [15]. The ‘stress-change’ property group was removed from the aluminium material properties, as these are piezoelectric properties; the model does not include the aluminium in its piezoelectric simulations, as the contribution by aluminium to this is very small as compared to LN, and would only increase computational overhead.

4.2.4 Physics Models

Two physics models must be defined in order for the COMSOL ‘Piezoelectric Multiphysics’ solver to work: solid mechanics and electrostatics.

For the solid mechanics physics model, the coordinate frame of the conservation law ‘linear elastic material’ is set to the global coordinate system, as we are only concerned with the behaviour of the device with respect to the world, rather than with itself. The boundary condition of the base of the device is set to ‘fixed’ with respect to the global coordinate system to provide an absolute reference frame for the model. All remaining boundary conditions are set to ‘free’, meaning the boundaries are unconstrained in their movement, and move with respect to the fixed boundary, as is the case in the real world. All initial values are set to zero, as the model assumes that no external mechanical forces are applied.

For the electrostatics physics model, we use the charge conservation law in order to be able to model the external electric components required for the device to function. All boundaries are set to 0 Coulombs, as any non-zero charge would imply a

charge discontinuity on the LN-air boundary. All domains – the COMSOL term for material regions – have an initial potential value of 0 V, as there is no potential applied to the material initially, nor is there an intrinsic potential in the material. A piezoelectric charge conservation law is additionally applied to all LN domains with the same boundary conditions and initial values as for the charge conservation law.

Finally, signal terminals are added to the model to allow for interfacing electronic components with the LN substrate and IDTs. A ground (0 V) signal terminal is added to alternating IDT fingers, as shown in Figure 2-2, and to the base of the model. A signal terminal is then added to each of the other set of alternating IDT fingers, so that the fingers of the IDT can connect to the external driving circuitry that generate and receive the SAWs.

4.2.5 Common External Circuitry

The external circuitry required for each of the models varies, depending on the type of modulation being simulated. However, the Tx/Rx IDT pair circuitry is common across all models. An external AC supply is required to create a SAW, and one must ensure that the impedances of both IDTs are matched to minimise losses.

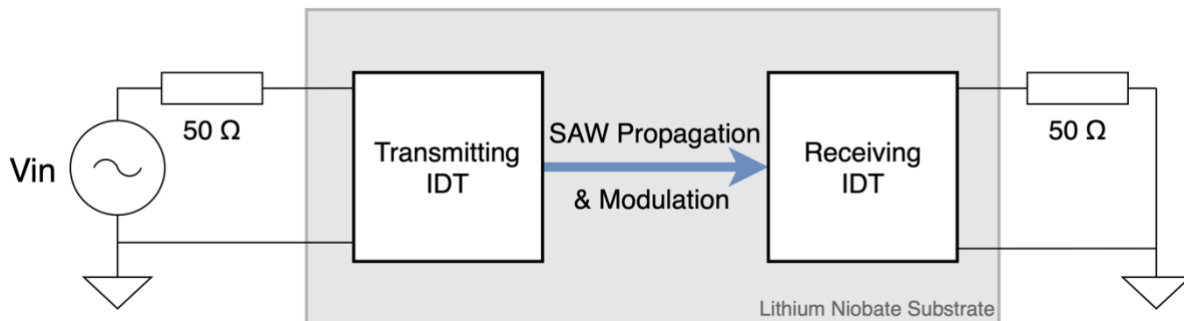


Figure 4-2: External circuitry for the Tx/Rx IDT pair with 50 Ω impedance matching.

V_{in} is the parameter that the solver will oscillate at 200 MHz. This parameter is a sine wave signal with a chosen amplitude of 10 V, as this would provide a good range over which to measure the results, and is reasonable given the power supply limitations outlined in the specifications. Any lower and the attenuation of the system would likely be too high to see a signal, and any higher may require a larger power supply than available in the lab. The external circuit for the receiving IDT is required in order to match the impedance of the transmitting IDT to minimise losses. 50 Ω is chosen as this is an impedance matching standard in signal processing [39].

4.2.6 Model Mesh

The model mesh defines the coordinates at which the modelling equations are numerically evaluated using the FEA method. In choosing the mesh characteristics, the size and geometry need to be balanced with computational resource availability and precision of the results required. COMSOL has a good default 'physics defined mesh' with qualitative descriptors like 'fine, finer, most fine', of which 'fine' was initially chosen to observe whether this would produce valid results without taking too much computation time.

Following initial runs of the identity model, as further discussed in section 4.3, the fineness of the mesh was increased; however, even at the 'most fine' setting, the largest distance between two mesh nodes was greater than the wavelength of the SAW, resulting in inaccurate calculations in subsequent nodes, as shown in Figure 4-3a. For the ultimate mesh configuration used for the project, a user defined triangular mesh is used, where the maximum spacing was limited to a fraction of the SAW wavelength parameter, $\lambda/4$. A triangular mesh was chosen, as that is what the default COMSOL physics defined mesh produced for both electrostatic and solid-state physics models. The results from this seemed to be the most realistic, as in Figure 4-3b.

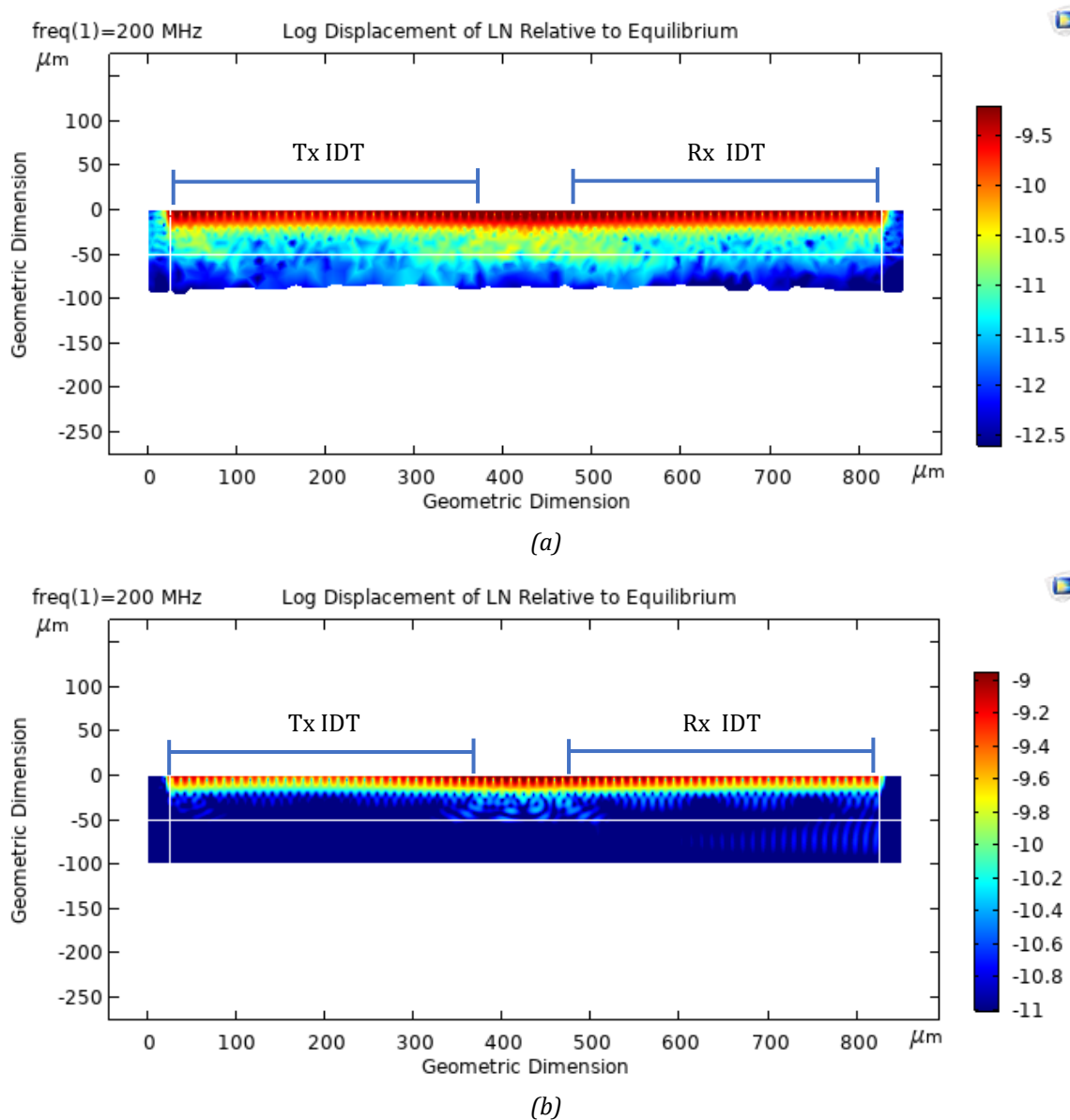


Figure 4-3: Identity model with a 200 MHz SAW. The Tx IDT is on the left and the Rx IDT is on the right as marked, with 50 μm spacing in the middle. White lines indicate the divides between regions 1-6. (a) 'Fine' mesh setting, with bulk transmission of the SAW and unrealistic displacement of the base observed. (b) Custom triangular mesh setting, where the maximum allowed spacing is, $\lambda/4$.

4.2.7 Model Output

Three types of studies were conducted for this project:

- 1) Frequency domain sweep (all models)
- 2) Gain parametric sweep (only gain models, discussed in section 4.4)
- 3) Phase parametric sweep (only phase models, discussed in section 4.5)

For the frequency domain sweep, a frequency analysis study was used. The frequency range was centred at the 200 MHz centre frequency. The frequency range and interval were adjusted as appropriate to the intention of the study – be that an initial coarse sweep to identify frequencies of interest or a narrow bandwidth fine sweep. In addition to the numerical data of the amplitude and phase of the output signal – obtained through the ‘global evaluation’ functionality, the logarithm of the displacement of the material from equilibrium was also produced, as this provided nice visuals with which to get an intuitive understanding of the results. These visuals are produced in 2D as the model itself is designed in 2D.

For the modulator parameter sweep studies, a ‘Parametric Sweep’ study is used for one given frequency. This method is chosen as it was established that conducting a 2D sweep over every combination of modulation parameters and frequency would take too long to compute – on the timescale of weeks. The parametric sweep study sweeps across a given range of the modulation parameter at a defined interval, while the frequency domain study is set to the centre frequency. The specific nature of the modulation parameters depends on the modulation technique, which is further discussed in sections 4.4 and 4.5 for gain and phase modulation respectively. The output is numerically evaluated in the Global Evaluation tool, and then plotted in MATLAB. In the case of the frequency domain sweep, a fixed value for the controlling parameter is chosen that minimises modulation, in order to accurately measure whether the frequency characteristics of the device meet the intrinsic loss specification.

In all these cases, the model is computed on the FASRC Cannon cluster visual desktop interface’s COMSOL installation, as they can take up to twenty hours to compute and evaluate.

4.3 Identity Model Geometry and Results

The identity case model was used to validate that the modelling technique produced expected results, and to verify that under ideal conditions, the specifications were met. The identity case is a simple Tx/Rx IDT pair with no other modulation structures on the chip. Therefore, in modelling the identity case, the only parameter that needed to be chosen was the number of finger-pairs in the Tx/Rx IDT pair. 20 finger-pairs was chosen, as the Loncar lab had previously identified this to be an effective balance between amplitude maximisation by having a larger area to generate the SAW, and attenuation due to losses by self-induced potentials from other SAWs generated in the

same IDT. Additionally this decision is not in the defined scope of this project, and so the ‘off-the-shelf’ approach is warranted. Finally, this value places the device well into the manufacturability and size specifications of no features smaller than $1\ \mu\text{m}$. The model geometry is shown in Figure 4-4.

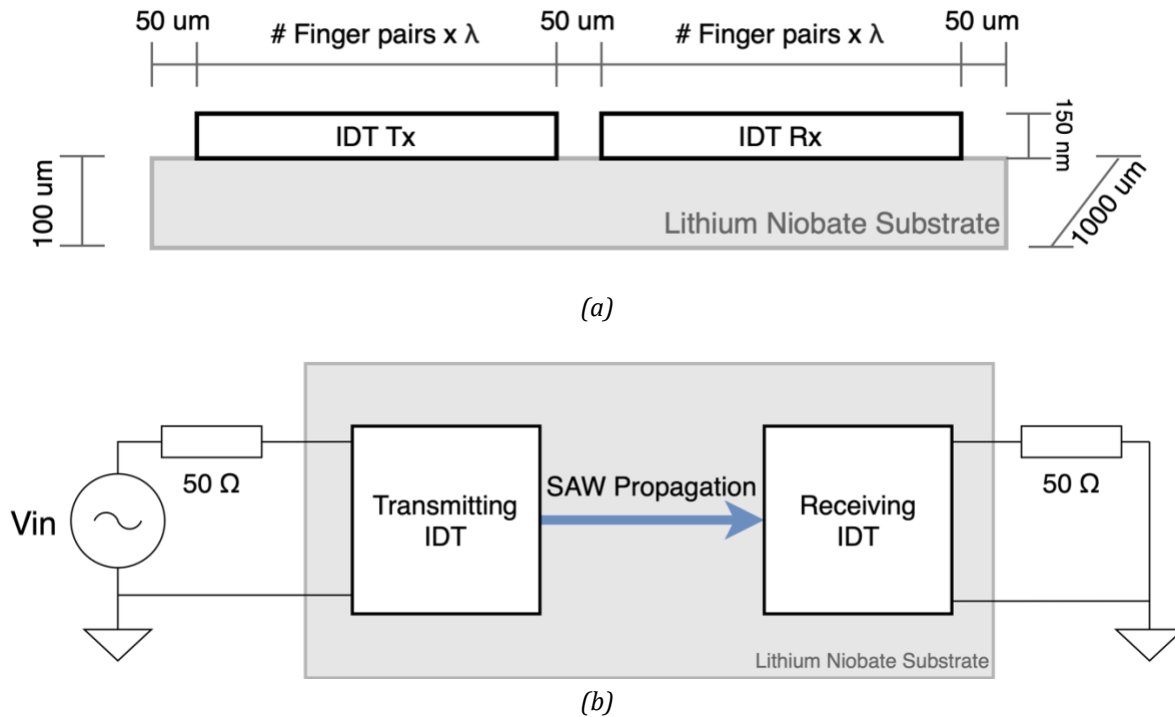


Figure 4-4: Geometry of the identity model, depicted not to scale in order to better visualise the geometry. Boxes labelled "IDT" represent the geometric extent of the fingers for a given IDT. (a) Side cross-sectional view. λ is the SAW wavelength. (b) Top-down view showing additional circuitry.

Initial modelling geometry used a calculated wavelength value of $20\ \mu\text{m}$. Only a frequency sweep study was performed on this model in order to validate the modelling technique and specification compliance. A coarse frequency sweep from 175 – 230 MHz at 5 MHz intervals was initially conducted. The visual representation of the propagating SAW wave, depicted in Figure 4-3, indicates that the model exhibited minimal bulk transmission of mechanical stress, and therefore minimal bulk SAW transmission, as desired. The attenuation results are shown in Figure 4-5.

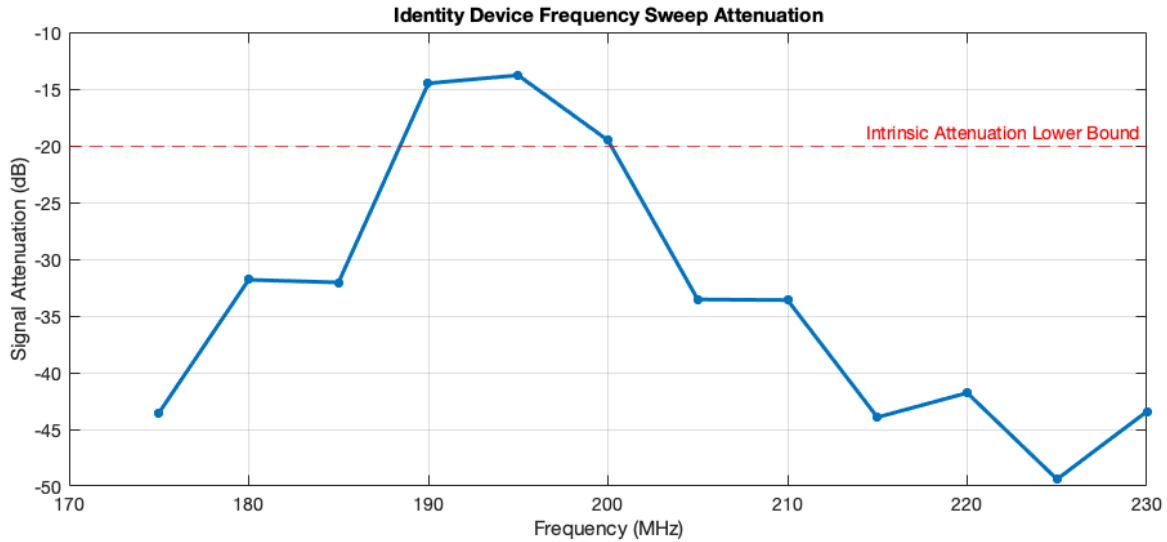


Figure 4-5: Identity model coarse frequency sweep results for $\lambda = 20\mu\text{m}$ geometry. The red dotted line indicates the specified lower bound for intrinsic attenuation.

The signal gain is above the lower bound for specified intrinsic attenuation for a bandwidth of about ± 6 MHz centred about 194 MHz. This is the expected shape of the curve from the identity case, with the gain maximum occurring close to the centre frequency, dropping off as the signal frequency deviates from the centre frequency. Thus, the overall modelling technique is verified.

However, the centre frequency is slightly off from the specified centre frequency of 200 MHz. As mentioned in section 4.2.2, this was due to the SAW transmission speed in the material datasheet, with which the SAW wavelength is calculated, not being accurate. Using instead another one of the lab's recent models to calculate a SAW propagation speed of 3800 m/s, the wavelength was updated to 19 μm . When a fine frequency sweep was conducted with this new geometry, the results in Figure 4-6 were obtained.

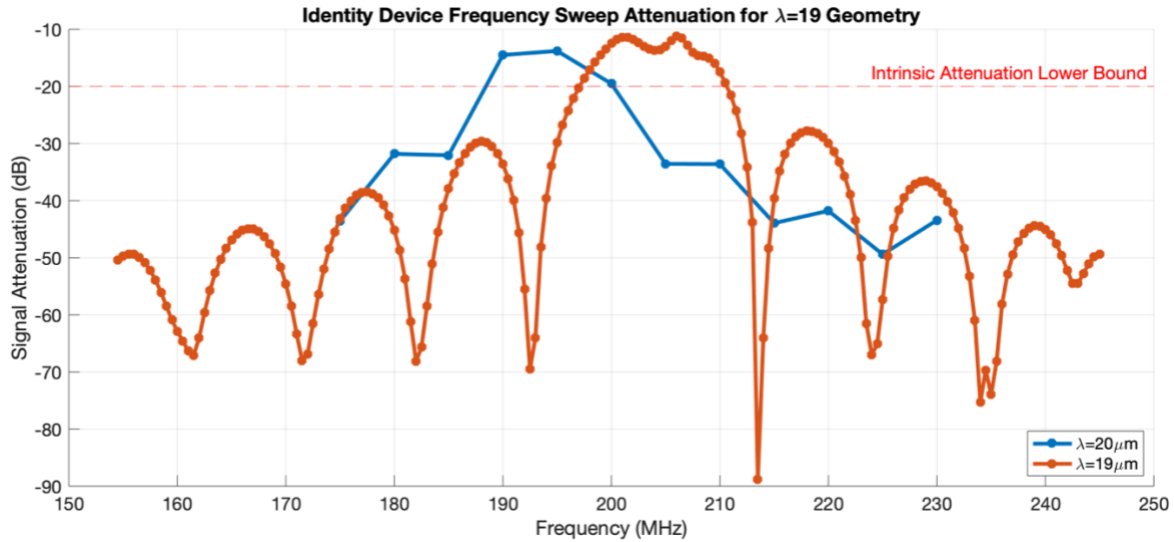


Figure 4-6: Identity model frequency sweep results for both wavelength geometries, as indicated by the legend. The red dotted line indicates the specified lower bound for intrinsic attenuation. The $\lambda = 20 \mu\text{m}$ data is lower resolution, as the peak can be identified from this data without the need for higher resolution studies. Further studies were only done on the new geometry.

It is clear from the data that the updated geometry resulted in better performance, with a bandwidth of ± 8 MHz centred about 200 MHz. The symmetrical attenuation curve shape is also expected, as the regularly spaced minima arise from destructive interference of SAWs from adjacent IDT fingers. While the bandwidth is not quite within the specification, the data provides confidence that this technique is viable.

4.4 Gain Modulator Geometry and Results

For the gain modulator architecture, another IDT is placed between the Tx/Rx IDT pair, and an impedance is placed across its terminals. This architecture has some promising results in recent literature, and does not require any additional complexities in the fabrication process, as it is simply another deposited IDT [11], [30]. As a SAW propagates through the material, the piezoelectric effect creates local potential differences within the LN substrate. When the SAW impinges on the gain IDT fingers, these potential differences give rise to a potential difference across the IDT terminals. If an impedance is placed across these terminals, the potential difference will result in a current through the impedance, thereby dissipating energy. This energy dissipation can be modulated by varying the impedance parameter, labelled as R_{gain} in the following discussion. The simulations only considered the resistive component of impedance to limit the analysis to one-dimension, and as adding

reactance would have necessitated more simulation time. The geometry is shown in Figure 4-7.

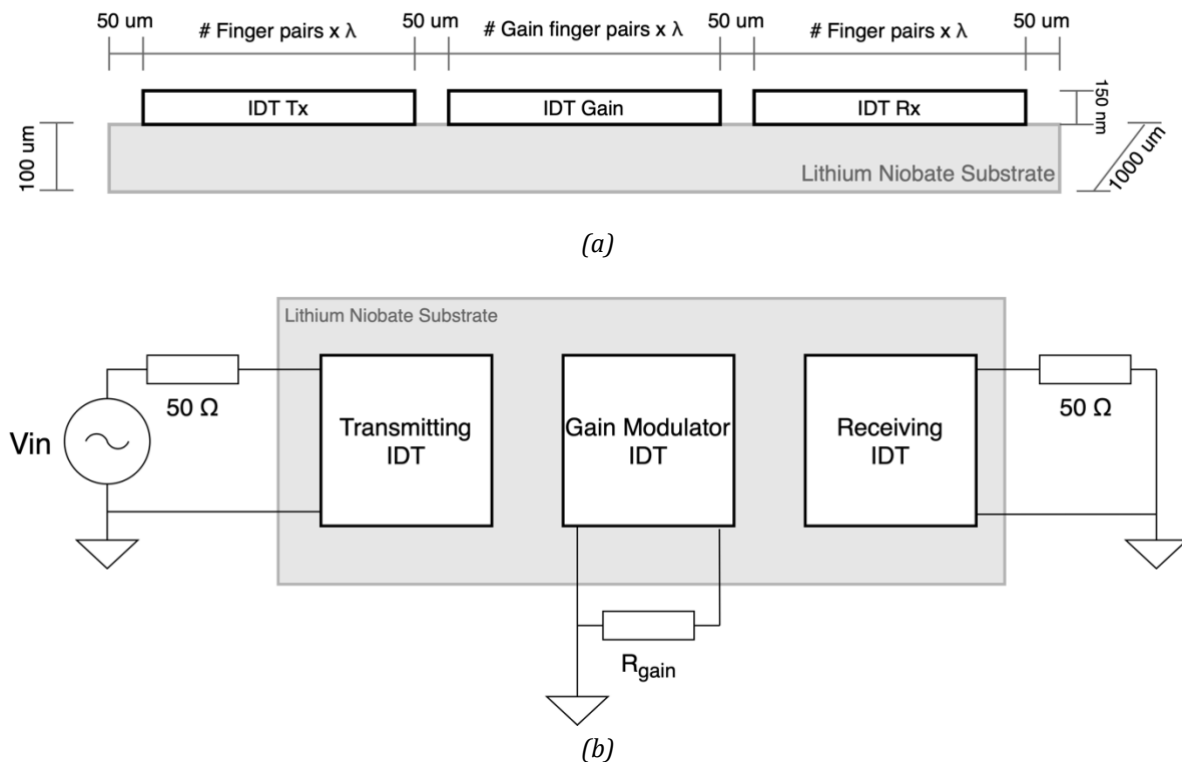


Figure 4-7: Geometry of the gain modulation model, depicted not to scale in order to better visualise the geometry. Boxes labelled "IDT" represent the geometric extent of the fingers for a given IDT. λ is the SAW wavelength. (a) Side cross-sectional view. (b) Top-down view showing additional circuitry.

An additional parameter that needed to be chosen was the number of gain IDT finger-pairs. A balance between having too few, where not enough attenuation would be achieved, and too many, which would have a higher intrinsic attenuation, was needed. 10, 20 and 30 finger-pairs were modelled separately, and the dynamic range and intrinsic attenuation observed to choose a value.

Initially, the geometry designed for a centre SAW wavelength of $20 \mu\text{m}$ (subsequently referred to as the $20 \mu\text{m}$ geometry) was modelled, as the wave propagation speed inconsistency had not yet been identified. A coarse frequency sweep was conducted in order to get an idea of how the devices behaved. A R_{gain} value of $10 \text{ M}\Omega$ was chosen for this in order to minimise the level of attenuation by ensuring that an effectively open circuit across the gain IDT terminals. The results are shown in Figure 4-8.

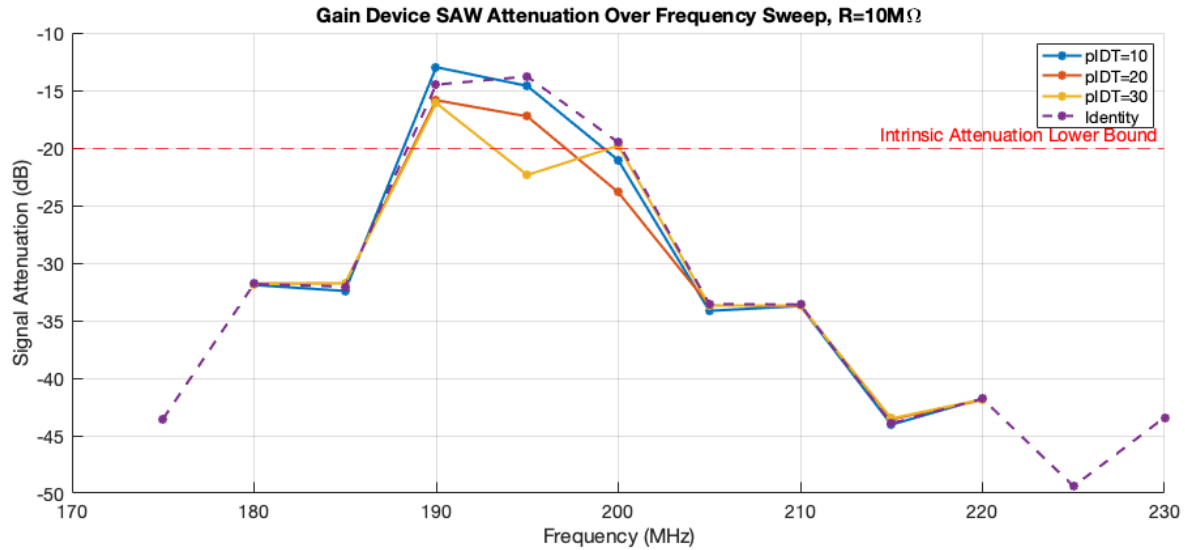


Figure 4-8: Gain modulator coarse frequency sweep results for $\lambda = 20\mu\text{m}$ geometry, showing attenuation levels for 10, 20 and 30 IDT finger-pairs. The identity case is included as a comparison. The red dotted line indicates the specified lower bound for intrinsic attenuation.

The three variants all gave similar attenuation curves, with 10 and 20 finger-pairs only exhibiting slight attenuation. The 30 finger-pair variant exhibits some odd behaviour around 195 MHz with a dip in the gain level, potentially due to reflection or resonant absorption.

Next, the resistance parameter sweep simulation is conducted for the three variants, with attenuation and phase shift measured. The resistance parameter values swept from 0 – 1 M Ω , using different interval steps for different ranges. For example, 1 Ω intervals were used around 50 Ω , given as this is where the most attenuation occurred due to impedance matching, while exponentially increasing intervals were used at higher resistance levels, as the signal properties no longer changed much. The gain and phase shift results are shown in Figure 4-9.

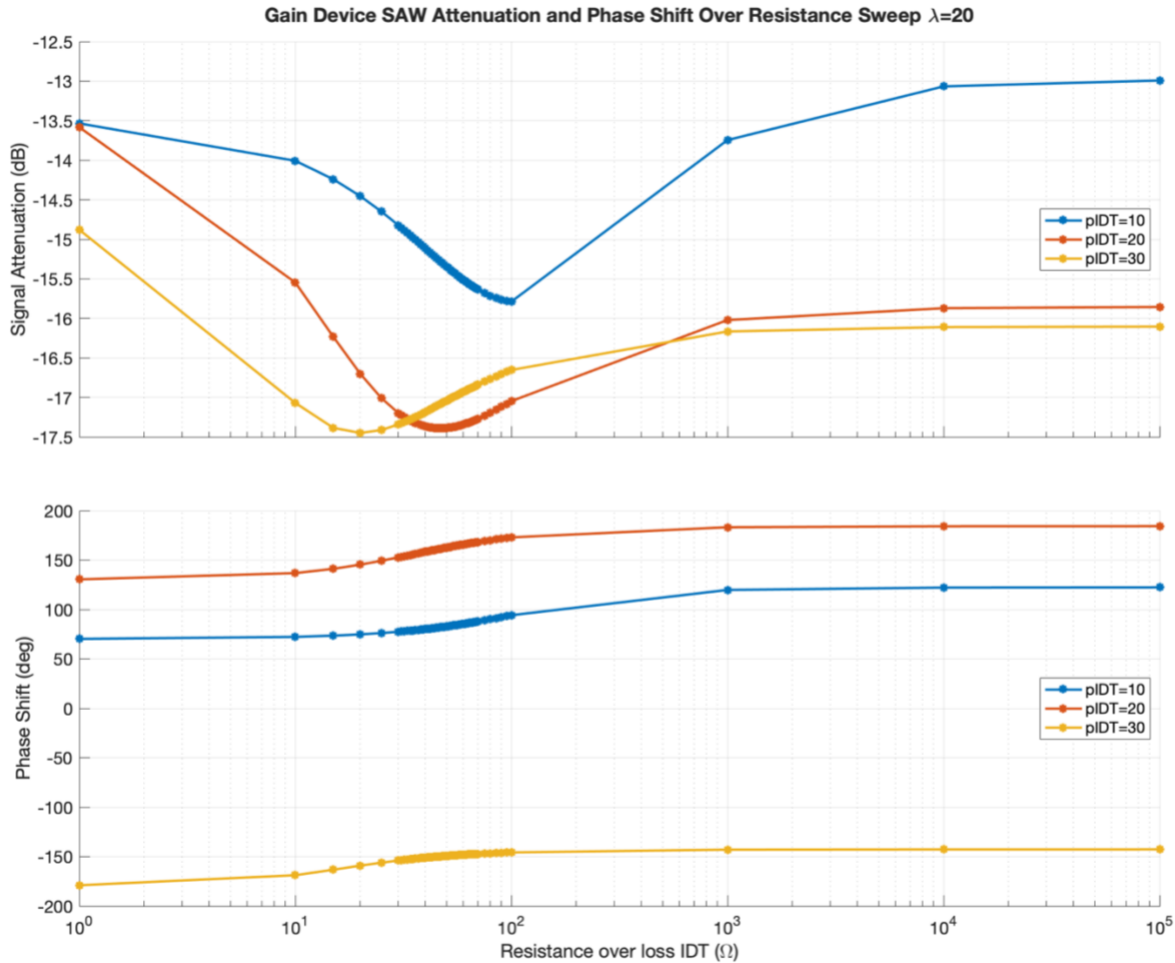


Figure 4-9: Gain modulator resistance parameter sweep results for $\lambda = 20\mu\text{m}$ geometry, showing attenuation and phase shift for 10, 20 and 30 IDT finger-pairs.

Likewise with the frequency sweep, the resistance parameter sweep gave similar profiles for all three variants of the device. The 10 finger-pair device has a dynamic range of 2.5 dB, the 20 finger-pair device has the largest dynamic range of 3.5 dB at the left of $50\ \Omega$, and the 30 finger-pair device has the smallest dynamic range. It is worth noting that ranges to the right of $50\ \Omega$ are more desirable, as they are easier to control, due to larger gaps between resistance values for a given gain change. However, given that the 20 finger-pair device exhibits the largest dynamic range, and good frequency sweep characteristics, this variant was chosen to move forward with.

When the geometry was updated to accompany the $19\ \mu\text{m}$ SAW wavelength, performance increased for the device in both the frequency sweep, as shown in Figure 4-10, and the resistance parameter sweep, shown in Figure 4-11. This data is presented with a comparison to the $20\ \mu\text{m}$ geometry.

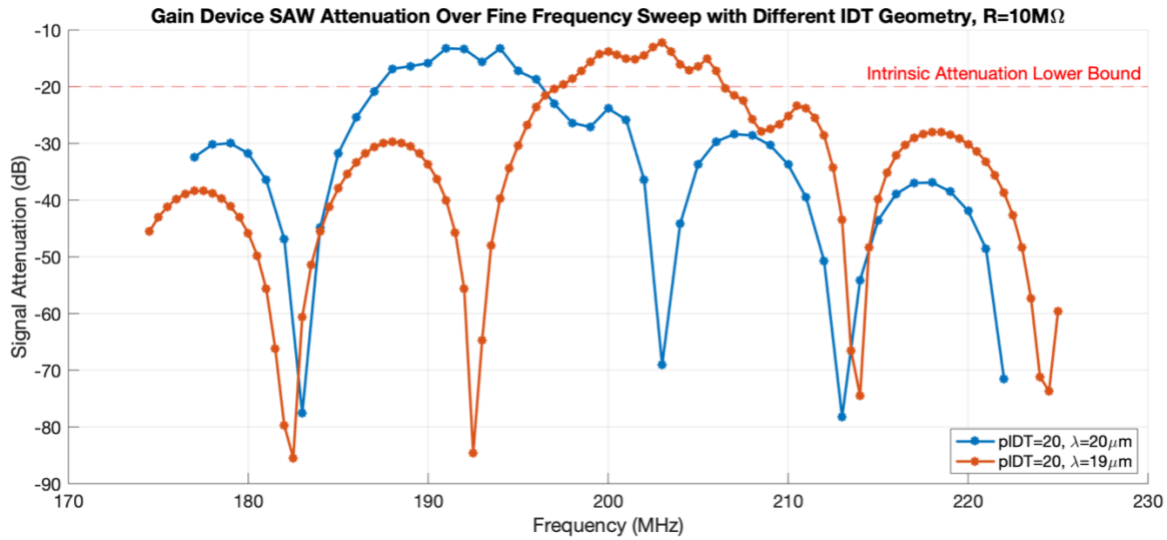


Figure 4-10: Gain model frequency sweep results for both wavelength geometries, as indicated by the legend.

In the frequency sweep results, the $19\mu\text{m}$ geometry is centred around the specified centre frequency of 200 MHz, while the bandwidth has not changed significantly, as shown by the distance between the points of intersection of the attenuation curve and the intrinsic lower attenuation bound line. The new geometry therefore better meets the specification in this case.

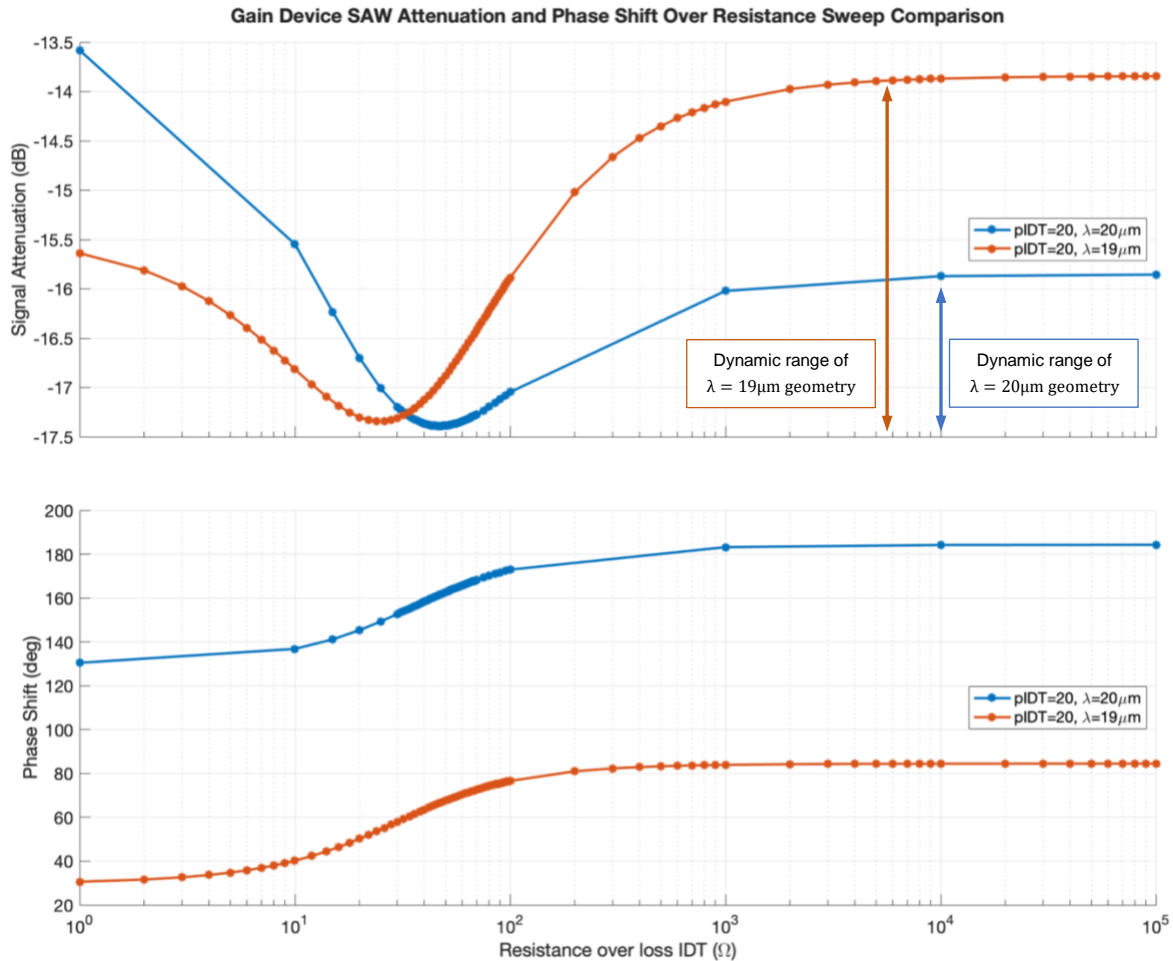


Figure 4-11: Gain modulator resistance parameter sweep results for $\lambda = 20\mu\text{m}$ and for $\lambda = 19\mu\text{m}$ geometry, showing attenuation and phase shift for the 20 IDT finger-pair variant. The orange and blue arrows visually indicate the dynamic range.

In the resistance parameter sweep, the $19\mu\text{m}$ geometry performed significantly better, with a dynamic range of 3.5 dB to the right of $50\ \Omega$, meaning that it has the same dynamic range as the $20\mu\text{m}$ geometry model, but is more easily controllable, as there are larger resistance intervals for a given gain change, meaning that the controllable resolution of a variable resistor does not need to be as high.

It is also worth noting that both geometries have very similar phase curves, where the maximum phase shift is 50° . The absolute offset is less important, as this changes with the location along the axis of SAW progression at which the SAW is received by the Rx IDT. As the geometries both have slightly different lengths, this difference in received phase is expected. However, the phase shift given by the amplitude modulator will need to be taken into account in the final device's control system.

4.5 Phase Modulator Geometry and Results

Little literature exists on the topic of active phase modulation of SAWs, although the phase shifting properties of some devices have been characterised [30]. In thinking through possible ways to modulate the phase, two methods came to mind that would be able to leverage the piezoelectric effect to change the wave propagation characteristics. By changing the mechanical forces in the substrate via the piezoelectric effect, the material wave propagation properties change, allowing one to potentially modulate the phase. It is also worth noting that only the new 19 μm geometry was modelled from this stage forward, as it was clear from the gain modulation models that it exhibited superior performance.

4.5.1 Surface Electrode Model Geometry and Results

Conceptually, this phase modulation approach simply applies a controllable electric field perpendicular to the axis of SAW propagation, and in doing so, changes the SAW propagation properties enough to allow for a full $\pm 90^\circ$ phase shift, as required for frequency modulation. The electric field is applied by electrodes placed onto the top and bottom surfaces of the modulator between the Tx/Rx IDT pair. A DC voltage applied between the two pads creates the electric field. Similar methods to achieve other goals have been documented in the literature. One example is where the change in propagation of a SAW in the presence of an electric field is sensed to detect acceleration [40]. Figure 4-12 shows the geometry of the simulated device.

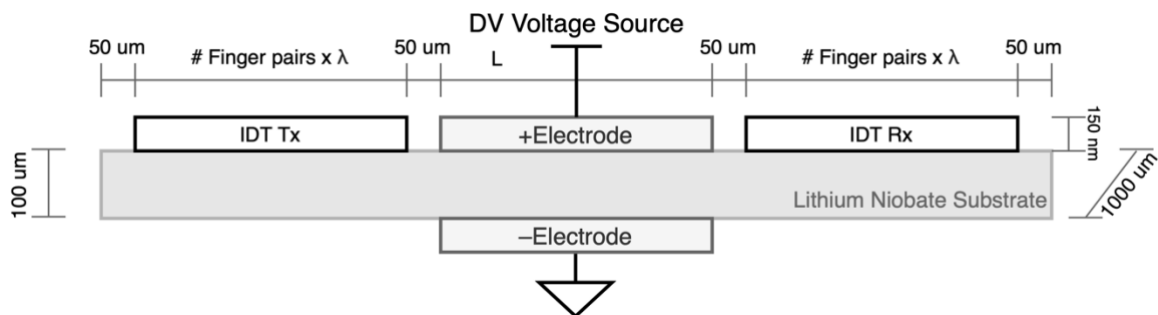


Figure 4-12: Surface electrode design of the SAW phase modulator. The positive and negative electrodes are connected to a DC power source. L represents the width dimension of the surface electrodes. λ is the SAW wavelength.

The two parameters that could be changed were the width of the surface electrodes and the voltage applied between them, V_{phase} . The model was simulated for two

electrode width cases initially – equivalent to the width and half the width of one of the Tx/Rx IDTs – with a voltage range of ± 100 V at 0.2 V intervals, in case there were changes at extremities or around tight voltage values. The SAW frequency was set to the centre frequency of 200 MHz. The simulation also took less time than any of the gain simulations – on the order of hours – allowing for this to be done time efficiently. The results are shown in Figure 4-13.

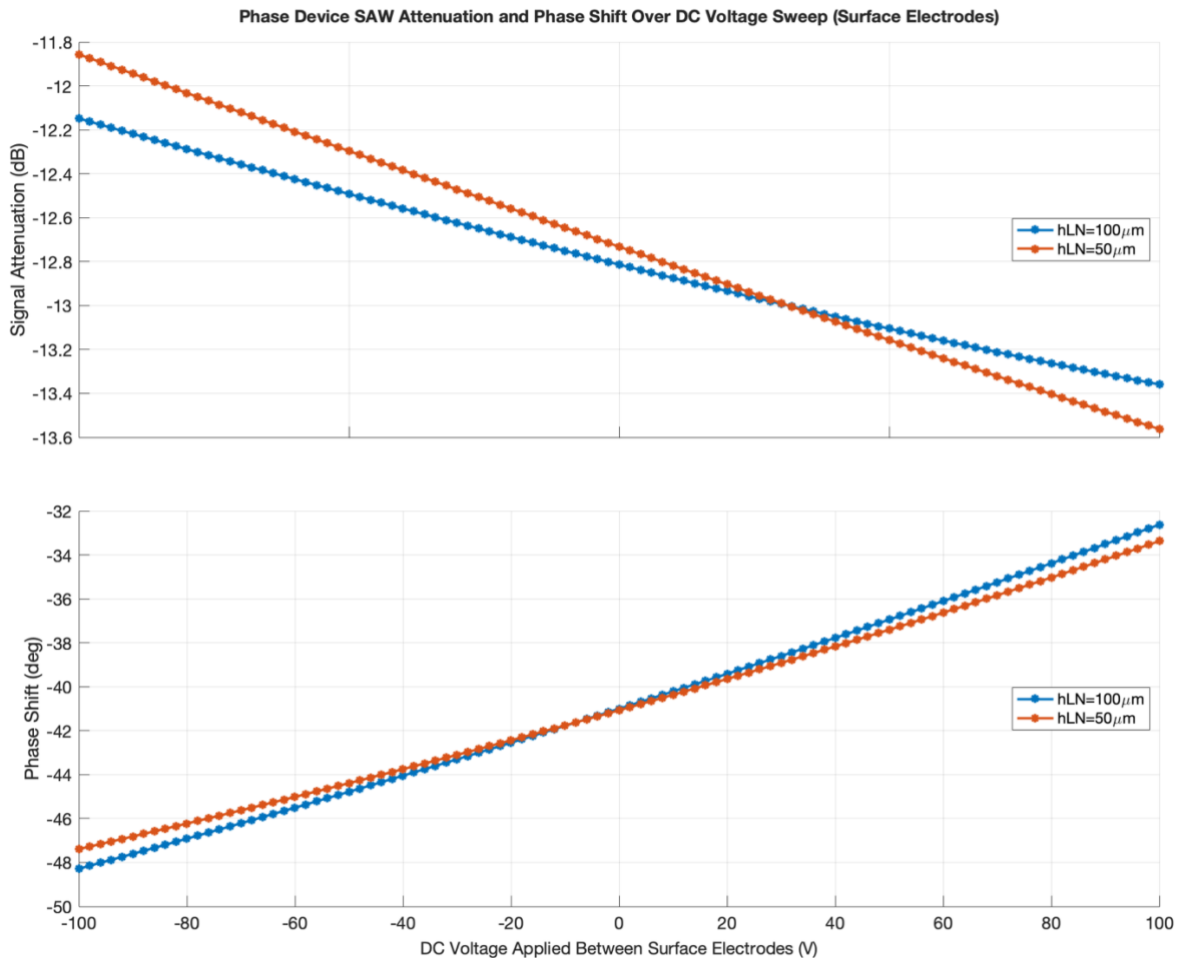


Figure 4-13: Surface electrode design phase modulator amplitude and phase shift data. Two electrode widths are tested. Every 10th data point is plotted for clarity.

Even at very high voltages, the degree of phase modulation is minimal, with only 16° shift between +100 V and -100 V. The electrode width also did little to impact the modulation. The signal amplitude was also impacted by this modulation, but only by 2 dB across the range. Given the much more complex fabrication process required for this method – arising from the fact that metal needs to be deposited on both the top and the bottom of the substrate – and given that the degree of modulation is minimal, this design was ruled out.

4.5.2 Naïve Model Geometry and Results

This approach is called the naïve design, as it relies on re-purposing the IDT for a use it is not intended for. The design simply consists of an IDT placed between the Tx/Rx IDTs. The terminals of this modulating IDT are connected to a DC power supply, which creates a steady-state potential difference between the IDT fingers. This potential difference results in a mechanical stress in the LN substrate that is applied parallel to the axis of SAW propagation. As above, the intent is to change the propagation properties sufficiently to result in phase modulation. Figure 4-14 shows the geometry for this approach.

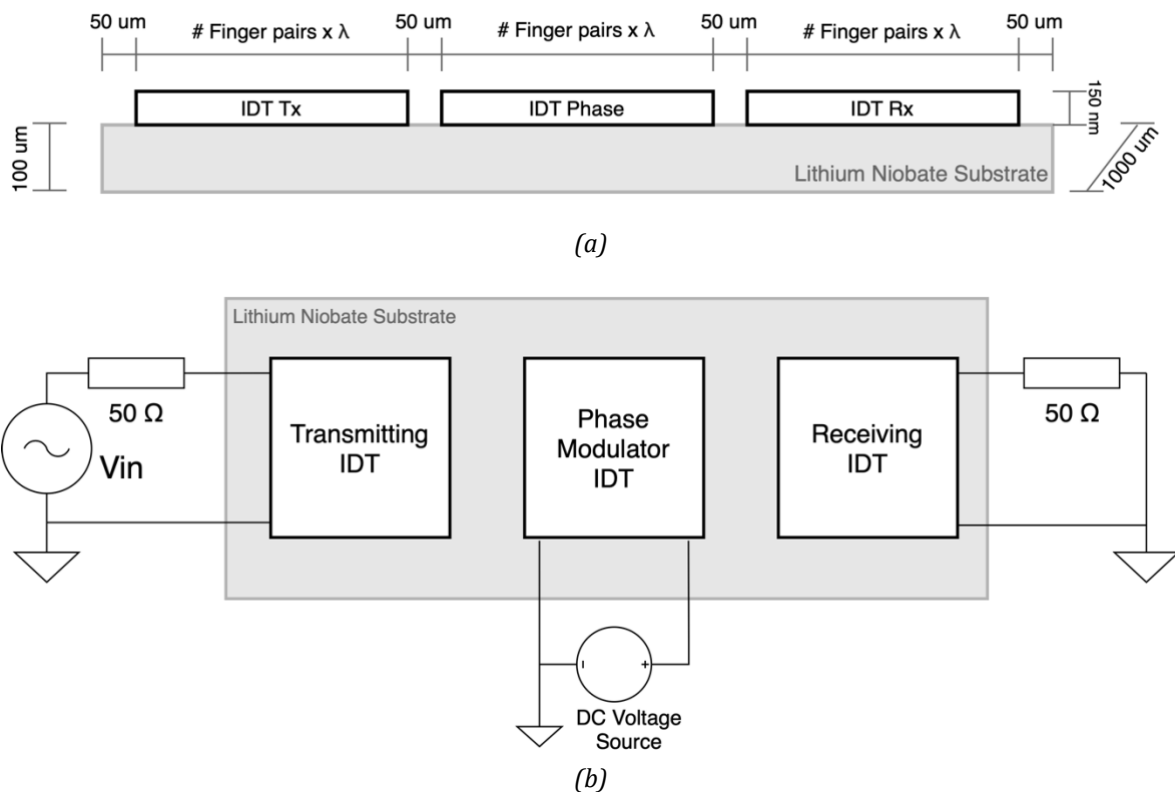


Figure 4-14: Geometry of the naïve phase modulation model, depicted not to scale in order to better visualise the geometry. Boxes labelled "IDT" represent the geometric extent of the fingers for a given IDT. λ is the SAW wavelength. (a) Side cross-sectional view. (b) Top-down view showing additional circuitry.

There are two parameters that need to be evaluated: the number of finger-pairs in the phase modulation IDT, and the DC voltage applied to the phase modulator IDT, V_{phase} . 10, 20, 30 and 40 finger-pairs were tested over a voltage range of ± 25 V at 0.2 V intervals, as rough preliminary simulations found this to be an adequate range. Simulation also took longer as compared to the surface electrode model, so sweeping

over a narrower range was more time efficient. The SAW frequency was set to the centre frequency of 200 MHz. The results can be seen in Figure 4-15.

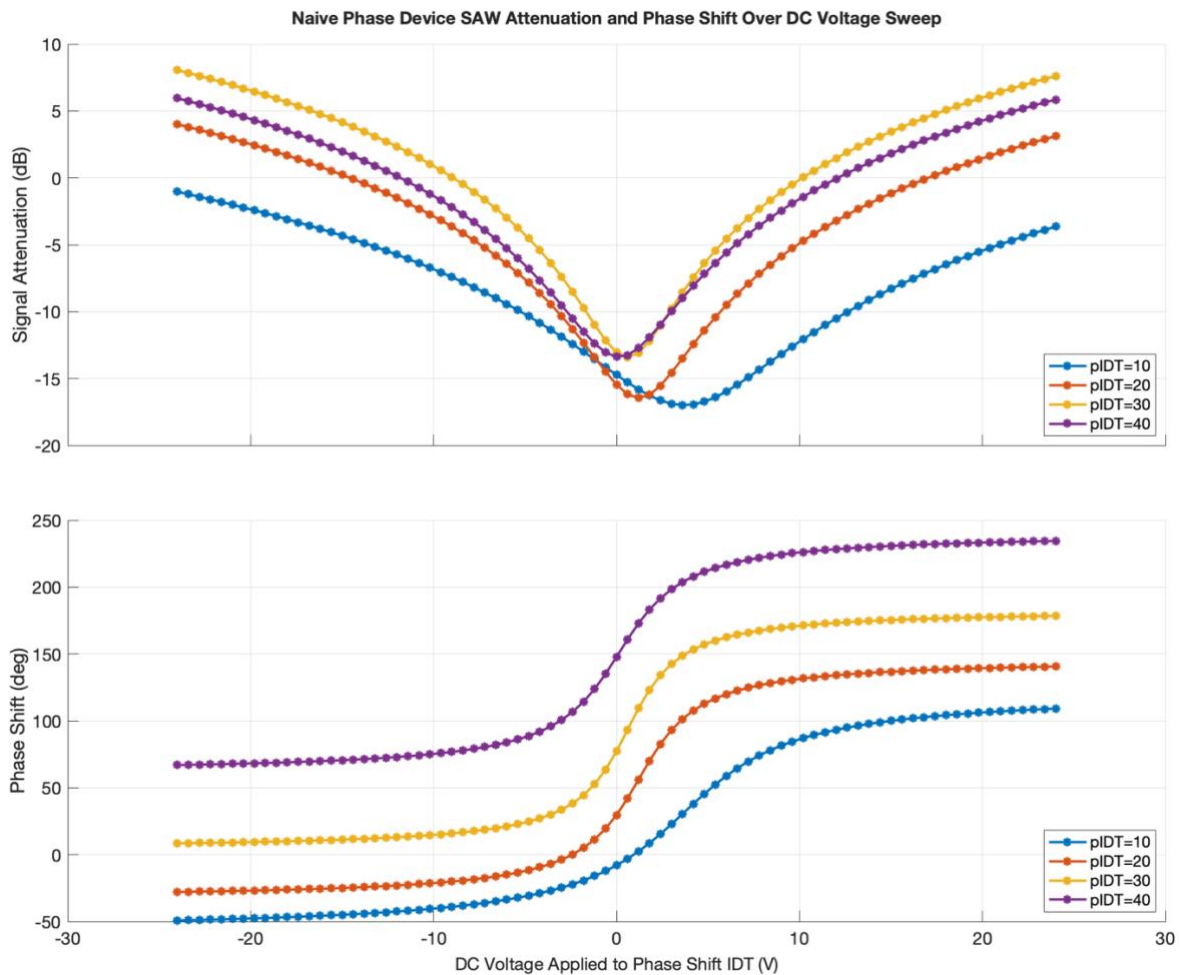


Figure 4-15: Naive design phase modulator amplitude and phase shift data. 10, 20, 30 and 40 finger-pairs on the phase modulation IDT is tested, as indicated in the legend. Every 3rd data point is plotted for clarity.

As is observable from the phase shift data in Figure 4-15, the 40 finger-pair variant performed the best, achieving $\pm 90^\circ$ phase shift within a ± 10 V range. Additionally, the 40 finger-pair variant did not show a significantly different attenuation curve as compared to the 20 and 30 variants, meaning that it has equally good attenuation performance as the other variants. Therefore, the 40 finger-pair variant is chosen as the phase modulator design.

It is interesting to note the shape of the attenuation curve. The minimum around 0 V can be explained by the SAW matching the IDT spacing geometry, inducing a potential difference, and thus losing energy to the IDT which is at a steady state DC potential itself. However, the positive signal gain observed outside of the ± 10 V range

is less clear. This could either be an artefact of an incorrectly set up model, or the SAW is in fact gaining energy when passing through the IDT set to this potential difference. Hardware validation data is a good starting point to further investigate this phenomenon.

Chapter 5

Device Fabrication

Having evaluated the designs from the computational models, the designs were fabricated at the Harvard Centre for Nanoscale Systems (CNS). The intent of this process is twofold. First, the results from the model need to be physically validated in order to proceed in further optimising the design with confidence. Secondly, one of the goals of this project is to create a device that is useful to the Lončar lab, and this requires building the physical device.

As the designs for the identity model, gain modulator model and phase modulator model all have metal structures on the surface of the LN substrate, the same fabrication technique can be used for all of them, and thus multiple devices can be made on a single piece of the substrate. Five device designs were chosen to be fabricated on a chip: the identity model, the three gain devices simulated with different numbers of gain IDT finger-pairs ($pIDT_g = 10, 20, 30$), and the naïve phase modulator design ($pIDT_p = 40$). This selection of devices allows for verification of the simulations and provides the lab with a useful device with which further research can be conducted. These all fit onto a single 10 mm x 10 mm LN chip comfortably with adequate spacing. The fabrication process used is a bilayer lift-off process using photoresist and metal deposition to create the surface structures, as further discussed in section 5.2.

5.1 Mask Design

As part of the bi-layer lift-off fabrication process, which is detailed in section 5.2, a photolithographic mask needs to be designed that allows only certain areas of the photoresist to be exposed to UV light. To do this, the python module *gdspsy* is used. The

gdspy package allows for the creation of GDSII stream files, which is the *de facto* industry standard file exchange format for microfabrication [41]. To use it, one draws polygons in Python and exports the result to a .gds file, for viewing in KLayout (a .gds viewer) and for import into the control software for the CNS OL-10 maskless photolithographer. OL-10 is referred to as ‘maskless’ as no physical mask is produced. Rather, the machine uses a UV laser to expose the chip in locations defined by the .gds file.

The Lončar lab had previously created many masks using *gdspy* and Python, so existing code was simply adapted to create the mask for this project (Appendix A). The code was modified to produce IDTs with the geometry modelled in COMSOL, and the electrical connection pad placement was also modified. Lastly, the positions of the IDTs were changed to reflect the model. The name of the project and date of fabrication were also included, along with alignment markers.

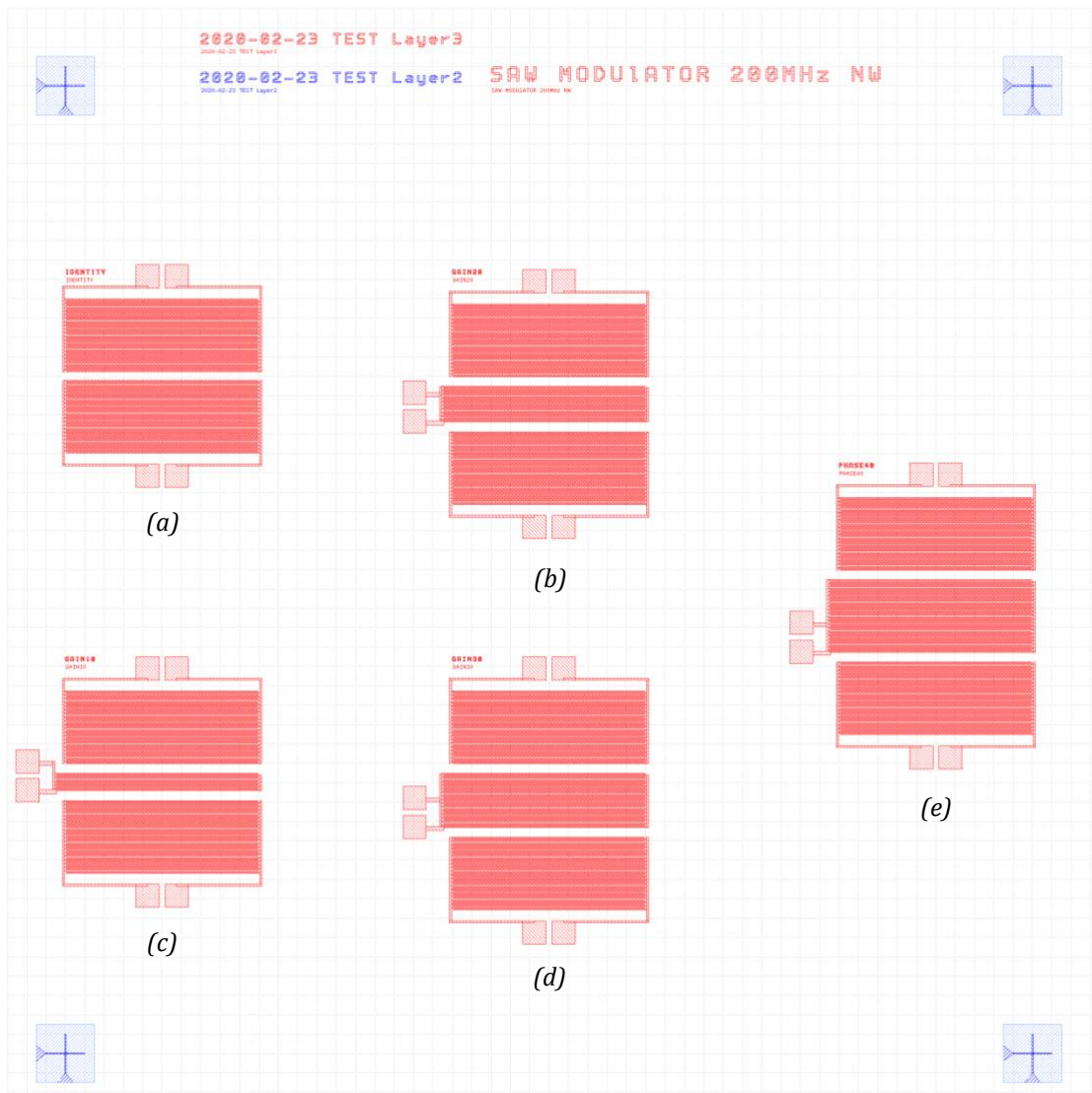


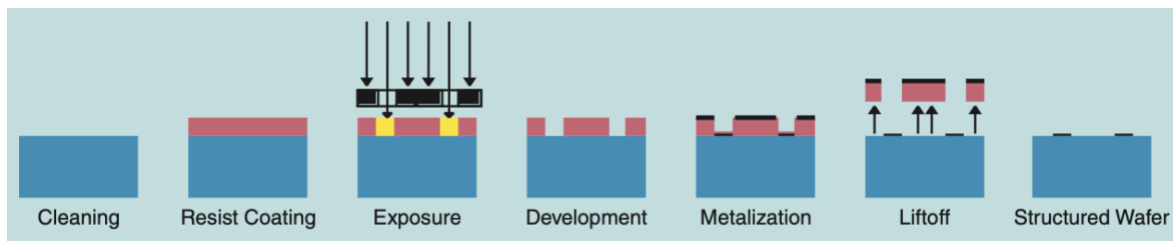
Figure 5-1: Screenshot of the mask in KLayout. The distance between the blue markers is 2.5 mm. (a) Identity device. (b) Gain device with 20 finger-pairs. (c) Gain device with 10 finger-pairs. (d) Gain device with 30 finger-pairs. (e) Phase device with 40 finger-pairs.

Unfortunately, during this process, there was some confusion regarding the number of fingers in the phase and gain modulation IDTs. While the Tx/Rx IDT pair each have the correct number of finger-pairs – e.g. 20 pairs, 40 fingers – the gain and phase modulation IDTs have half the amount of IDT finger-pairs specified – e.g. 10 pairs, 20 fingers for 20 pairs specified. While unfortunate that this error was not caught prior to the start of the fabrication process, it does not render the devices useless. Of the five produced, three have been modelled already – the identity model, the phase model with 20 finger-pairs (labelled as having 20 finger-pairs), and the gain model with 10 finger-pairs (labelled as having 20 finger-pairs). While not the optimal design, they can still be used to verify that the model is valid and are still useful for the

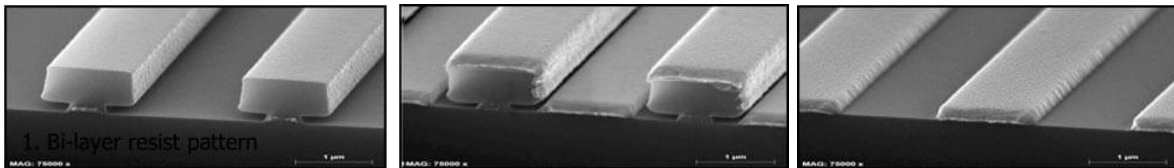
research agenda of the Lončar lab. Given the timescale of the project, there was not enough additional time for another round of fabrication.

5.2 Fabrication Protocol

The fabrication process used is a bilayer lift-off process, as shown in Figure 5-2. A positive photoresist was used, such that the exposed photoresist would be removed following the development stage. The undercutting between the substrate and the photoresist as seen in Figure 5-2b is a function of how long the LN chip undergoes development for, and it is important that this undercutting is present to allow for a clean lift-off.



(a)



(b)

(c)

(d)

Figure 5-2: (a) SAW device fabrication: bilayer lift-off technique with photolithography and metal deposition of aluminium [27]. Red is the photoresist, the black in the exposure step is the mask, and the black in subsequent steps is the deposited metal. The bottom row are scanning electron microscope image of IDT fingers after (a) development, (b) metallisation, and (c) lift-off [42].

The fabrication protocol followed is a standard protocol that makes use of the standard material library available at CNS. Images corresponding to some of the fabrication process are shown below in Figure 5-3. The fabrication protocol is as follows:

- 1) Dice the LN substrate into 10 mm x 10 mm squares
- 2) Clean the sample to remove residue from dicing
 - a. Place sample in Remover PG+ sonicate for 5 minutes

- b. Place sample in Methanol + sonicate for 3 minutes ¹
- c. Place sample in isopropyl alcohol (IPA) + sonicate for 3 minutes
- d. O₂ Plasma clean at 100 W, 40sccm, for 3 minutes
- 3) Spin-coat the substrate with photoresist (PR)
 - a. Spin coat PR LOR 3A at 3000 rpm for 1 minute ²
 - b. Bake for 5 minutes at 180C
 - c. Spin coat PR S1813 at 3000 rpm for 1 minute ³
 - d. Bake for 2 minutes at 115C
- 4) Place the sample in CNS OL-10 maskless lithographer for direct UV laser writer exposure of mask
 - a. Set the laser wavelength to 405 nm
 - b. Set dose to 180 mJ/cm²
- 5) Develop the sample to remove PR previously exposed to the UV laser
 - a. Place the sample in MF-319 developer for 65 seconds ⁴
 - b. Rinse the sample with distilled water + blow dry
- 6) Clean the sample in O₂ plasma at 60W, 40sccm, for 20 seconds
- 7) Deposit metal onto substrate using Sharon E-Beam Evaporator (CNS EE-3)
 - a. Place and secure the samples on metal deposition plate
 - b. Place the aluminium crucible in EE-3
 - c. Pump the EE-3 chamber down to vacuum pressure
 - d. Deposit 150 nm aluminium onto the samples
- 8) Lift-off metal in Remover PG overnight ⁵
- 9) Clean the samples to remove residue metal
 - a. Place the samples in IPA + blow dry
 - b. Place the samples in Methanol + blow dry

¹ 'Remover PG' is the trade name for the solvent stripper commonly used in fabrication.

² This is a 'lift-off resist' photoresist with properties given by the '3A' marker [43].

³ This is another kind of commercially available photoresist [44].

⁴ MF-139 is a developer, meaning that it removes the photoresist that was exposed to UV light [45].

⁵ Remover PG removes the remaining photoresist from the surface of the substrate [46].

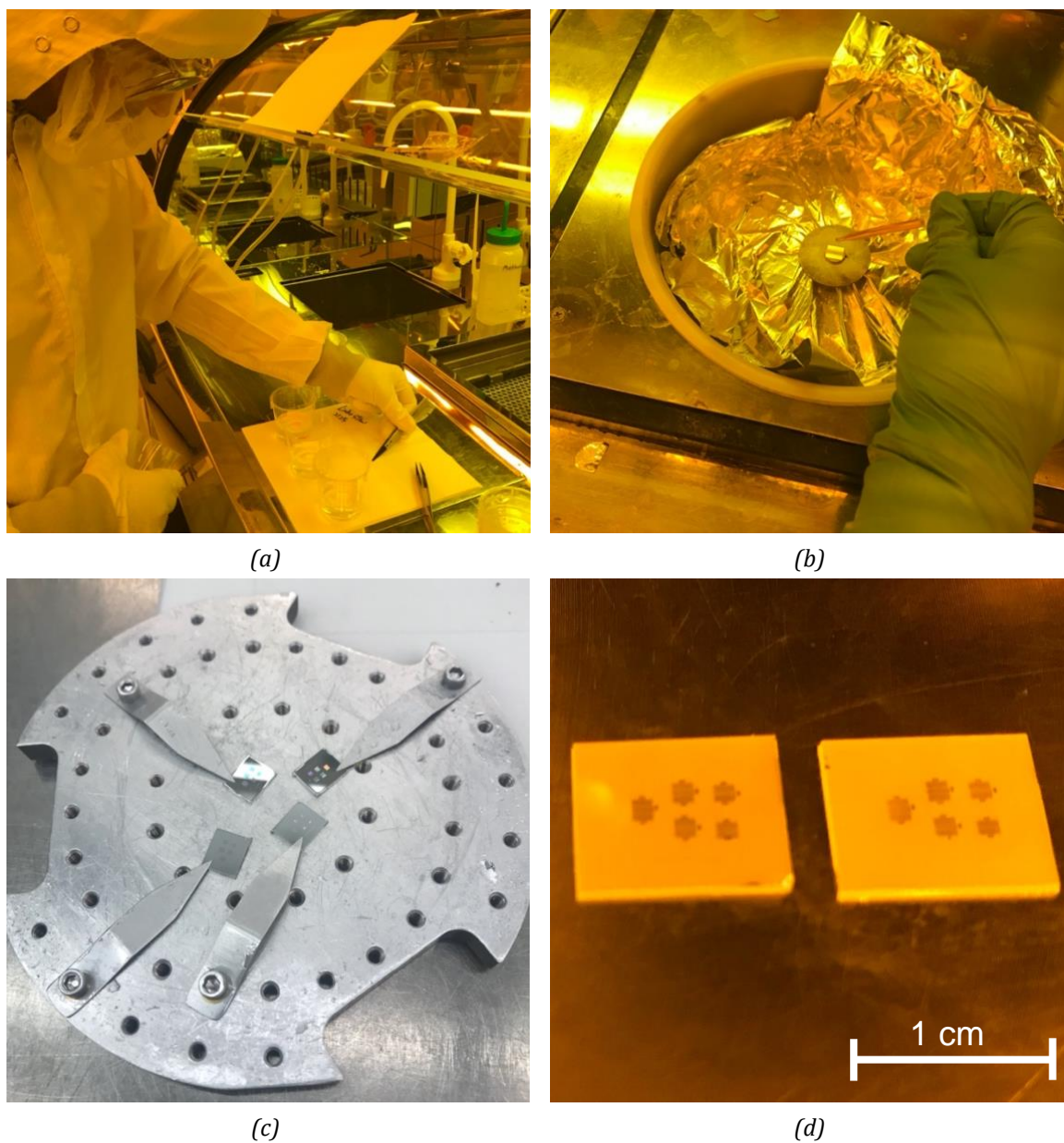


Figure 5-3: Select images from the fabrication process. (a) Sample cleaning to remove residue from dicing. (b) Photoresist spin-coating. (c) Samples after EE-3 metal deposition. (d) Two of four samples after lift-off and clean.

5.3 Fabrication Results

Of six samples initially prepared, one did not spin-coat adequately, one failed during the development process, and one failed to produce usable devices after lift-off. Of the three remaining, at least one usable device was obtained of each of the five designs, as shown in Figure 5-4.

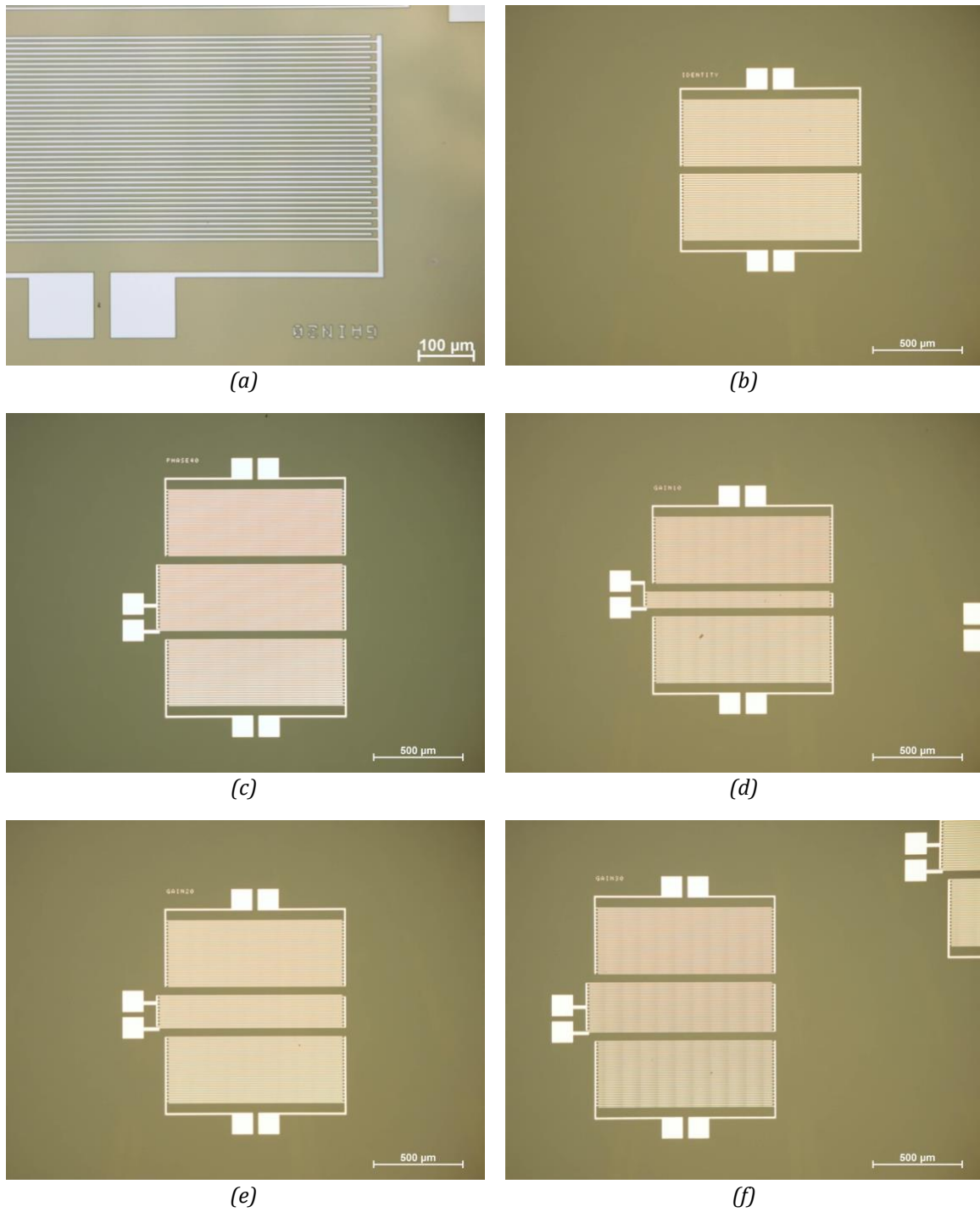


Figure 5-4: Optical images of fabricated devices. (a) Zoomed in photo of an IDT showing the individual fingers. (b) Identity device. (c) Phase device (with 20 fabricated finger-pairs). (d)-(f) Gain devices (with 5, 10, and 20 fabricated finger-pairs).

Chapter 6

System Design and Construction

In order to package the final product in such a way that it can be easily used by the lab, there must be a way to interface with the fabricated devices in a manner that does not require specialized equipment or training. To do this, the LN chip needs to be mounted on a printed circuit board (PCB) that has the requisite connections and electronics to allow a user to interface with the chip and control the SAW modulation properties. The full schematic and layout are available in Appendix B.

6.1 Printed Circuit Board

The decision to mount the LN chip on a PCB was a straightforward one. The only other way in which nanoscale electronics are able to interface with the macro world is via a specialised probe device that takes time to set up for every use, requires specialised training and is not easily usable on a benchtop with other devices. A well-designed PCB on the other hand is easy to interface with, has a small physical footprint, and can be easily wire-bonded to a microfabricated device. Likewise, external signals can be easily routed to the chip via industry standard and widely used SubMiniature version A (SMA) shielded connectors.

In thinking about the design of the PCB, versatility was very important. Given the budgetary and time restrictions of the project – especially with regards to the current COVID-19 virus epidemic placing pressure on PCB manufacturers globally – it was unlikely that there would be enough time to design and order a second round of PCBs. Additionally, there are many devices on one chip that this PCB would interface with, as not all devices on the three successfully fabricated chips were usable. This meant that one PCB design needed to be able to interface with at least two gain devices, the identity device and the phase device.

6.1.1 Identity Circuit

The circuitry required for the identity device is very simple, as there is no modulation required, and thus is nothing more than a simple passthrough trace for the coaxial SMA (*SubMiniature version A*) connector to wire-bond pads, as shown in Figure 6-1. The shield connector is connected to the PCB ground plane in order to provide a stable reference.

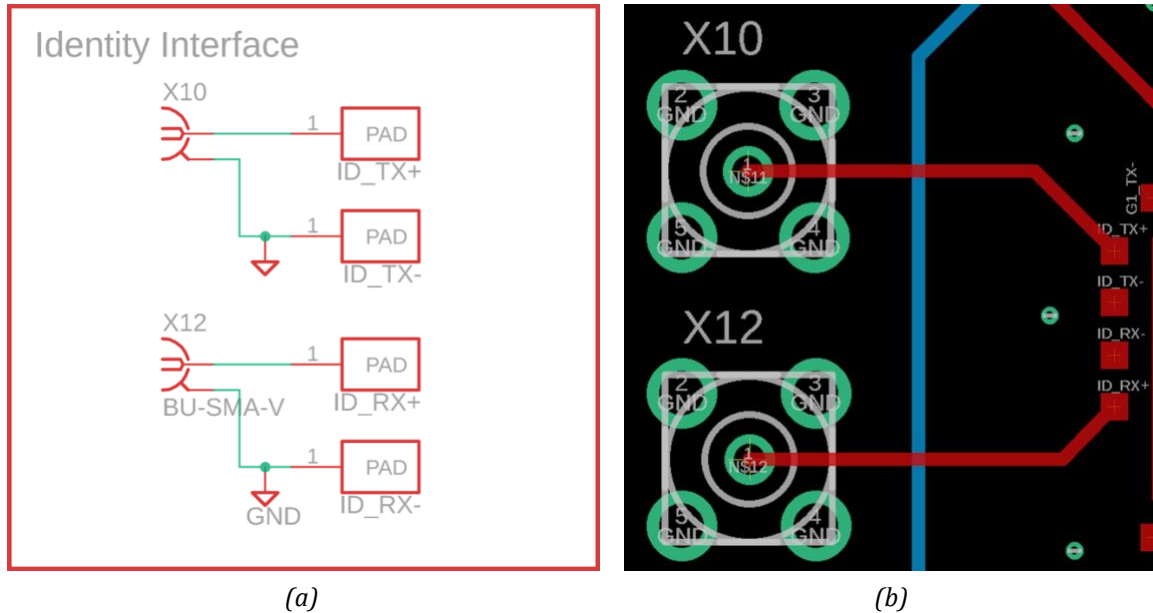


Figure 6-1: Identity circuit. (a) Schematic with SMA connectors and wire-bond pads. (b) Corresponding PCB layout.

6.1.2 Gain Circuit

The gain device requires a resistive load to be placed across the terminals of the gain modulating IDT between the Tx/Rx IDT pair. From the simulation, it can be concluded that the largest dynamic range of signal is attained with resistance values ranging from 50 Ω – 10 k Ω . This range is very hard to achieve dynamically in hardware with the required interval resolution. From the simulation, a small change around the 50 Ω range has a comparatively larger impact on the gain than a similar change above 1 k Ω . However, it can be hard to achieve these resolutions with the required range, as if the range increases for a given resolution, the difference between steps increases. Two options were assessed:

- 1) Manual rheostat, as previous projects at the Lončar lab have done,
- 2) Digital rheostat.

The first is undoubtedly the easiest of the two to implement in hardware; however the major drawback of this solution is that it cannot be electronically controlled, meaning that as an end-user product, it only serves to provide proof-of-concept. The second solution involving a digital rheostat is more challenging to implement, given that it requires a controller and additional circuitry, and to select the correct component that balances range with resolution. However, this solution allows for digital control of the resistance and thus the degree of amplitude modulation. For this reason, the digital rheostat solution was chosen.

There are several challenges associated with using a digital rheostat in this context:

- The resistance range needs to span three orders of magnitude and be selectable with an appropriate resolution.
- The digital communication protocol used by the chip needs to be simple to use and selectively addressable, given that may be two copies of the device on the PCB.
- The maximum voltage across the resistance terminals needs to be considered. Looking at the simulation data, this does not exceed ± 2.4 V in the case of least attenuation.
- There is a resistive offset associated with the wiper resistance of the digital rheostat that needs to be considered.

The chosen digital rheostat was the AD5174 from Analog Devices [47]. This device was readily available from commercial vendors and was available in the hand-solderable SMD 10-MSOP package. It has a rheostat voltage rating of ± 2.5 V nominal, ± 2.8 V maximum and requires a ± 2.5 V dual-supply, which is available from a lab power supply. This is adequate, as the simulation data shows that the SAW is attenuated to ± 2.5 V by the time it interacts with the gain modulation IDT. The wiper resistance is 35Ω , which is the lowest readily available in a suitable package. Given that the minimum required resistance is 50Ω , this value is suitable. The resistance range without the offset is $0 \Omega - 10 \text{ k}\Omega$. The AD5174 is controlled via an SPI connection with internal clamping diodes that allow it to interface with 3.3 V and 5 V logic devices, and with chip-select functionality to allow several devices to be on the same SPI bus. This makes interfacing with the device using simple microcontrollers like the ubiquitous 5 V Arduino UNO straightforward, and as a result the software on the microcontroller that controls the digital potentiometer can be easily changed without needing access to specialised software or programming interfaces. Finally, the device has a 10-bit resolution (1024 positions), giving a resolution of 9.7Ω , which is

the highest resolution available without requiring custom ICs within the above constraints. Assuming ± 5 V SAW at the modulator and 4 dB dynamic range – a value consistent with simulation results – this resistance resolution gives a 3 mV modulation resolution, which is adequate. The external components required for the AD5174 are one capacitor, one pull-up resistor and supply decoupling capacitors, as shown in Figure 6-2.

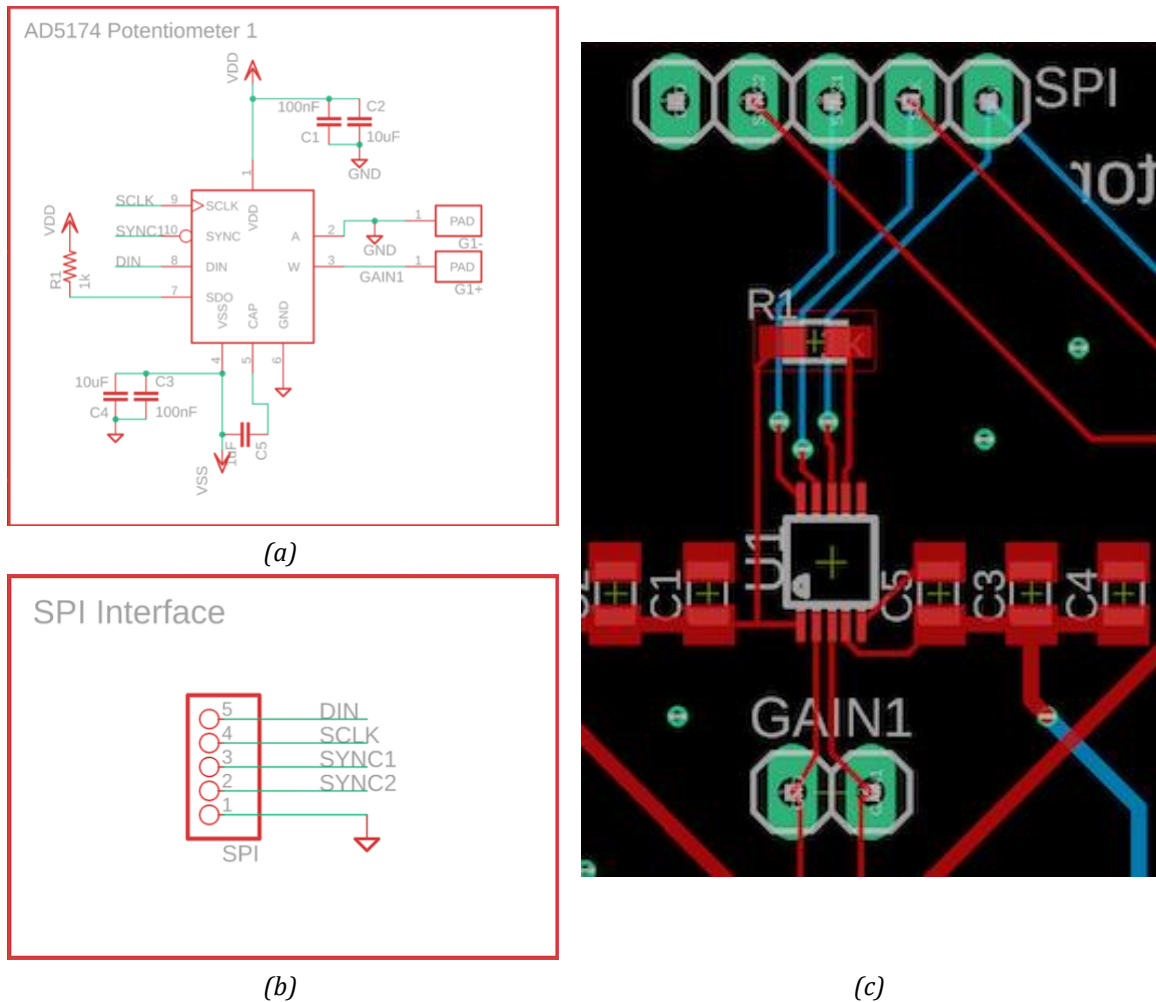


Figure 6-2: Gain control circuit. (a) AD5174 digital rheostat schematic. (b) SPI digital interface schematic. (c) corresponding PCB layout, which also show the headers for the manual rheostat (labelled GAIN1).

In the case that the AD5174 digital rheostat proves to be inadequate to drive the desired range of modulation, or in the case that it is damaged in PCB population, two 0.1" header connections are broken out to allow a user to insert a manual potentiometer on a breadboard. This is not intended to be used, but is included on the PCB for versatility purposes. The interface schematic is shown in Figure 6-2. For the

Tx/Rx IDT pair of the gain devices, SMA connectors route the signal directly to the chip, as in the identity case, as shown in Figure 6-3.

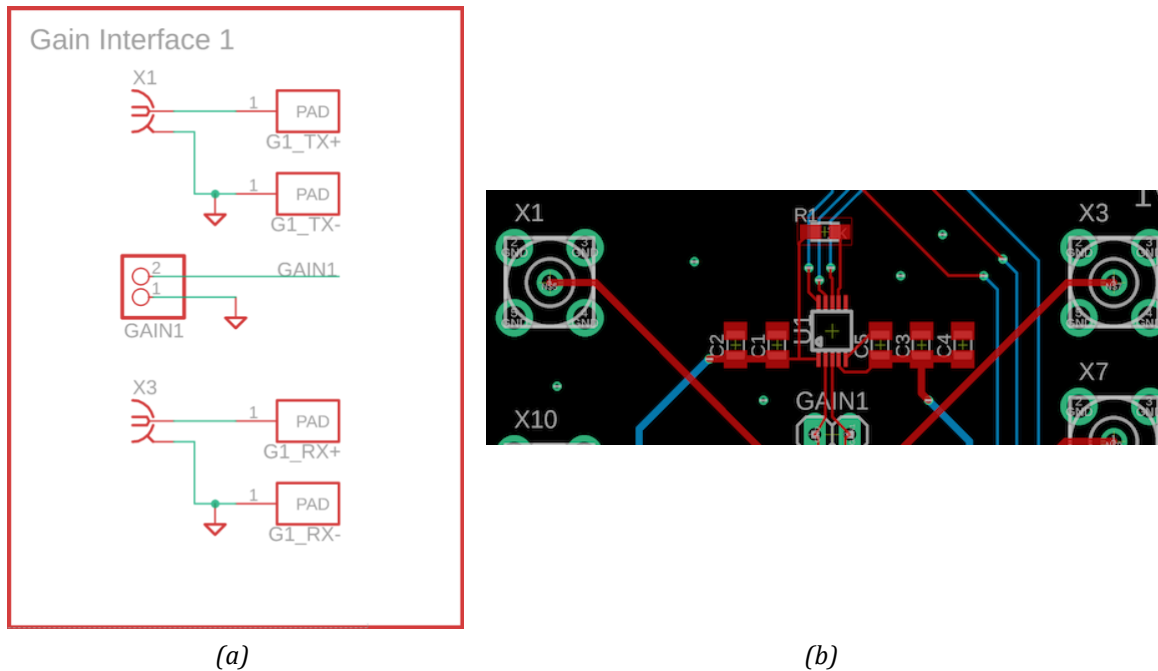


Figure 6-3: (a) Gain circuit Tx/Rx IDT interface schematic with 2x1 0.1" header connected to gain modulation IDT. (b) Corresponding PCB layout, showing the SMA connectors X1, X3 and the manual rheostat header GAIN1

6.1.3 Phase Circuit

Given the large $\pm 10\text{V}$ voltage requirements for this device, the circuitry for the phase modulator would have required a specialised digital-to-analog voltage converter (DAC) and a $\pm 10\text{V}$ supply; for example, the AD660 from Analog Devices is a $\pm 10\text{V}$ DAC, costing upwards of \$40 per chip [48]. Additionally, as the phase modulation circuit was not as fully characterised as the gain modulation circuit due to time constraints, more complex electronics would have been less likely to function as expected. The same effect could instead be achieved by connecting the phase IDT directly to an SMA connector, like the Tx/Rx IDT pair, as this would allow an operator to connect an external power supply to the phase IDT. While this is less versatile for control purposes, it will still allow for validation of the COMSOL model. Figure 6-4 shows the relevant schematic and PCB layout. The traces to the Tx/Rx IDT pair are designed to be equally long to maximise impedance matching and reduce timing error.

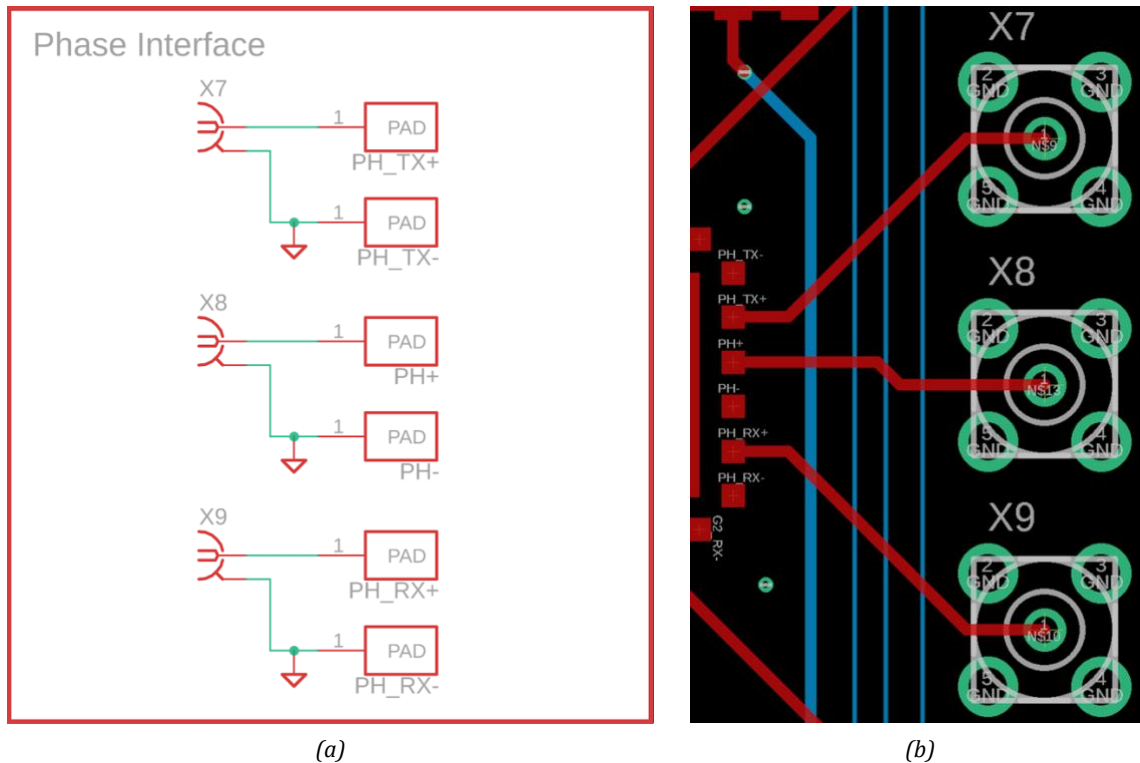


Figure 6-4: Phase circuit. (a) Schematic with additional SMA connector for the phase modulator, (b) corresponding PCB layout.

6.1.4 Additional Design Considerations

In addition to the above, there are additional design considerations that were made during the design of the PCB.

- *Surface-mount (SMD) components* – as the PCB is the platform on which the wire-bonding from the chip to the electrical contacts is done, it is important that it can be placed flat onto the wire-bonding tool’s workbench. Therefore – with exception of the connectors – all components must be SMD.
- *Good grounding* – given the volume of different analog and digital signals on the PCB, good grounding to a 0 V reference is essential. Both copper layers are ground planes with copper infill and are connected with multiple vias across the PCB. The surface onto which the chip is mounted is also grounded to prevent static build-up on the surface.
- *Organisation of Layout* – as some of the components may not need to be installed (e.g. if only one gain control circuit is needed, or some of the SMA connectors do not need to be installed) and to assist in operation by the end-

user, the components are spaced out in a logical fashion so as to make their function clearer.

- *Off-board connectors located on the edge of the board* – this is to make user operation easier, and to prevent a tangle of cables above the PCB.
- *Standard connector footprints* – SMA is a common connector standard for analog signals, and 0.1" header footprints for power, SPI and the gain-bypass connections allow the user to install their preferred connector (e.g. simple male headers, Molex-KK connector, etc.).
- *Decoupling Capacitors between ground plane and power buses* – this helps in buffering against power rail noise and momentary fluctuations, helping to reduce noise in the circuit overall. A range of capacitor values are chosen to buffer different noise frequencies (Figure 6-5).

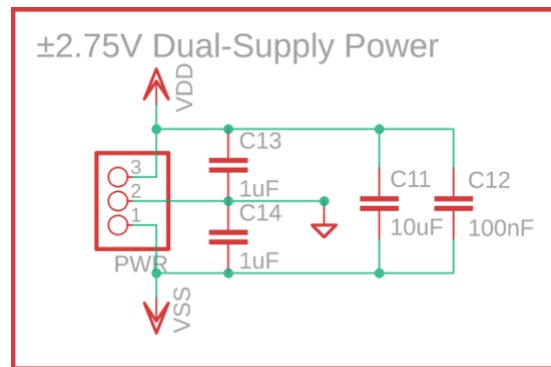


Figure 6-5: Dual-supply power bus connector with decoupling capacitors.

6.1.5 Considerations for Future PCB Iterations

In the prototype presented above, two minor mistakes were made, both with regards to the digital interface of the digital potentiometer.

The SPI protocol is a four-wire protocol, requiring MISO (master in, slave out), MOSI (master out, slave in), SCLK (system clock) and CS (chip select). The AD5174 digital potentiometer's interface maps onto these connections. However, during the design phase, the datasheet was misread and the AD5174's SDO pin (serial data out), which serves as the MISO connection of breaking out, was not broken out on the digital interface header (labelled SPI on the PCB). While less than ideal, the pull-up resistor connected to it, as per the datasheet recommendation, means that the device would still function as expected; however, the control system software would have to be modified to account for the lack of feedback.

Secondly, the SYNC2 connection, which serves as the chip-select connection for both of the AD5174s on the PCB is not strictly necessary, as the AD5174 datasheet suggests that the SDO pin of the first device can be daisy-chained to the DIN pin of the second device, effectively creating one SPI device without the need to explicitly select which one to communicate to. This modification would save a pin on the digital interface header and routing complexity, as the SYNC1 header pin could just be connected to both SYNC1 and SYNC2 pins. It still needs to be connected to the microcontroller, as the AD5174 uses the rising and falling edges on the SYNC pin to shift data to its internal registers [47].

There are further additional changes that could be made. These include adding a ± 10 V DAC for the phase modulator, rounding the corners to avoid sharp edges, and adding mounting holes to make integration into a mechanical housing easier.

6.2 Control System

In order for the PCB circuitry to be able to perform SAW modulation, it needs to be connected together into a single control system, where the user or other software is able to control the SAW modulation characteristics. As the phase modulation circuitry was not integrated onto into the PCB in this prototype, but rather relies on an external power supply to provide the required voltage for the phase modulator, the initial design of the control system focused on controlling the gain modulator.

The requirements for controlling this circuit are not very computationally taxing. The component in the gain modulator circuit that is controllable is the digital potentiometer, which is accessible via a SPI connection. This protocol is available on the majority of modern microcontrollers and does not necessitate any special timing requirements beyond those commonly available in microcontrollers. While it would be possible to interface with SPI using a more powerful microprocessor (like that found on the Raspberry Pi, or in a computer), this would add additional complexity, power requirements and complex circuitry requirements. Especially seeing as more than adequate microcontrollers exist today on accessible and well documented platforms, like the Arduino UNO.

The ATMEGA328P on an Arduino UNO platform was chosen for the controller hardware. The UNO is also readily available in the Lončar lab. The 5 V digital logic level on the UNO is not a concern, as the selected digital potentiometer has internal shunt diodes on its SPI bus to allow interfacing with 5 V logic devices. The device is wired to the PCB as shown in Figure 6-6.

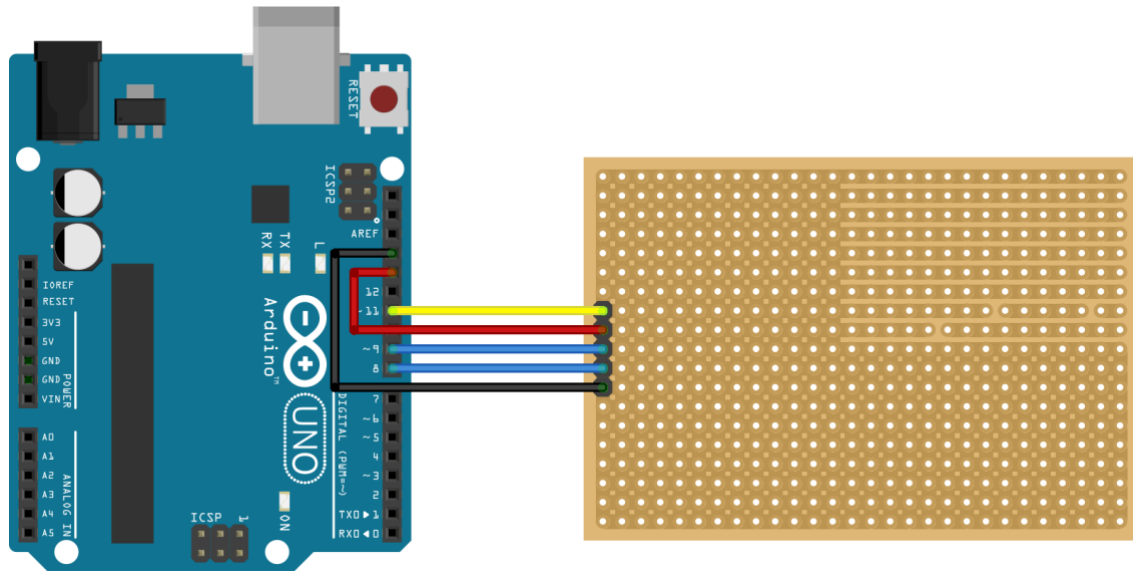


Figure 6-6: A drawing indicating the SPI connections to an Arduino UNO. The protoboard depicted is the size of the PCB. Black: ground. Blue: SYNC1/2. Red: SCLK. Yellow: DIN. The graphic is made using Fritzing.

Interfacing with the microcontroller itself is most easily done via the UNO's on-board UART connection over USB. The interface can take the form of a command-response protocol for setting the resistance level, or a higher-level protocol, where the microcontroller is sent a desired frequency shift and does the necessary calculations to evaluate the resistance level to be set. As final build of the project did not take place, this software was not written.

Further improvements could be made in the future by creating a feedback loop between the set modulation level and the actual modulation level. This would be a complex project, as the controller would need to interface with a device capable of measuring the SAW at the Tx IDT. This feedback principle could also be applied to the phase modulator controller. In both cases, a detailed description of how the modulation parameters impact the SAW is needed, perhaps stored as a lookup table on the controller.

Chapter 7

Design Evaluation and Testing

Once the PCB was assembled and the SAW devices wire-bonded to the relevant pads, the next step would have been to test and evaluate the design, and verify that it meets the required specifications. Unfortunately, due to the extenuating circumstances caused by the emergency de-densifying measures Harvard University took due to the spread of COVID-19 in the spring of 2020, this step was unable to be completed. While the PCB and all the components had arrived, not enough time remained for assembly and verification. While the Lončar lab offered to complete the testing and produce the data, the university ultimately decided to suspend all on-site research activities. What is presented here is a detailed methodology of what tests would have been conducted, had the semester progressed as usual.

7.1 Testing Methodology

The tests that were to be conducted on the device would have served two purposes. The first is to validate whether the COMSOL model of the device was accurate in how it predicted the SAW transmission behaviour, and the second is to see whether the fabricated devices themselves met the project specifications.

In the first case, model validation would indicate whether the assumptions made in Chapter 4, the given material properties or the physics engine setup were indeed valid, and are reflective of reality. If this were not the case, the model setup would need to be reviewed, perhaps leading to a change in design of the devices once the models were re-evaluated. For example, if an observed frequency sweep curve for the gain modulator were a significantly different shape to the one from the simulation, this may indicate that the physics engine configuration is incorrect, as there may be a

miscalculation in how the materials interact with each other. On the other hand, if the curve is the same shape but shows more attenuation, this may indicate that while the physics engine is configured correctly, the implicit assumption of high efficiency piezoelectric coupling may need to be revisited.

In the second case, compliance with the specification validation is checked. Given that the project goal is to ultimately produce a device that is useful to the Lončar lab, it is important that the specifications are met. If key specifications were not met – such as the SAW phase and gain modulation specifications, and intrinsic insertion loss – testing the SAW transmission characteristics of the devices may illuminate why this is the case, and may present a way forward to being able to meet the specification in a future iteration of the device, such as geometry or control circuitry modifications.

In order to achieve these goals, two sets of tests were designed. The first set would attempt to re-create the model simulation results, by performing the same frequency and parameter sweeps as was done in simulation. This would produce a dataset that could be directly compared to the simulation data in order to determine whether the simulation is accurate. Using a mean squared error approach, this accuracy can be quantified to determine whether a device replicates simulation results. Acceptable error thresholds would be set for this as appropriate to result in less than 5% mean error. The data should also be visually inspected to catch outlying datapoints that may skew the results or that may not be reflected in the mean error. The second set of tests is to derive a numerical model of behaviour of each device in the frequency domain in order to fully characterise the real-life behaviour of the devices, which is ultimately needed to design control software for the modulator, as this data may differ from the simulation slightly. A summary of these tests is given below in Table 7-1.

Table 7-1: Summary of tests to be conducted. The test description and parameters are also given.

| Identity Device | | | |
|------------------------|-------------------------------------|---------------------------------|------------------|
| <i>Equipment</i> | <i>Test</i> | <i>Parameter Range</i> | <i>Constants</i> |
| VNA | Frequency sweep | 170 – 230 MHz, 0.5 MHz interval | – |
| VNA | Measure numerical transfer function | | |

| Gain device | | | |
|--------------------|-------------------------------------|--|--|
| <i>Equipment</i> | <i>Test</i> | <i>Parameter Range</i> | <i>Constants</i> |
| Multimeter | Characterize digital potentiometer | | |
| VNA | Frequency sweep | 170 – 230 MHz, 0.5 MHz interval | $R_{\text{gain}} = 10 \text{ k}\Omega$ |
| VNA, controller | R_{gain} sweep | 35 – 10 k Ω , 9.7 Ω interval | f=200 MHz |
| VNA | Measure numerical transfer function | | |

| Phase device | | | |
|---------------------|-------------------------------------|-------------------------------------|----------------------------------|
| <i>Equipment</i> | <i>Test</i> | <i>Parameter Range</i> | <i>Constants</i> |
| VNA | Frequency sweep | 170 – 230 MHz, 0.5 MHz interval | $V_{\text{phase}} = 0 \text{ V}$ |
| VNA, DC supply | V_{phase} sweep | $\pm 10 \text{ V}$, 0.5 V interval | f = 200 MHz |
| VNA | Measure numerical transfer function | | |

The equipment that would have been used in addition to the project hardware include a function generator for generation of the SAWs, an adjustable $\pm 10 \text{ V}$ DC power supply for the phase modulator, and a vector network analyser (VNA). A VNA provides signal characteristic measurements over a range of frequencies, such as relative phase and amplitude for a given frequency, and speed of propagation [49]. A VNA makes measurements with respect to a reference signal – the signal that enters the device to produce the SAW, as shown in Figure 7-1. In doing so, a VNA is able to evaluate the transmission characteristics of the signal, and subsequently present data that allows for direct comparison to the simulation data. This also allows for characterisation of the device’s signal transfer properties. The function generator, DC power supply and VNA should all be centrally controllable by a single computer so

that sweeps over parameters can be conducted and data recorded without repeated manual intervention. This is important, as for the two-dimensional parameter tests to measure the device's transfer function, several hundred parameter combinations will be tested.

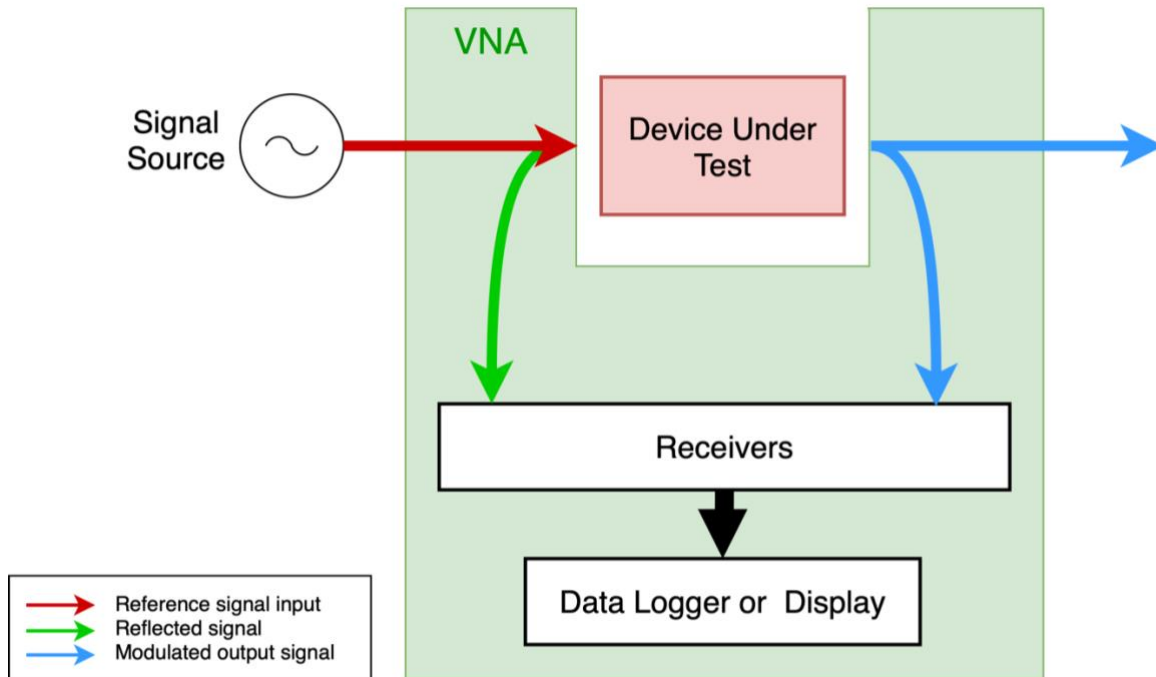


Figure 7-1: A VNA makes measurements with respect to a reference signal. The measurements are presented to the user on a display or logged on a computer for further analysis.

7.2 Identity Device Testing

The purpose of this device is to evaluate whether the simple case of passthrough SAW generation, transmission and reception functions as expected, both in simulation and on a fabricated device. As such, the tests that would have been performed on the identity device would have served to verify that the testing equipment functions as expected and that the test protocol produces the desired data. It would also serve as a baseline for comparison against the results from other devices.

The first test that would have been conducted is a frequency sweep of the SAW generation sine signal, in order to reproduce the simulation results. The VNA records the signal amplitude for the given frequency under test. The following parameters are used:

- *Frequency range: 170 – 230 MHz*

- *Frequency interval: 0.5 MHz*
- *Signal amplitude: 10 V*

This frequency range is chosen such that we are able to see the response of the device to different harmonics of the wavelength, as was indicated in the simulation data. The small frequency interval also allows us to characterise the frequency response of the device accurately, in addition to replicating the simulation study. In comparing with the measurements with the simulation data, the mean squared error of the gain for given frequencies would be calculated. If the error is below 5%, then it is concluded that the model is accurate.

In addition to this test, this device would also allow us to observe any baseline odd behaviour of the Tx/Rx IDT pair architecture, if it were present. Such behaviour could include parasitic losses or harmonic attenuation. While hard to predict without access to test data, one could imagine that the intrinsic insertion loss at the centre frequency peak as in Figure 4-6 is lower due to noise or energy loss due to imperfect IDT interfacing with the LN substrate. The peak itself may not be located at the desired 200 MHz centre frequency, due to imperfections in the crystalline structure of the substrate or temperature variation changing the SAW propagation speed, which would require updating the geometry of the device accordingly to shift the centre frequency to 200 MHz.

7.3 Gain Device Testing

The first test that needs to be conducted on the gain device is to characterise the digital potentiometer to make sure that it works and to know whether there are any component-specific variations in the resistance, as the datasheet suggests there may be $\pm 17.5 \Omega$ variation in the intrinsic wiper resistance [47]. It is important that this offset is known, as it would impact the amplitude. For example, the lowest controllable value on one device may be 20Ω , but on another it is 37.5Ω , and this offset would be present between any given values. In order to test this, the digital potentiometer would be set to its lowest configuration via SPI. The command for this can be found on page 13 of the digital rheostat datasheet. [47]. The pre-programmed tolerance – which is constant for all resistance values – would also need to be obtained from the component's memory [47].

The following tests to be performed would be to replicate the simulation results. The tests would be performed on the fabricated 10 finger-pair gain device and the 20 finger-pair phase modulator (which has the same geometry as the 20 finger-

pair gain device would have had without the mask error). These two devices would be tested as there is simulation data to compare against. Like with the identity device, a frequency sweep would be performed, with the R_{gain} gain modulating resistance parameter set to the highest setting on the digital potentiometer – nominally 10 k Ω – where the least attenuation would be observed in order to match the simulation resistance parameter value of 10 M Ω . The following other parameters would be used:

- *Frequency range:* 170 – 230 MHz
- *Frequency interval:* 0.5 MHz
- *Signal amplitude:* 10 V
- *Resistance R_{gain} :* 10 k Ω

The resistance sweep test would then be performed, making use of the fact that the modulator controller PCB can be interfaced with a computer to automatically change the resistance parameter across the gain IDT. The VNA would record both relative amplitude and phase shift for this test. The resistance sweep test would have the following parameters:

- *Resistance range:* 35 – 10³ Ω
- *Resistance interval:* 9.7 Ω (given by the resolution limit of the device, as calculated in section 6.1.2)
- *Signal frequency:* 200 MHz
- *Signal amplitude:* 10 V
- *Resistance R_{gain} :* 10 k Ω

The amplitude and phase data from these tests would be compared to the model simulation data to see whether there are discrepancies. Discrepancies may include a lower average signal gain due to losses given by material imperfections, different phase shift properties due to non-uniform metal deposition density, or inadequate gain resolution (any step change greater than 5% of the signal amplitude). In addition to verifying the model technique, this data would have also been used to inform changes to the device geometry, such as the IDT finger width, and changes to the external circuitry. An example may be the addition of a reactance component to the gain impedance.

Finally, a two-dimensional parameter sweep over both frequency and resistance would be done. While this would have taken several days to run in simulation, this test could be done in a few hours, as the physical SAW propagation and measurement thereof is much faster than the numerical calculations for the same effect. This data would be used to create a lookup table of amplitude and phase effects for a given combination of frequency and resistance, and to see whether the project

specifications are met – such as the intrinsic insertion loss – at the edge cases of the parameters. This test would have the following parameters, totalling 122,880 combinations:

- *Resistance range*: 35 – 10³ Ω
- *Resistance interval*: 9.7 Ω (given by the resolution limit of the device, as calculated in section 6.1.2)
- *Frequency range*: 170 – 230 MHz
- *Frequency interval*: 0.5 MHz
- *Signal amplitude*: 10 V

Assuming each combination takes one second to measure, the test would take 34 hours to complete. If there are time constraints, the frequency range and interval could be changed to 185 – 215 MHz and 1 MHz respectively, or the resistance interval could be changed above 1 kΩ to 100 Ω, as the impact on attenuation is likely less at larger resistance values. This test would then only take 5 hours. Alternatively, a 2D sweep with a larger frequency interval could be conducted first in order to identify combinations where the gain changes the most. This test would only need to be run once, as the signal transmission characteristics would not change between tests.

7.4 Phase Device Testing

The phase device testing follows much the same reasoning as the gain device testing. The tests are performed on the 20 finger-pair modulator device, as this is the geometry closest to the intended 40 finger-pair geometry. As with the gain device, two parameter sweeps are performed, as well as a 2D parameter sweep.

The frequency sweep test is conducted with the V_{phase} phase modulating voltage parameter set to 0 V as in the simulation. The VNA would record both relative amplitude and phase shift data. The following other parameters would be used:

- *Frequency range*: 170 – 230 MHz
- *Frequency interval*: 0.5 MHz
- *Signal amplitude*: 10 V
- *Voltage V_{phase}* : 0 V

The voltage sweep test would then be performed, making use of the fact that the DC supply chosen can be interfaced with the experiment controller to automatically change the voltage parameter across the phase IDT. The VNA would record both relative amplitude and phase shift for this test. The voltage sweep test would have the following parameters:

- *DC Voltage range: ± 10 V*
- *Voltage interval: 0.5 V*
- *Frequency range: 170 – 230 MHz*
- *Frequency interval: 0.5 MHz*
- *Signal amplitude: 10 V*

The amplitude and phase data from these tests would be compared to the model simulation data to see whether there are discrepancies. Discrepancies may include different phase shift properties due to non-uniform metal deposition density, or inadequate phase shift (less than $\pm 90^\circ$). The results would be used to inform changes to the design that could result in better phase shift performance, such as changing the IDT geometry.

Finally, a two-dimensional parameter sweep over both frequency and voltage would be done. While this would have taken several days to run in simulation, this test could be done in a few hours, as the physical SAW propagation and measurement thereof is much faster than the numerical calculations for the same effect. This data would be used to create a lookup table of amplitude and phase effects for a given combination of frequency and voltage, and to see whether the project specifications are met at the edge cases of the parameters. This test would have the following parameters, totalling 4,800 combinations:

- *DC Voltage range: ± 10 V*
- *Voltage interval: 0.5 V*
- *Frequency range: 170 – 230 MHz*
- *Frequency interval: 0.5 MHz*
- *Signal amplitude: 10 V*

Assuming each combination takes one second to measure, the test would take 1.3 hours to complete.

The test results would inform future updates to the device and control circuitry. As discussed in section 8.2, geometric changes could include changes to the phase and gain modulating IDT geometries, such as making the fingers wider on the gain IDT, or changing the spacing between fingers on the phase IDT to minimise the intrinsic attenuation. Additional changes could be made to the gain modulation circuit by adding a reactance component to the impedance to create a frequency-sensitive modulator. Further, changes to the Tx/Rx IDT could be considered, such as IDT geometry or number of finger-pairs, despite being initially outside the project scope.

Chapter 8

Conclusion

This project set out to research, design, fabricate and construct a surface acoustic wave (SAW) modulator, that was able to modulate a SAW in transit on a Lithium Niobate (LN) substrate. While the final build and validation of the prototype did not take place due to the emergency measures Harvard University took to de-densify the campus officials in early March, significant progress and understanding towards a future prototype device has been gained, along with simulations of potential modulator designs.

Many of the specifications were met during the design process, and the remaining specifications were not able to be measured. In the case where the model simulations showed that the specification was unlikely to be met – for example, the maximum allowable intrinsic insertion loss – proposed future solutions may be able to meet the specification, as discussed later. Table 8-1 shows a summary of the project specifications and which ones were met.

8.1 Specification Evaluation

Table 8-1: Summary of the project specifications. Green means that they have been met. Yellow means that they were unable to be tested.

| | Description | Specification | Sub-System |
|------|--|---|----------------------------------|
| 1.1 | Physical size of all the features on the LN substrate | Between 1 mm x 1 mm and 10 μ m x 10 μ m | Overall System Size |
| 1.2 | Max. final product dimensions | 15 cm x 15 cm | |
| 1.3 | Fabricated with the equipment available at Harvard CNS | No features less than 1 μ m | Manufacturability and usefulness |
| 1.4 | Max. allowable intrinsic insertion loss with no amplitude modulation | -20 dB | |
| 1.5 | Max. allowable noise factor | 20 dB | |
| 2.1 | Frequency shift about centre frequency | (200 \pm 10) MHz | Phase Modulator |
| 3.1 | Dynamic range of the amplitude modulator | 0 dB to -10 dB | Amplitude Modulator |
| 4.1a | Power | 120 V AC RMS at 60 Hz | Control System |
| 4.1b | Computer interfaces | USB or Ethernet | |
| 4.2 | Connections to and from the control system to the PCB | Coaxial | |

The reasons why some specifications are marked as not having been fully met are described here, along with potential paths forward that will be expanded upon in section 8.2.

Specification 1.1 is not met, as the physical dimensions of the devices exceed 1 mm in the axis of SAW propagation. The dimensions of the largest device, the phase modulator, are 1 mm x 2.7 mm. However, this does not impair the ultimate function of

the project, and indeed was a necessary concession to optimise the performance of the device. Given the results presented, it is unlikely that the device can feasibly be made smaller. Therefore, while this specification was not strictly met, meeting it would have compromised the performance of the device, and so review of this specification is advised.

Specification 1.4 could not be tested before we had to vacate campus. However, from the simulations, it is unlikely that this would have been met, as even under optimal conditions and no modulation, the full bandwidth was not above this threshold. It is likely that the results would have been better had on-chip modulation taken place, rather than modulating the input signal, as only the receiving IDT would have caused significant attenuation, rather than both the transmitting and receiving IDTs currently.

Specification 1.5 could not be measured in time, and the simulations do not provide an indication of whether this would have been met. Every reasonable precaution was taken to protect against signal noise, including the use of shielded coaxial cable, so it is possible the specification was met.

Specification 2.1 could not be directly measured, as the device and control system were not completed. While the input signal could be varied and modulated, actual on-chip modulation of frequency could not be demonstrated. However, the gain and phase results, as well as the intrinsic attenuation levels of the Tx/Rx IDTs, are promising, suggesting that on-chip frequency modulation and reception thereof is a possibility.

Specification 3.1 could not be verified before we vacated campus. From the simulations it can be suggested that it is unlikely the dynamic range specification would have been met, as under the optimal simulation circumstances, the most dynamic range achieved was 4 dB. However, there are potential solutions to this, as discussed in section 8.2.

The remaining specifications were all met, or the design could verify that they were met. The minimum dimension of a fabricated structure is 4.75 μm , and the overall system is not larger than 15 cm x 15 cm, at 5.2 cm x 7.1 cm – the size of the PCB. The control system specifications were all met, as the design thereof makes use of devices connected to 12 V AC RMS at 60 Hz supplies, interfaces with a computer over USB, and makes use of coaxial connections for substrate signal lines.

8.2 Potential Future Work

While the project demonstrated useful results and fabricated a handful of prototypes, ongoing work is required in order to realise the ultimate design goal of an electro-acoustic on-chip SAW modulator.

Naturally, the devices designed as part of this project need to first be fully verified and tested in order to identify potential issues in the design or fabrication of them. This would also allow the control circuitry on the PCB to be validated and iterated upon for higher performance operation if required. For example, if it was shown that the digital potentiometer resolution was too low for useful operation of the gain modulator, there are solutions available with higher resolution that require specialised equipment to solder, or that are only available direct from the manufacturer. Further, a ± 10 V DAC and the microcontroller could be integrated onto the board to further consolidate the control system into a single unit, which is useful from an end-user standpoint.

Further modelling of other geometries or parameters may also help increase modulation performance of the devices. The effect of changing the number of finger-pairs in the Rx/Tx IDTs could be considered, as this value was taken as an off-the-shelf value from previous lab models in the models described in Chapter 4. Different IDT finger geometry may also help increase the energy transduction efficiency to and from the LN substrate, which could be achieved by making the fingers of the IDT wider than a quarter of the wavelength, but not changing the spacing between them.

In the gain modulator model, a higher dynamic range could be achieved by adding a reactive component to the impedance across the gain modulation IDT and optimising for this parameter. This may result in a controllable RLC filter architecture, potentially allowing selective frequency amplitude manipulation, and an increased dynamic range. Other options include a 'negative resistance' circuit, which may be able to increase the amplitude of the SAW while propagating, rather than just attenuate it, allowing the intrinsic insertion loss issue to be overcome. Evidence for this solution has been shown in the literature [33]. A 2D parameter sweep over both frequency and impedance could be performed (or 3D if the impedance includes reactance) in order to validate that the design meets the specification even at the edge cases.

In the phase modulator model, further investigation into the signal amplification phenomenon discussed in section 4.5.2 could be conducted to isolate whether it is an artefact of the simulation or whether signal gain is actually occurring. Efforts could also be made to minimise the local minimum in amplitude around the

centre frequency, perhaps by changing the IDT geometry spacing to be significantly greater than the wavelength of the centre frequency, or by gradually changing the spacing along the axis of propagation.

Future work needs to also be dedicated towards integrating both the gain and phase modulator onto a single chip, in order to be able to do on-chip frequency modulation. This would involve creating the device geometry and modelling it in order to verify device behaviour, followed by fabrication. If this were achieved, on-chip frequency modulation could be tested against the specification, likely leading to a lower insertion loss for the overall device.

Finally, the control system code needs to be designed and written to suit the chosen modulation paradigm and be integrated into an end-user-friendly design that can be deployed in the Lončar lab. This would require careful characterisation of the device propagation properties, and an analysis of the modulation space the device can achieve, given the physical limitations of the modulator. For example, the modulator may not be able to modulate towards a specific phase and amplitude, as the modulation spaces of the gain and phase modulator cannot reach that point when combined.

This project has ample future pathways to explore, and the suggestions above may only serve as a starting point for ongoing work. However, the project scope achieved in this report nevertheless provides a valuable stepping stone in realising the design goals of the project.

Acknowledgements

First and foremost, I would like to thank Dr. Linbo Shao, my supervising thesis advisor for this project. Linbo has never failed to make himself available if I had questions – of which I had many throughout the course of this project. He led me from minimal understanding of a very specific subject area to being able to conduct this project independently with patience and sincere understanding. A small example of this was spending eight hours with me at night in the Harvard Center for Nanoscale Systems, fabricating the devices. I would also like to thank Marko Lončar, my thesis faculty advisor, who brought me onto the project and had faith that an initially clueless undergraduate could indeed do this project justice. I am extremely thankful to the both of them.

I would also like to extend my thanks to the whole ES100 teaching staff, who over the course of an academic year, guided us through what was initially a daunting prospect. I would like to extend a special thanks to Michelle Rosen, who led my section with a light-hearted humour and diligent resolve, without which this project would have not come to fruition. I would also like to thank Christopher Lombardo for advising me over the four years of my undergraduate career, and to Salma Abu Ayyash for coordinating a class of occasionally uncooperative engineers through the thesis writing process.

Finally, I would like to thank the countless individuals who have helped me along this path – not just in this project, but also through my undergraduate career. From my fellow Class of 2020 engineers, with whom I have endured impossible problem sets, changing degree requirements and more, to my blockmates and other dear friends, and to my family, all have never wavered in their support as I tried my best to stay above the waterline over these four whirlwind years.

While the conclusion to my undergraduate career may have been less than ceremonial, I have no doubt that I will look fondly back at this time and remember all those who helped me along the way.

References

- [1] M. M. Waldrop, 'The chips are down for Moore's law', *Nature*, vol. 530, no. 7589, pp. 144–147, Feb. 2016, doi: 10.1038/530144a.
- [2] C.-C. Chang, Y. Cho, L. Wang, and J. Zou, 'Micromachined silicon acoustic delay lines for ultrasound applications', *J. Micromechanics Microengineering*, vol. 23, no. 2, p. 025006, Feb. 2013, doi: 10.1088/0960-1317/23/2/025006.
- [3] J. L. O'Brien, A. Furusawa, and J. Vučković, 'Photonic quantum technologies', *Nat. Photonics*, vol. 3, no. 12, pp. 687–695, Dec. 2009, doi: 10.1038/nphoton.2009.229.
- [4] D. R. Morgan, 'Surface acoustic wave devices and applications', *Ultrasonics*, vol. 11, no. 3, pp. 121–131, May 1973, doi: 10.1016/0041-624X(73)90608-2.
- [5] J. D. Maines and E. G. S. Paige, 'Surface-acoustic-wave devices for signal processing applications', *Proc. IEEE*, vol. 64, no. 5, pp. 639–652, 1976, doi: 10.1109/PROC.1976.10189.
- [6] R. M. White and F. W. Voltmer, 'DIRECT PIEZOELECTRIC COUPLING TO SURFACE ELASTIC WAVES', *Appl. Phys. Lett.*, vol. 7, no. 12, pp. 314–316, Dec. 1965, doi: 10.1063/1.1754276.
- [7] S. Kapfinger *et al.*, 'Dynamic acousto-optic control of a strongly coupled photonic molecule', *Nat. Commun.*, vol. 6, no. 1, p. 8540, Dec. 2015, doi: 10.1038/ncomms9540.
- [8] D. A. Golter, T. Oo, M. Amezcuca, K. A. Stewart, and H. Wang, 'Optomechanical Quantum Control of a Nitrogen-Vacancy Center in Diamond', *Phys. Rev. Lett.*, vol. 116, no. 14, p. 143602, Apr. 2016, doi: 10.1103/PhysRevLett.116.143602.
- [9] M. M. de Lima and P. V. Santos, 'Modulation of photonic structures by surface acoustic waves', *Rep. Prog. Phys.*, vol. 68, no. 7, pp. 1639–1701, Jul. 2005, doi: 10.1088/0034-4885/68/7/R02.
- [10] C. C. W. Ruppel, 'Acoustic Wave Filter Technology—A Review', *IEEE Trans. Ultrason. Ferroelectr. Freq. Control*, vol. 64, no. 9, pp. 1390–1400, Sep. 2017, doi: 10.1109/TUFFC.2017.2690905.
- [11] L. Shao *et al.*, 'Microwave-to-optical conversion using lithium niobate thin-film acoustic resonators', *ArXiv190708593 Phys. Physicsquant-Ph*, Jul. 2019, Accessed: Sep. 04, 2019. [Online]. Available: <http://arxiv.org/abs/1907.08593>.
- [12] L. Shao *et al.*, 'Phononic Band Structure Engineering for High-Q Gigahertz Surface Acoustic Wave Resonators on Lithium Niobate', *Phys. Rev. Appl.*, vol. 12, no. 1, p. 014022, Jul. 2019, doi: 10.1103/PhysRevApplied.12.014022.

- [13] D. P. Morgan, *Surface acoustic wave filters: with applications to electronic communications and signal processing*, 2nd ed. Amsterdam ; London: Academic Press, 2007.
- [14] C. Campbell, *Surface Acoustic Wave Devices and Their Signal Processing Applications*. Saint Louis: Elsevier Science, 2014.
- [15] A. V. Varlamov, V. V. Lebedev, P. M. Agruzov, I. V. Ilichev, and A. V. Shamrai, 'Optimal configuration of the waveguide acousto-optic TE-TM polarization mode convertor on X-cut lithium niobate substrate', *J. Phys. Conf. Ser.*, vol. 1236, p. 012034, Jun. 2019, doi: 10.1088/1742-6596/1236/1/012034.
- [16] C. Gorecki, F. Chollet, E. Bonnotte, and H. Kawakatsu, 'Silicon-based integrated interferometer with phase modulation driven by surface acoustic waves', *Opt. Lett.*, vol. 22, no. 23, p. 1784, Dec. 1997, doi: 10.1364/OL.22.001784.
- [17] 'Surface acoustic wave', *Wikipedia*. Apr. 06, 2020, Accessed: Apr. 08, 2020. [Online]. Available: https://en.wikipedia.org/w/index.php?title=Surface_acoustic_wave&oldid=949496632.
- [18] D. A. Golter, T. Oo, M. Amezcua, I. Lekavicius, K. A. Stewart, and H. Wang, 'Coupling a Surface Acoustic Wave to an Electron Spin in Diamond via a Dark State', *Phys. Rev. X*, vol. 6, no. 4, p. 041060, Dec. 2016, doi: 10.1103/PhysRevX.6.041060.
- [19] S. J. Whiteley *et al.*, 'Spin-phonon interactions in silicon carbide addressed by Gaussian acoustics', *Nat. Phys.*, vol. 15, no. 5, pp. 490-495, May 2019, doi: 10.1038/s41567-019-0420-0.
- [20] T. Aref *et al.*, 'Quantum Acoustics with Surface Acoustic Waves', in *Superconducting Devices in Quantum Optics*, R. H. Hadfield and G. Johansson, Eds. Cham: Springer International Publishing, 2016, pp. 217-244.
- [21] Y. Chu *et al.*, 'Quantum acoustics with superconducting qubits', *Science*, vol. 358, no. 6360, pp. 199-202, Oct. 2017, doi: 10.1126/science.aao1511.
- [22] D. Castelvecchi, 'IBM's quantum cloud computer goes commercial', *Nature*, vol. 543, no. 7644, pp. 159-159, Mar. 2017, doi: 10.1038/nature.2017.21585.
- [23] M. C. Kuzyk and H. Wang, 'Scaling Phononic Quantum Networks of Solid-State Spins with Closed Mechanical Subsystems', *Phys. Rev. X*, vol. 8, no. 4, p. 041027, Nov. 2018, doi: 10.1103/PhysRevX.8.041027.
- [24] X. Li, M. C. Kuzyk, and H. Wang, 'Honeycomblike Phononic Networks of Spins with Closed Mechanical Subsystems', *Phys. Rev. Appl.*, vol. 11, no. 6, p. 064037, Jun. 2019, doi: 10.1103/PhysRevApplied.11.064037.
- [25] M.-A. Lemonde *et al.*, 'Phonon Networks with Silicon-Vacancy Centers in Diamond Waveguides', *Phys. Rev. Lett.*, vol. 120, no. 21, p. 213603, May 2018, doi: 10.1103/PhysRevLett.120.213603.
- [26] K. J. Satzinger *et al.*, 'Quantum control of surface acoustic-wave phonons', *Nature*, vol. 563, no. 7733, pp. 661-665, Nov. 2018, doi: 10.1038/s41586-018-0719-5.
- [27] C. C. W. Ruppel, L. Reindl, and R. Weigel, 'SAW devices and their wireless communications applications', *IEEE Microw. Mag.*, vol. 3, no. 2, pp. 65-71, Jun. 2002, doi: 10.1109/MMW.2002.1004053.
- [28] Y. Yang, R. Lu, T. Manzanegue, and S. Gong, 'Toward Ka Band Acoustics: Lithium Niobate Asymmetrical Mode Piezoelectric MEMS Resonators', in *2018 IEEE*

- International Frequency Control Symposium (IFCS)*, Olympic Valley, CA, May 2018, pp. 1–5, doi: 10.1109/FCS.2018.8597475.
- [29] H. Roder, ‘Amplitude, Phase, and Frequency Modulation’, *Proc. IRE*, vol. 19, no. 12, pp. 2145–2176, Dec. 1931, doi: 10.1109/JRPROC.1931.222283.
- [30] L. Shao, W. Mao, S. Maity, N. Sinclair, Y. Hu, and L. Yang, ‘DRAFT: Nonreciprocal Transmission of Microwave Acoustic Waves using Nonlinear Parity-Time-Symmetric Resonators’, p. 14.
- [31] ‘Maskless Photolithography MLA150 | Heidelberg Instruments’.
<https://www.himt.de/index.php/MLA150.html> (accessed Oct. 06, 2019).
- [32] ‘Nikon’s Museum of Microscopy | Eclipse E600POL’, *Nikon’s MicroscopyU*.
<https://www.microscopyu.com/museum/eclipse-e600pol> (accessed Mar. 01, 2020).
- [33] L. Shao, W. Mao, S. Maity, N. Sinclair, Y. Hu, and L. Yang, ‘DRAFT: Supplementary Materials for Nonreciprocal Transmission of Microwave Acoustic Waves using Nonlinear Parity-Time-Symmetric Resonators’, p. 14.
- [34] J.-M. Hode, M. Doisy, and P. Dufilie, ‘Application of low loss SAW filters to RF and IF filtering in digital cellular radio systems’, in *IEEE Symposium on Ultrasonics*, Honolulu, HI, USA, 1990, pp. 429–434, doi: 10.1109/ULTSYM.1990.171402.
- [35] V. D. Kuptsov, ‘Noise optimization of surface acoustic wave devices in electronic systems’, in *2016 IEEE International Ultrasonics Symposium (IUS)*, Tours, France, Sep. 2016, pp. 1–4, doi: 10.1109/ULTSYM.2016.7728524.
- [36] ‘3rd Generation Partnership Project; Technical Specification Group Radio Access Network; Evolved Universal Terrestrial Radio Access (E-UTRA); User Equipment (UE) radio transmission and reception.’, 3GPP, 3GPP TS 36.101, Jul. 2013.
- [37] ‘Lithium Niobate Properties’.
<http://www.roditi.com/SingleCrystal/LiNbO3/liNBO3-Properties.html> (accessed Nov. 03, 2019).
- [38] R. E. Newnham, *Properties of materials: anisotropy, symmetry, structure*. Oxford ; New York: Oxford University Press, 2005.
- [39] ‘Impedance and Impedance Matching - National Instruments’.
<https://www.ni.com/en-gb/innovations/white-papers/06/impedance-and-impedance-matching.html> (accessed Apr. 08, 2020).
- [40] W. Wang, Y. Huang, X. Liu, and Y. Liang, ‘Surface acoustic wave acceleration sensor with high sensitivity incorporating ST-X quartz cantilever beam’, *Smart Mater. Struct.*, vol. 24, no. 1, p. 015015, Jan. 2015, doi: 10.1088/0964-1726/24/1/015015.
- [41] ‘GDSII | LayoutEditor Documentation’.
<https://www.layouteditor.org/layout/file-formats/gdsii> (accessed Apr. 08, 2020).
- [42] ‘Polymethylglutarimide (PMGI) Resists | Kayaku Advanced Materials’, *Kayaku Advanced Materials, Inc.* <https://kayakuam.com/products/pmgi-lor-lift-off-resists/> (accessed Mar. 01, 2020).
- [43] ‘LOR Lift-Off Resists Datasheet’. [Online]. Available: https://amolf.nl/wp-content/uploads/2016/09/datasheets_LOR_datasheet.pdf.
- [44] ‘Microposit S1800 Series Photoresists Datasheet’. [Online]. Available: https://amolf.nl/wp-content/uploads/2016/09/datasheets_S1800.pdf.

-
- [45] 'Microposit MF-139 Developer Datasheet'. [Online]. Available: http://micromaterialstech.com/wp-content/dow_electronic_materials/datasheets/MF-319%20Developer.pdf.
- [46] 'Remover PG Datasheet'. [Online]. Available: http://www.cen.iitb.ac.in/chemical_approval/policy/28_policy.pdf.
- [47] 'AD5174: Single-Channel, 1024-Position, Digital Rheostat with SPI Interface and 50-TP Memory'. Analog Devices, Accessed: Mar. 01, 2020. [Online]. Available: <https://www.analog.com/media/en/technical-documentation/datasheets/AD5174.pdf>.
- [48] 'AD660: Monolithic 16-Bit Serial/Byte DACPORT datasheet'. Analog Devices, Accessed: Mar. 01, 2020. [Online]. Available: <https://www.analog.com/media/en/technical-documentation/datasheets/AD660.pdf>.
- [49] 'Introduction to Vector Network Analyzers Basics'. Tektronix, Accessed: Apr. 09, 2020. [Online]. Available: <https://www.tek.com/document/primer/introduction-vector-network-analyzers-basics>.

Appendices

A. Fabrication Mask Generation Code

This mask generation code was adapted from code my advisor Linbo Shao wrote. Functions that he authored are titled with (LS), while functions I authored are titled (NW) .

```
#####  
# created by Linbo Shao #  
# updated by Nicolas Weninger #  
# description: Create SAW mask #  
# date: Aug 30, 2017 #  
#####  
  
import numpy as np  
import re  
import gdspy  
  
print('Using gdspy module version ' + gdspy.__version__ )  
  
index = 1  
  
#####  
# Contact PAD (LS) #  
#####  
# configuration 'gsg'  
# Origin at center of Signal pad  
# Seting parameters #  
# UNIT in micron #  
def contactPad(pitch=150.0, size=120.0, configuration='gsg', cellname="ContactPad",  
layer=3):  
    cell10 = gdspy.Cell(cellname + "_gen")  
    if 'gsg' == configuration:  
        rectangleS = gdspy.Rectangle((-size / 2, -size / 2), (size / 2, size / 2),  
layer=layer)  
        rectangleGr = gdspy.Rectangle((pitch - size / 2, -size / 2), (pitch + size / 2, size  
/ 2), layer=layer)  
        cell10.add([rectangleS,
```

```

        #                rectangleGl,
        rectangleGr])

    print("contact pad generated.")
    return cell0
#####

#####
#   IDT generation -- contacts at end (LS/NW)   #
#####
def metalIDTgen(widthx=150.0, widthy=2.0 / 2.0, pitch=2.0, n=10, shift=5.0,
cellname="metalIDT", layer=1, padlayer=3):
    cell0 = gdspy.Cell(cellname + "_gen")

    positions = [pitch * i for i in range(0, n)]
    ##### build connections #####
    gnd = -1
    for position in positions:
        shiftx = gnd * shift
        rectangle = gdspy.Rectangle((- shiftx - widthx / 2.0, position - widthy / 2.0),
                                   (- shiftx + widthx / 2, position + widthy / 2),
layer=layer)
        cell0.add(rectangle)
        gnd = gnd * -1

    ##### Draw connection #####
    rectangle = gdspy.Rectangle((-shift - widthx / 2.0 - 10.0, - widthy / 2.0),
                                (-shift - widthx / 2.0, max(70.0, pitch * n + 50.0)),
layer=layer)
    cell0.add(rectangle)

    rectangle = gdspy.Rectangle((+shift + widthx / 2.0, - widthy / 2.0),
                                (+shift + widthx / 2.0 + 10.0, max(70.0, pitch * n + 50.0)),
layer=layer)
    cell0.add(rectangle)

    ##### Extra connection for large pad #####
    if widthx > 250.0:
        rectangle = gdspy.Rectangle((-shift - widthx / 2.0 - 10.0, max(70.0, pitch * n +
50.0)),
                                   (-75.0, max(70.0, pitch * n + 50.0) + 10.0),
layer=layer)
        cell0.add(rectangle)
        rectangle = gdspy.Rectangle((+shift + widthx / 2.0 + 10.0, max(70.0, pitch * n +
50.0)),
                                   (75.0, max(70.0, pitch * n + 50.0) + 10.0), layer=layer)
        cell0.add(rectangle)

    ##### Draw Pads #####
    ## assuming pitch = 150 um #####
    rectangle = gdspy.Rectangle((-150.0 / 2.0 - 120.0 / 2.0, max(70.0, pitch * n + 50.0)),
                                (-150.0 / 2.0 + 120.0 / 2.0, max(70.0, pitch * n + 50.0) +
120.0), layer=padlayer)
    cell0.add(rectangle)

    rectangle = gdspy.Rectangle((+150.0 / 2.0 - 120.0 / 2.0, max(70.0, pitch * n + 50.0)),

```

```

                (+150.0 / 2.0 + 120.0 / 2.0, max(70.0, pitch * n + 50.0) +
120.0), layer=padlayer)
    cell0.add(rectangle)

    print("metalIDT generated.")
    return cell0
#####

#####
# IDT generation -- contacts at side (LS/NW) #
#####
def metalSideIDTgen(widthx=150.0, widthy=2.0 / 2.0, pitch=2.0, n=10, shift=5.0,
cellname="metalsideIDT", layer=1, padlayer=3):
    global index
    index = index + 1
    cell0 = gds Spy.Cell(cellname + "_gen%d" % (index))

    positions = [pitch * i for i in range(0, n)]
    ##### build connections #####
    gnd = -1
    for position in positions:
        shiftx = gnd * shift
        rectangle = gds Spy.Rectangle((- shiftx - widthx / 2.0, position - widthy / 2.0),
                (- shiftx + widthx / 2.0, position + widthy / 2.0),
layer=layer)
        cell0.add(rectangle)
        gnd = gnd * -1

    ##### Draw connection #####
    rectangle = gds Spy.Rectangle((-shift - widthx / 2.0 - 10.0, pitch - widthy / 2.0),
                (-shift - widthx / 2.0, max(pitch * (n - 1) + widthy / 2.0,
150.0)), layer=layer)
    cell0.add(rectangle)

    rectangle = gds Spy.Rectangle((+shift + widthx / 2.0, - widthy / 2.0),
                (+shift + widthx / 2.0 + 10.0, pitch * (n - 2) + widthy /
2.0), layer=layer)
    cell0.add(rectangle)

    rectangle = gds Spy.Rectangle((-shift - widthx / 2.0 - 80.0, 130.0),
                (-shift - widthx / 2.0 - 10.0, 150.0), layer=layer)
    cell0.add(rectangle)

    rectangle = gds Spy.Rectangle((-shift - widthx / 2.0 - 80.0, + widthy / 2.0),
                (shift - widthx / 2.0, min(- widthy / 2.0, + widthy / 2.0 -
20.0)), layer=layer)
    cell0.add(rectangle)

    ##### Draw Pads #####
    ### Assumeing 150 um pitch
    rectangle = gds Spy.Rectangle((-shift - widthx / 2.0 - 80.0 - 120.0, -120.0 / 2.0),
                (-shift - widthx / 2.0 - 80.0, 120.0 / 2.0), layer=padlayer)
    cell0.add(rectangle)

    rectangle = gds Spy.Rectangle((-shift - widthx / 2.0 - 80.0 - 120.0, 150.0 - 120.0 / 2.0),

```

```

                                (-shift - widthx / 2.0 - 80.0, 150.0 + 120.0 / 2),
layer=padlayer)
    cell10.add(rectangle)

    print("metalIDT at center generated.")
    return cell10
#####

#####
# add text      (LS)                                     #
#####
def textCell(text="Loncar Group", size=20, cellname="text", layer=2):
    cell11 = gdsapy.Cell(cellname)
    # Same goes for Labels & Text
    text1 = gdsapy.Text(text, size, (0, 0), layer=layer)
    label1 = gdsapy.Label(
        text, (0, -5), 'nw', layer=layer)
    cell11.add(text1)
    cell11.add(label1)
    print("textadded : " + text)
    return cell11
#####

#####
# add alignment Marker  (LS)                             #
#####
def alignmentMarker(cellname="alignmentmarker", layer=1, layerOPEN=5, layerOpenwindow=4):
    cell11 = gdsapy.Cell(cellname)
    # cell11.add(gdsapy.Polygon([(0, 100), (-50, 250), (50, 250)], layer = layer)) # UP
    cell11.add(gdsapy.Polygon([(0, -100), (-40, -150), (40, -150)], layer=layer)) # Down
    # cell11.add(gdsapy.Polygon([(100, 0), (250, 50), (250, -50)], layer = layer)) # right
    cell11.add(gdsapy.Polygon([(-100, 0), (-150, 40), (-150, -40)], layer=layer)) # left

    cell11.add(gdsapy.Rectangle((-100, -3), (-5, 3), layer=layer))
    cell11.add(gdsapy.Rectangle((100, -3), (5, 3), layer=layer))
    cell11.add(gdsapy.Rectangle((-3, 100), (3, 5), layer=layer))
    cell11.add(gdsapy.Rectangle((-3, -100), (3, -5), layer=layer))

    cell11.add(gdsapy.Rectangle((0, 0), (3, 3), layer=layer))
    cell11.add(gdsapy.Rectangle((0, 0), (-3, -3), layer=layer))

    # open window for fox etching
    # cell11.add(gdsapy.Rectangle((-300, -300), (300, 300), layer=layerOpenwindow))

    # open window for ebeam alignment
    cell11.add(gdsapy.Rectangle((-150, -150), (150, 150), layer=layerOPEN))

    return cell11
#####

#####
# IDENTITY      (NW)                                     #
#####

```

```

def IDTIdentityCell(n=200, gap=50, IDTpitch=1.683, IDTwidth=1000.0,
cellname1="IDTIdentity"):
    global index
    index = index + 1
    wIDT = IDTpitch*2*n #length of IDT
    cell1 = gdspy.Cell(cellname1 + "%d" % (index))

    metalIDTcell = metalIDTgen(n=n, widthx=IDTwidth, widthy=IDTpitch/2, pitch=IDTpitch,
cellname="idt1_%d" % (index), layer=3)

    text1 = textCell(text="IDENTITY", size=30, cellname="%dn%d_gap%.0f" % (index, n, gap),
layer=3)

    # add text
    cell1.add(gdspy.CellReference(text1, (-IDTwidth/2, wIDT-240)))

    # the first IDT
    cell1.add(gdspy.CellReference(metalIDTcell, (0, gap / 2.0)))

    # the other IDT
    cell1.add(gdspy.CellReference(metalIDTcell, (0, - gap / 2.0), rotation=180))

    return cell1
#####

#####
#   GAIN   (NW)   #
#####
def IDTGainCell(n=200, gap=50, IDTpitch=1.683, IDTwidth=1000.0, pIDT_gain=20,
cellname1="IDTGain"):
    global index
    index = index + 1
    wIDT = IDTpitch*2*n #length of IDT
    wIDT_Gain = IDTpitch*pIDT_gain # length of gain IDT

    cell1 = gdspy.Cell(cellname1 + "%d" % (index))

    metalIDTcell = metalIDTgen(n=n, widthx=IDTwidth, widthy=IDTpitch/2, pitch=IDTpitch,
cellname="idt1_%d" % (index), layer=3)

    metalSideIDTcell = metalSideIDTgen(n=pIDT_gain, widthx=IDTwidth+50, widthy=IDTpitch/2,
pitch=IDTpitch, layer=3, cellname="idt1_%d" % (index))

    text1 = textCell(text="GAIN%d"%(pIDT_gain), size=30, cellname="%dn%d_gap%.0f" % (index,
n, gap), layer=3)

    # add text
    cell1.add(gdspy.CellReference(text1, (-IDTwidth/2, wIDT-240)))

    # the first IDT
    cell1.add(gdspy.CellReference(metalIDTcell, (0,0)))
    # the other IDT
    cell1.add(gdspy.CellReference(metalIDTcell, (0, -2*gap-wIDT_Gain), rotation=180)) #(-
gap/2.0)-wIDT_Gain+45)

```

```

# add gain IDT
cell1.add(gdspy.CellReference(metalSideIDTcell, (-25, -wIDT_Gain-gap+5))) #-gap-
wIDT_Gain+125)

return cell1
#####

#####
# PHASE (NW) #
#####
def IDTPhaseCell(n=200, gap=50, IDTpitch=1.683, IDTwidth=1000.0, pIDT_phase=20,
cellname1="IDTPhase"):
    global index
    index = index + 1
    wIDT = IDTpitch*2*n #length of IDT
    wIDT_phase = IDTpitch*pIDT_phase # length of phase IDT

    cell1 = gdspy.Cell(cellname1 + "%d" % (index))

    metalIDTcell = metalIDTgen(n=n, widthx=IDTwidth, widthy=IDTpitch/2, pitch=IDTpitch,
cellname="idt1_%d" % (index), layer=3)

    metalSideIDTcell = metalSideIDTgen(n=pIDT_phase, widthx=IDTwidth+50, widthy=IDTpitch/2,
pitch=IDTpitch, layer=3, cellname="idt1_%d" % (index))

    text1 = textCell(text="PHASE%d"%(pIDT_phase), size=30, cellname="A%dn%d_gap%.0f" %
(index, n, gap), layer=3)

# add text
cell1.add(gdspy.CellReference(text1, (-IDTwidth/2, wIDT-240)))

# the first IDT
cell1.add(gdspy.CellReference(metalIDTcell, (0,0)))
# the other IDT
cell1.add(gdspy.CellReference(metalIDTcell, (0, -2*gap-wIDT_phase), rotation=180))
# add phase IDT
cell1.add(gdspy.CellReference(metalSideIDTcell, (-25, -wIDT_phase-gap+5)))

return cell1
#####

#####
# MAIN program (NW) #
#####
if __name__ == '__main__':
    wavelength = 19 #microns
    IDTpitch0 = wavelength/2.0
    IDTwidth0 = 1000

    ref_cell = gdspy.Cell('eBeam')

    text3 = gdspy.CellReference(textCell(text="SAW MODULATOR 200MHz NW", cellname="title3",
layer=3, size=100), (-300, 2500))
    text1 = gdspy.CellReference(textCell(text="2020-02-23 TEST Layer2", cellname="title1",
layer=2, size=70), (-1800, 2500))

```



```

text2 = gdspy.CellReference(textCell(text="2020-02-23 TEST Layer3", cellname="title2",
layer=3, size=70), (-1800, 2700))

##### IDENTITY #####
Ident = gdspy.CellReference(IDTIdentityCell(n=40, gap=50, IDTpitch=IDTpitch0,
IDTwidth=IDTwidth0), (-2000, 1000))

##### GAIN #####
Gain10 = gdspy.CellReference(IDTGainCell(n=40, gap=50, IDTpitch=IDTpitch0,
IDTwidth=IDTwidth0, pIDT_gain=10), (-2000, -1000))
Gain20 = gdspy.CellReference(IDTGainCell(n=40, gap=50, IDTpitch=IDTpitch0,
IDTwidth=IDTwidth0, pIDT_gain=20), (0, 1000))
Gain30 = gdspy.CellReference(IDTGainCell(n=40, gap=50, IDTpitch=IDTpitch0,
IDTwidth=IDTwidth0, pIDT_gain=30), (0, -1000))

##### PHASE #####
Phase40 = gdspy.CellReference(IDTPhaseCell(n=40, gap=50, IDTpitch=IDTpitch0,
IDTwidth=IDTwidth0, pIDT_phase=40), (2000, 0))

ref_cell.add([

    text1, text2, text3,
    Ident, Gain10, Gain20, Gain30, Phase40,

])
alignmentmark0 = alignmentMarker(layer=2)
alignmentmark1 = gdspy.CellReference(alignmentmark0, origin=(2500, 2500))
alignmentmark2 = gdspy.CellReference(alignmentmark0, origin=(2500, -2500))
alignmentmark3 = gdspy.CellReference(alignmentmark0, origin=(-2500, 2500))
alignmentmark4 = gdspy.CellReference(alignmentmark0, origin=(-2500, -2500))
alignmentmarks_cell = gdspy.Cell('ebeam_alignment')
alignmentmarks_cell.add([alignmentmark1, alignmentmark2, alignmentmark3,
alignmentmark4])

#### for OL-10 add marker to the file
ref_cell.add([alignmentmark1, alignmentmark2, alignmentmark3, alignmentmark4])
# create corrodinate

# ----- #
#      OUTPUT
# ----- #

exportname = "500um_SAW_200MHz"

faltten_cell = ref_cell.flatten()
gdspy.write_gds('C' + exportname + '_flattened.gds', cells=[faltten_cell], unit=1.0e-6,
precision=1.0e-10)

# ----- #
#      DISPLAY
# ----- #
# View the layout using a GUI. Full description of the controls can
# be found in the online help at http://gdspy.sourceforge.net/
gdspy.LayoutViewer()
print("exit")

```

B. PCB Schematic and Board Layout

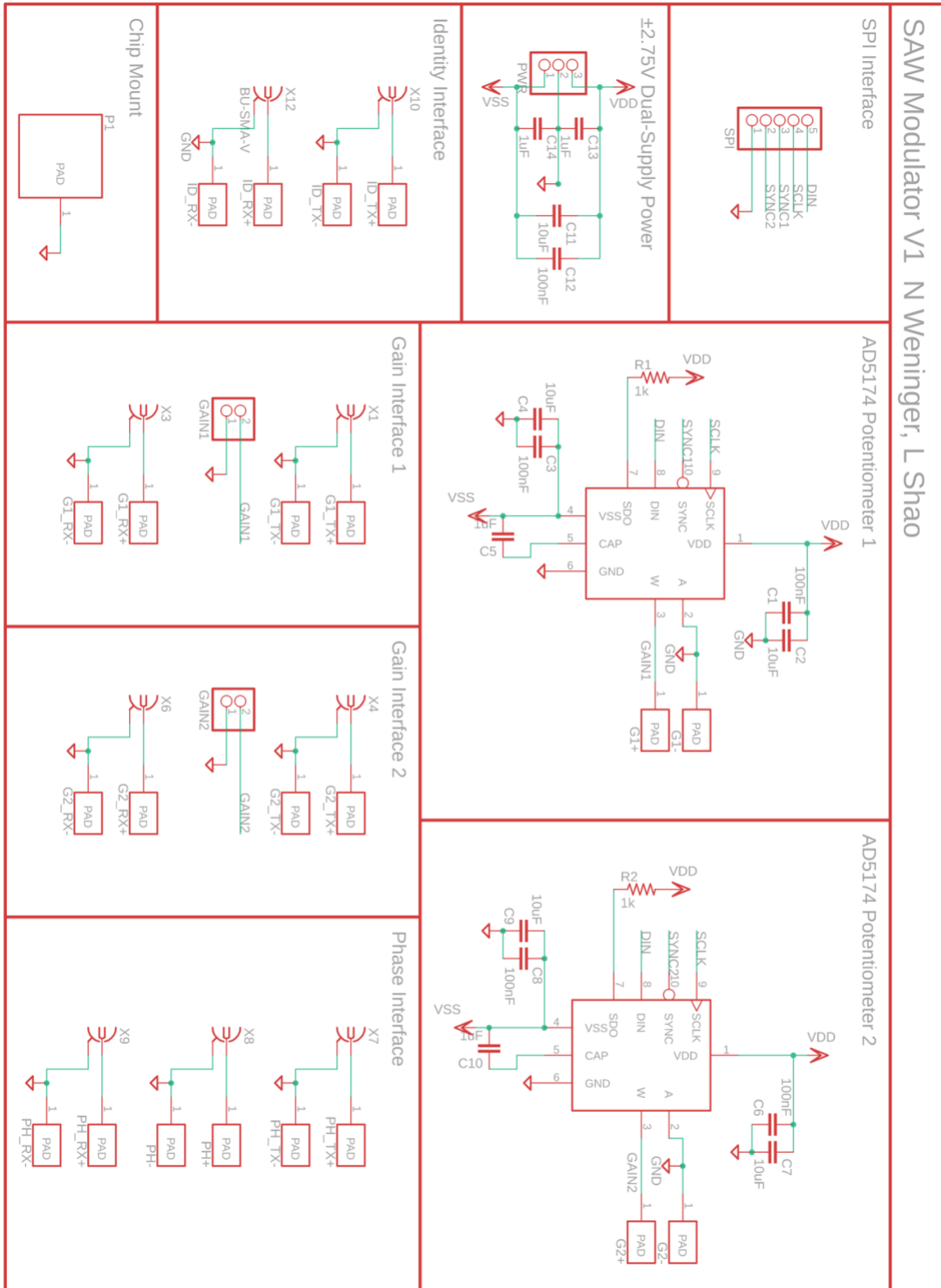


Figure B-1: Full schematic of the PCB as ordered.

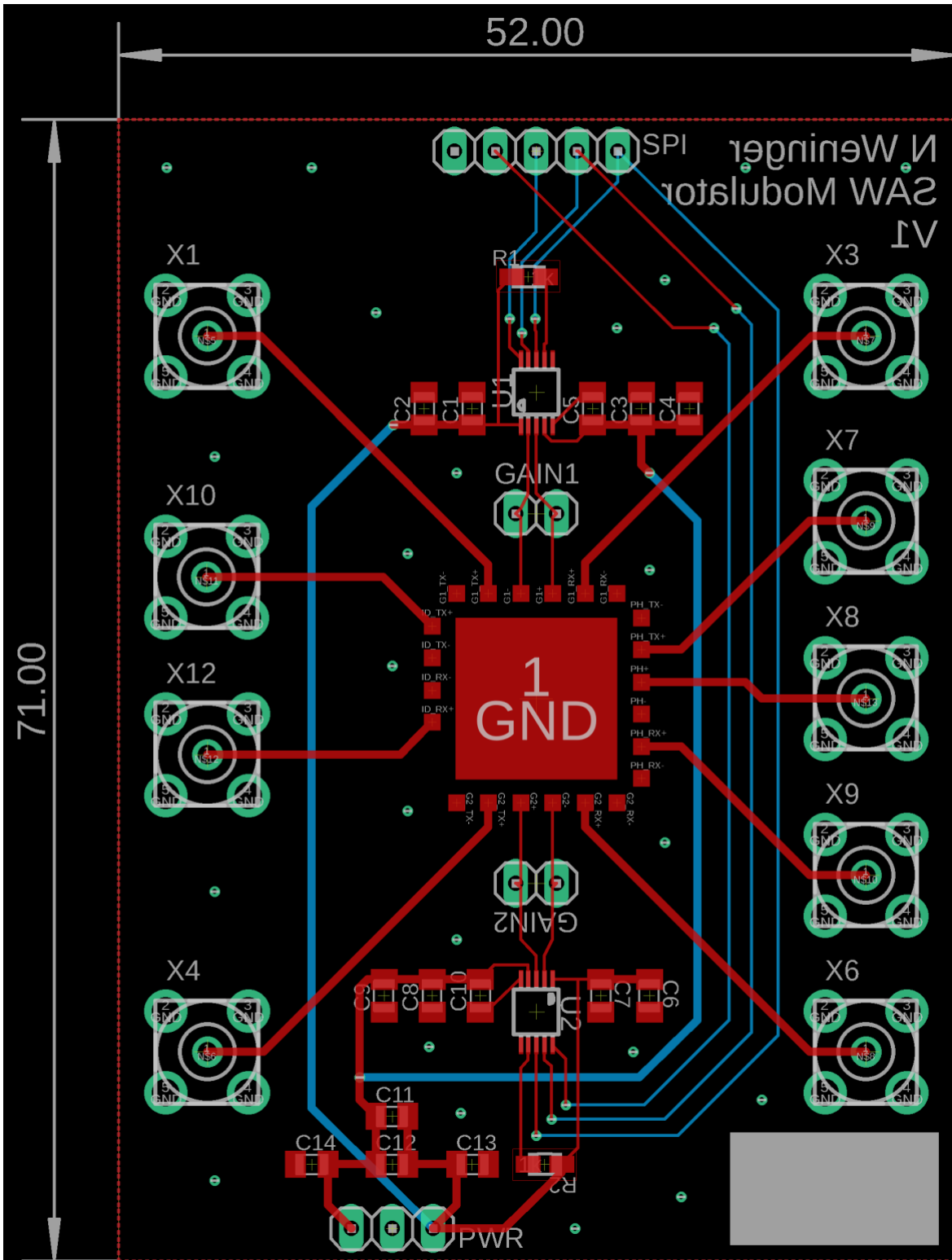


Figure B-2: Screenshot of the PCB layout as ordered, without ground plane infill.

C. PCB Bill of Materials

Bill of Materials for 3 PCBs

| Qty/PCB | Description | Value | Parts | Supplier | Catalogue No. | Unit Price | No. Ordered | Total Price | |
|--------------|-----------------------|----------|--------------------------------------|----------|------------------|------------|-------------|-------------|---------------|
| 2 | PIN HEADER 1X02 | | GAIN1, GAIN2 | Digikley | 609-3465-ND | \$1.46 | 2 | \$2.92 | |
| 1 | PIN HEADER 1X03 | | PWR | Digikley | N/A | \$0.00 | 0 | \$0.00 | |
| 1 | PIN HEADER 1X05 | | SPI | Digikley | N/A | \$0.00 | 0 | \$0.00 | |
| 5 | CAPACITOR 0805 | 100nF | C1, C3, C6, C8, C12 | Digikley | 399-1177-1-ND | \$0.10 | 40 | \$4.00 | |
| 5 | CAPACITOR 0805 | 10uF | C2, C4, C7, C9, C11 | Digikley | 399-3138-1-ND | \$0.16 | 40 | \$6.40 | |
| 4 | CAPACITOR 0805 | 1uF | C5, C10, C13, C14 | Digikley | 399-8011-1-ND | \$0.12 | 40 | \$4.80 | |
| 2 | RESISTOR 0805 | 1k | R1, R2 | Digikley | 311-1.0KARCT-ND | \$0.10 | 20 | \$2.00 | |
| 2 | DIGITAL POTENTIOMETER | AD5174 | U1, U2 | Digikley | AD5174BRMZ-10-ND | \$4.08 | 8 | \$32.64 | |
| 9 | FEMALE SMA CONNECTOR | BU-SMA-V | X1, X3, X4, X6, X7, X8, X9, X10, X12 | Digikley | WM5543-ND | \$3.14 | 27 | \$84.78 | |
| TOTAL | | | | | | | | | 137.54 |

Table C-1: PCB Bill of Materials and total quantities ordered for the project.

D. Project Budget

Table D-1: Total project budget

| CNS Costs | | | |
|-------------------------------------|------------------|---------------------------|-------------|
| Instrument | Cost / hr | Hours Used | Cost |
| EE-5 PVD E-Beam Deposition System | \$ 50.00 | 5 | \$ 250.00 |
| OL-10 Heidelberg MLA | \$ 35.00 | 1 | \$ 35.00 |
| NF-07 General LISE Cleanroom Access | \$ 39.00 | 8 (Max. 3 hrs charged) | \$ 117.00 |
| | | Subtotal | \$ 402.00 |

| FAS RC Cluster Costs | | | |
|-----------------------------|------------------|-------------------|-------------|
| Instrument | Cost / hr | Hours Used | Cost |
| 4 cores, 16 GB RAM, COMSOL | \$ 0.08 | 100 | \$ 8.20 |
| | | Subtotal | \$ 8.20 |

| PCB Hardware BOM Costs | | | |
|-------------------------------|--|----------|-----------|
| BOM Materials | | | \$ 137.54 |
| PCB (5) | | | \$ 148.40 |
| | | Subtotal | \$ 285.94 |

| | |
|---------------------------|------------------|
| Total Project Cost | \$ 696.14 |
|---------------------------|------------------|

Note: CNS Costs and FAS RC computing cluster costs were covered by the Lončar lab and are estimates. The PCB hardware BOM costs were covered by the ES100 budget through the SEAS Active Learning Labs.

E. Supplemental ES100 Questions

Table E-1: Supplemental ES100 Budget Questions

| | Total \$ | Exact or estimated? |
|---|-----------|---------------------|
| Total Development cost: everything that was spent on your project including prototypes, transportation to research locations, renting of equipment, orders from a lab you worked at, your own money, etc. | \$ 696.14 | Estimated |
| Minimum cost to make one prototype of your project | \$ 440.40 | Estimated |
| Total cost of items purchased through the <i>Active Learning Labs (ALL)</i> , if any | \$ 285.94 | Exact |
| Total cost covered by the <i>Harvard Research Lab(s)</i> you are affiliated with, if any | \$ 410.20 | Estimated |
| Total cost of items purchased personally, if any | \$ - | Exact |
| Total cost covered by a <i>non-Harvard lab</i> and/or company, if any | \$ - | Exact |

Table E-2: Supplemental ES100 Questions on Harvard CNS Usage.

| | |
|---|---|
| If you had to use CNS space and equipment, please answer the following questions: | |
| Why did your project require the use of CNS facilities? | The project required a device to be fabricated. |
| Roughly much time did you spend using CNS facilities? | Approximately 8 total hours. |
| What equipment did you need to use? | OL-10, EE-5, wet benches for photolithography. |
| Who did you interact with at CNS and how? | My advisor Dr. Linbo Shao accompanied me at CNS. We did not interact with any CNS staff. |
| If you are affiliated with a research lab that arranged for your use of CNS facilities, please specify which lab (and research administrator who arranged your access, if you know) | I am affiliated with the Lončar lab. My access was arranged by my advisor Dr. Linbo Shao. |
| If you didn't work through a research lab directly, did the Active Learning Lab sponsor/arrange your use of CNS resources? | N/A |
| What could we have done better to make your CNS experience more productive? | N/A |

